FINITE ELEMENT ANALYSIS OF WIDE-TYPE LARGE CAPACITY END-PLATE CONNECTIONS

G. Shi，* H. Fan，Y.J. Shi and Y.Q. Wang

Key Laboratory of Civil Engineering Safety and Durability of China
Education Ministry，Department of Civil Engineering，
Tsinghua University，Beijing，100084，China
* Email：fanh05@sina.com

KEYWORDS

Wide end plate，large capacity end-plate connection，finite element analysis.

ABSTRACT

With the increase of the height and span of the steel structure，the size and the inner force of the beam and column is becoming larger，which beyond the loading capacity of the traditional end-plate connection. However，end-plate connections with the four bolts in a row both at the inner and external sides of the tension flange of the beam usually possess greater loading capacity，which could satisfy the large capacity requirement. Although with this outstanding advantage，seldom research on the static behavior of the wide-type end-plate connection has been done in China. In this paper，detailed verified finite element model will be employed to analyze the static behavior of 6 wide-type end-plate connections. The influence of parameters such as end-plate thickness，bolt layout，end-plate extend or not and the geometry of the stiffener have been investigated. The simulation results demonstrate that（1）the shear force in the connection is mainly transferred by the contact surface of the end-plate；（2）whether the compression part of the end-plate is extended or not has little effect on the static behavior of the whole connection；（3）at ultimate state the other bolts located between the beam flange have significant contribution to the loading capacity of the connections while it shows little contribution in the elastic state. A bolt tension force distribution model for connection design is proposed；the bolt tension force of the inner column distributes approximately linearly with the neutral axis located at the beam axis and the bolt tension force of the outer column is equal to 0.32P. What's more，a yield line model of the end plate tension part has been proposed.

INTRODUCTION

Traditional end-plate connection（see Figure 1）is a type of commonly used connection in steel frames[1]. However，with the increase of the size and inner force of the components，this traditional layout（two bolts in a row）could not satisfy the strength requirements. To increase the loading capacity，the wide-

type configuration featured by four bolts in a row (see Figure 2) might be employed. The performance of the unstiffened type (see Figure 2(b)), has been identified by the U. S. and European researchers, and corresponding design methods have been established [2-5], which demonstrated that the tension force transferred by the bolts located far from the beam web was much lower than those of the nearer ones.
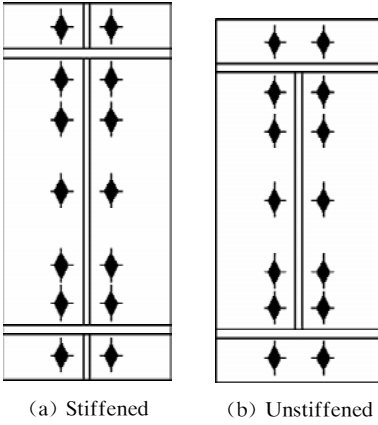

(a) Stiffened	(b) Unstiffened

Figure 1   Bolt layout of traditional configuration

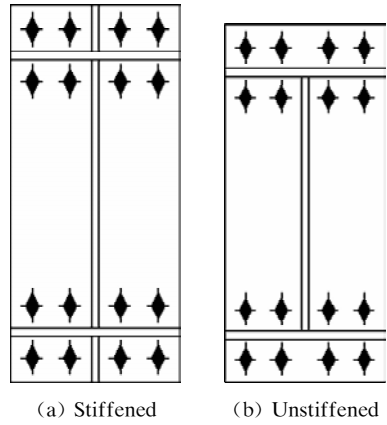|	
(a) Stiffened	(b) Unstiffened

Figure 2   Bolt layout of wide-type configuration

However, investigations showed that the stiffener located at the extended part of the end plate could reduce the end plate thickness requirement and prevent the brittle failure of the weld, thus enhance its seismic performance[6, 7]. Therefore, the static behavior of the stiffened type (see Figure 2(a)) will be investigated. Besides, researchers all over the world[3, 8, 9], especially in China[10, 11] in recent years, simulated the behavior of the end-plate connections with finite element methods, which showed high accuracy compared to the corresponding test results. Hence, the performance of the stiffened wide-type end-plate connections, will be studied by finite element analysis, where the behavior of the key components such as the end plate and the bolts would be detailed investigated.

VERIFYING THE FINITE ELEMENT MODEL

To simulate the behavior of the end-plate connections, no matter traditional or wide-type configuration, the contacting and the pre-tension behavior are two major difficulties. Investigations proved that the former can be solved by creating contact pair between the contacting surfaces while the latter by inserting pre-tension elements into the bolt. The validation of the finite element model is proved as the following.

Choosing Element Type

The finite element model of the bolt and the complete specimen are shown in Figure 3, where the contact surfaces between the bolt nut and its contacting plates are glued together and the effective diameter, but not the nominator diameter is used to model the bolt shank.

Constitutive Model of the Steel

The stress-strain model shown in Figure 4(a), considering both the yielding and hardening behavior, is adopted for all the steel plate, while that in Figure 4(b) is for the bolts. If no coupon tension test data is

given，the constitutive model for Q345 steel plate listed in Table 1[12] will be used and the yielding strength and the tension strength for the Grade 10.9 bolts are 940 MPa and 1 040 MPa[13]，respectively.
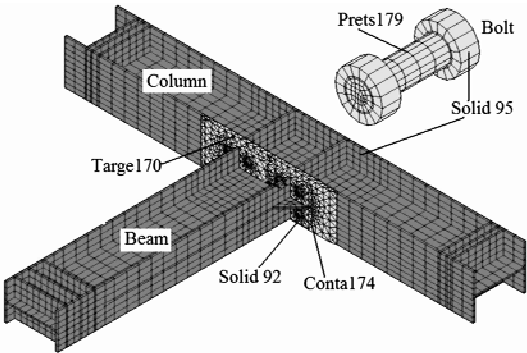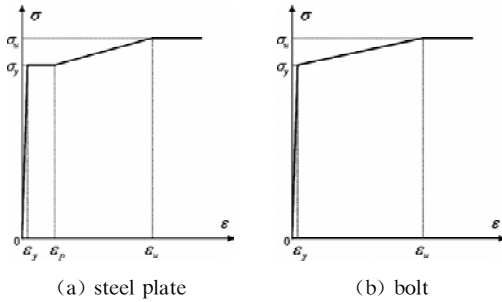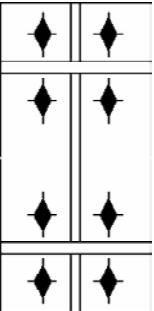

Figure 3　Finite element model

(a) steel plate　　(b) bolt

Figure 4　The adopted stress-strain model

TABLE 1　THE VALUE OF THE CONSTITUTIVE MODEL OF Q345 STEEL PLATE WITHOUT COUPON TEST

Plate thickness	$t \leqslant 16$ mm			$t > 16$ mm		
strain	0.001 675	0.025	0.100 2	0.001 675	0.020	0.095 2
stress	345	345	500	345	345	500

Simulation Results

The predicted loading capacity of specimens in Refs. [6] and [14] are listed in Table 2，where the corresponding experimental results are shown for comparison. For the failure mode of the specimens in Ref. [14] is the local buckling of the beam，the maximum local geometrical imperfection is setting as 1.5 mm for these specimens. The difference for most specimens is no more than 10%，while it is more than 20% for some specimens in Ref. [14]，which could attribute to the scatter of the test specimens. As the established finite element model has been verified by 19 experimental specimens in the literature to prove its accuracy，it can be used to study the performance of the wide-type stiffened end-plate connections.

TABLE 2　THE LOADING CAPACITY COMPARISON OF END-PLATE CONNECTIOINS IN REFS. [6] AND[14]

Ref.	Typical bolt layout	Specimen	Loading capacity		
			Test(kN)	FEM(kN)	FEM / Test
[6]		SC1	155.3	153.9	0.99	
		SC2	286.4	270.8	0.95	
		SC3	256.8	241.1	0.94	Average：
		SC4	256.6	257.7	1.00	0.98
		SC5	268.4	275.4	1.03	Standard deviation：
		SC6	325.3	328.5	1.01	0.10
		SC7	342.3	349.9	1.02	
		SC8	296.1	279.1	0.94	

continued

Ref.	Typical bolt layout	Specimen	Loading capacity		
			Test(kN)	FEM(kN)	FEM / Test
[14]		A1−1EM	156.7	158.0	0.99
		A2−1EM−2	156.7	150.0	1.04
		B1−1EM	244.7	204.0	1.20
		B2−1EM	244.7	228.0	1.07
		B2−4EM	261.6	208.0	1.26
		C1−2EM	170.0	183.0	0.93
		C3−2EM	170.0	197.0	0.86
		C3−5EM	183.5	201.0	0.91
		D1−2EM	422.6	444.0	0.95
		D3−2EM	422.6	462.0	0.91
		D4−2EM	422.6	448.0	0.94

Average：1.01
Standard deviation：0.13

PARAMETRICAL ANALYSIS

Joint Configuration

The typical T-shape side joint of steel frame，as the experimental joint specimens in Ref. [6]，with the wide-type end-plate connection，is used for analysis. Both the beam and column are welded H-section with the geometry of $950 \times 350 \times 16 \times 18$ and $800 \times 350 \times 16 \times t_{ep}$ (t_{ep} is the end-plate thickness)，respectively. The 10.9 grade M24 high strength bolt and Q345 steel plates are adopted. Three types of bolt group layouts（see Figure 5）are covered，where type A is a standard layout fulfilling the requirements of current steel specifications，the compression part of the end-plate of type B is flushed，type C is the most efficient bolt layout but violates the maximum bolt spacing requirement. In addition，two types of stiffeners（in Figure 6）are analyzed，where stiffener I is recommended by FEMA−350[15] and stiffener II is used in the domestic practices and literatures. The configuration details of all the finite element models are listed in Table 3.

Figure 5   3 types of bolt layout

Finite Element Model

The finite element model，verified in section 2，is used to study the performance of the stiffened wide-type end-plate connections，with the material model shown in Figure 4 and Table 1. Considering the calculating efficiency and the symmetry of the specimen，we establish the half-model for all the specimens in Table 3.
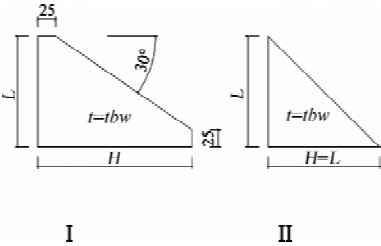

Figure 6　Two types of stiffener

TABLE 3　THE CONFIGURATION DETAILS OF THE ANALYZED END-PLATE CONNECTIONS

Specimen	Bolt layout	End plate thickness	Stiffener type	Specimen	Bolt layout	End plate thickness	Stiffener type
SJA24I	A	24	I	SJA24II	A	24	II
SJA16I	A	16	I	SJB24I	B	24	I
SJA32I	A	32	I	SJC24I	C	24	I

Simulation Results

Bolt Transferred Tension Force

In China，the design strength of the transferred tension force by a high strength bolt must not exceed 0.8P，where P is the pre-tension force of the bolt. To investigate the distribution of the bolt transferred tension force，the bolt tension force F and the compression force C in the vicinity of the bolts have to be known.

To obtain the compression force C，firstly，the contact surface of the end-plate were divided into several rectangle parts（see Figure 7）with a bolt hole in each part. Secondly，the contact compression force was extracted from each rectangle surface respectively. When the dividing lines passed through the middle point of two adjacent bolts，the tension force and the compression force were approximately equal to each other when there was no external loading，which proved that the dividing was reasonable.

Figure 8 shows the development of the bolt transferred tension force of specimen SJA24I with the increase of the moment，in which the horizontal dashed line represents the design tension force of a high strength bolt （180 kN here）. In a wide range（even beyond the point that the maximum bolt transferred force reaches 0.8P），the bolt transferred tension force increases linearly as the external loading grows. When the maximum bolt transferred force reaches 0.8P，the transferred force by the bolt group are plotted in Figure 9，where "（1）" represents the bolt column far from the beam web and "2" identifies the nearer ones.
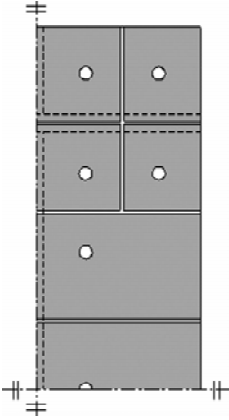
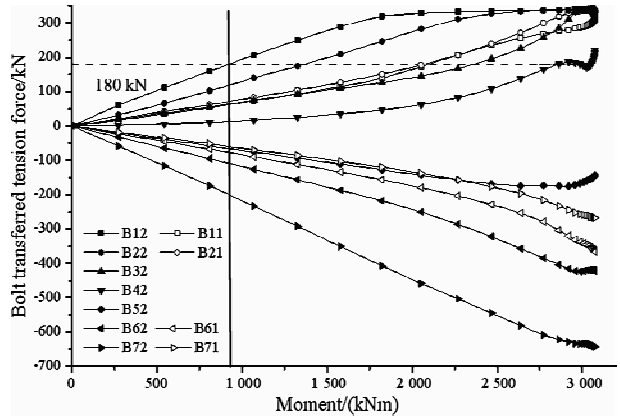**Figure 7   Division scheme of the contact surface**

Figure 8   Bolt transferred force-moment curves of SJA24I

Generally，the transferred force of B12 is always the maximum，while B22 follows. When the transferred tension force by B12 reaches $0.8P$, tension force transferred by the bolts located far from the web is far less than those of nearer ones，about 0.4 times of the former. The end-plate thickness has notable effect on the transferred force of B22 and B42. With thicker end-plate，the transferred force of B22 is smaller while that of B42 is much closer to 0.

Comparison between SJA24I and SJA24II indicates that the weaker the stiffener the evener the tension force transferred by the bolts near the tension flange. Results of SJB24I and SJB24I signify that the extended end-plate at the compression part has little effect on the bolt transferred force，which implies that the compression force is actually transferred by the beam web/stiffener and the beam compression flange. The difference between SJA24I and SJC24I indicates that bolt B42 make little contribution to the bending capacity in elastic state for the neutral axis of the bolt group is close to the beam axis. And，the tension force transferred by the bolts near the beam web is not linearly distributed where the tension force transferred by bolts in the inner part of the beam flange is less than the assumption of linear distribution. However，the compression force of the connection transferred by the compression part of beam web and beam compression flange could be assumed as symmetrically distributed with tension force transferred by the bolt located at the tension region.

Bolt Transferred Shear Force

Bolt shear force always exists in the end-plate connection for the local bending deformation of the end-plate，as shown in Figure 10，among which the shear force of bolts located at the external part of the end-plate are larger than those of others. Further study shows that the thicker the end-plate the smaller the bolt transferred shear force because less bending deformation would generate in thicker end-plate. As a whole，the bolt transferred shear force is so small that their effect can be ignored.

The Loading Capacity the Connection

In Table 4，term M_u means the maximum moment when the plastic equivalent strain of the high strength bolt and end-plate are less than 0.1 and 0.2, respectively. Therefore，choosing M_u as the ultimate loading capacity of the connection could guarantee the safety. φ_u is the connection rotation corresponding
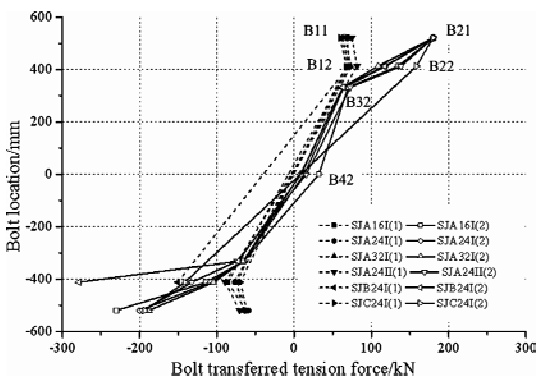
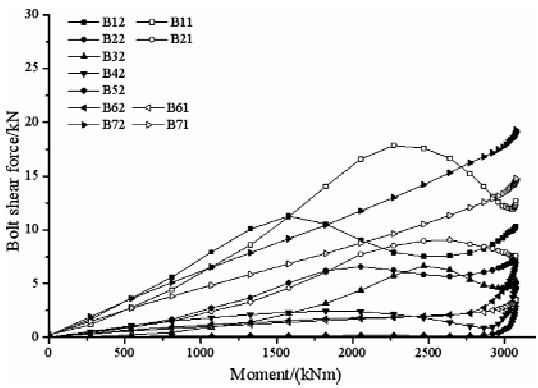Figure 9　The bolt transferred force in elastic range

Figure 10　Bolt shear force development of SJA24I

to the moment M_u (The connection rotation is the gap rotation in Ref.[6] composed by the deformation of bolt tension, end-plate bending and column flange bending.). Compared M_u of the 14 specimens, it can be seen that (1) when the end-plate is thick, the change of the end-plate thickness has little effect on the connection loading capacity, which is the opposite case when thinner end-plate is employed; (2) the effect of whether the compression part of the end-plate and the geometry of the stiffener can be ignored; (3) bolts far from the beam tension flange contribute greatly to the loading capacity of the connection as M_u of SJA24I is about 20% higher than that of SJC24I. Therefore, when design a wide-type end-plate connection, consider the loading capacity contribution of the bolts located in the inner part of the beam flange, the linear distribution assumption could be still valid to calculate the loading capacity of the bolt group. In addition, the bolt transferred force at ultimate state is plotted in Figure 11.
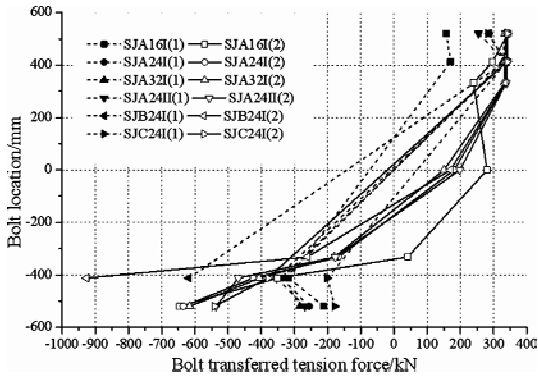
Figure 11　Bolt transferred force at ultimate state

M_{ou} is the calculated loading capacity of the traditional end-plate connections as shown in Figure 1(a), whose only difference from the wide-type end-plate connection is the absence of the bolt column far from the beam web. The last column of Table 4 indicates that M_u is 24%~88% greater than M_{ou} and when the end-plate is thin, the increase of the loading capacity is relatively small.

The Yield Line of the End-plate

Based on the observation of the stress contour (see Figure 12), a yield line model as shown in Figure 13 is proposed to calculate the loading capacity and the thickness of the end-plate.
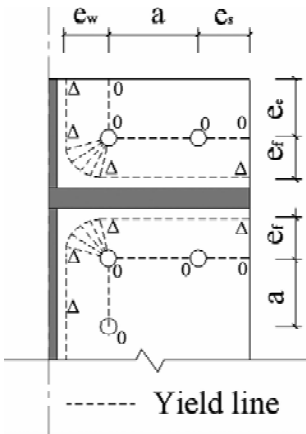
Figure 12 Stress contour of SJA16I

Figure 13 Yield line model

TABLE 4 LOADING CAPACITY OF ALL 6 SPECIMENS

Specimen	M_u /kNm	φ_u /mrad	M_{ou} /kNm	M_u/M_{ou}	Specimen	M_u /kNm	φ_u /mrad	M_{ou} /kNm	M_u/M_{ou}
SJA24I	2 987	3.03	2 028	1.47	SJA24II	2 955	4.01	2 010	1.47
SJA16I	2 455	6.01	1 975	1.24	SJB24I	2 903	3.01	1 981	1.47
SJA32I	3 139	3.41	2 135	1.47	SJC24I	2 480	3.36	1 319	1.88

CONCLUSIONS

The finite element model has calculated 19 experimental specimens and the static behavior of the wide-type end-plate connection has been detailed investigated，where parameters such as end-plate thickness，stiffener geometry, and bolt layout are considered. It can be concluded as the following：

(1) The established finite element models were widely verified and had high accuracy，which could be used to predict the behavior of end-plate connections with different configurations.

(2) Most of the shear force is transferred by friction while shear force in the bolt group can be ignored.

(3) The stiffener geometry has great influence on the bolt transferred tension force at the beginning stage. And the bolt rows located near the beam axis has little contribution in the elastic range while its effect to the ultimate loading capacity of the connection is notable. However，whether the compression part of the end-plate is flushed or extended has little influence on the static performance of the wide-type end-plate connection.

(4) When design a wide-type end-plate connection，the transferred tension force by the bolt columns in the vicinity of the beam web could be assumed as linear distribution with the neutral axis located at the beam axis，where the bolt columns far from the beam web transferred equal tension force，about $0.32P$. And the compression force transferred by the connection could be assumed as symmetrically distributed with tension force transferred by the bolt located at the tension region.

(5) A yield line model of the tension part of the end-plate has been proposed.

REFERENCE

［1］China Engineering Construction Standardization Association，"Technical specification for steel structure of light-weight buildings with gabled frames"，CECS 102：2002.（in Chinese）

［2］Murray，T. M.，"Extended End-Plate Moment Connections"，Chicago，AISC，IL，1990.

［3］Krishnamurthy，N.，"A fresh look at bolted end-plate behavior and design"，Engineering Journal，1978，2nd Quarter，pp.39-49.

［4］Demonceau，J. F.，Weynand，K.，Jaspart，J. P. and Muller，C.，"Application of Eurocode 3 to steel connections with four bolts per horizontal row"，SDSS'Rio 2010 Stability and Ductility of Steel Structures，Rio de Janeiro，Brazil，September 8-10，2010.

［5］Grundy，P.，Thomas，I. R. and Bennetts，I. D.，"Beam-to-column moment connections. Journal of the structural division"，ASCE，1980，106(ST1)，pp.313-330.

［6］Shi，G.，Shi，Y. J.，Wang，Y. Q.，Li，S. F. and Chen，H.，"Experimental study of semirigid end-plate connections in multi-story steel frames"，Journal of Tsinghua University (Science and Technology)，2004，44(3)，pp.395-397.（in Chinese）

［7］Tsai，K. and Popov，E. P.，"Cyclic Behavior of End-Plate Moment Connections"，Journal of Structural Engineering，1990，116(11)，pp.2917-2930.

［8］Murray，T. M. and Kukreti，A. R.，"Design of 8-bolt stiffened moment end-plates"，Engineering Journal，AISC，1988，2nd Quarter，pp.45-53.

［9］Chasten，C. P.，Lu，L. W. and Driscoll，G. C.，"Prying and shear in end-plate connection design"，Journal of structural engineering，1992，118(5)，pp.1295-1311.

［10］Shi，G.，Shi，Y. J. and Wang，Y. Q.，"Nonlinear finite element analysis of end-plate connections in steel frames"，Engineering Mechanics，2008，25(12)，pp.79-85.（in Chinese）

［11］Guo，B.，"Analysis of prying force in extended end-plate bolted connections"，Building Structure，2006，36(8)，pp.10-11，19.（in Chinese）

［12］GB/T 1987-2005，"Steel plates for building structure".（in Chinese）

［13］GB/T 1231-92，"Specification of high strength bolts with large hexagon head，large hexagon nuts，plain washers for steel structures".（in Chinese）

［14］Chen，Y. Y.，Wang，S. F.，Wang，S. N.，Liu，C. Z. and Chen，Y. Q.，"Experimental research on joint behavior of H-section beams with flanges and end-plates connected by non-completely penetrated welds"，Journal of Building Structures，2005，26(3)，pp.70-77.（in Chinese）

［15］Federal Emergency Management Agency."FEMA-350 Recommended Seismic Design Criteria for New Steel Moment-Frame Buildings"，2000.

EXPERIMENTAL ANALYSIS ON THE LOCAL BUCKLINGBEHAVIOR AT PANEL ZONE OF BEAM-TO-COLUMN CONNECTION IN STEEL GABLED FRAMES

* Y. Shi[1, 2]，Y. Chen[1]，Y. Xu[1] and X. Z. Zhao[1]

[1] State Key Laboratory for Disaster Reduction in Civil Engineering，Tongji University，
Shanghai 200092，China
[2] Disaster Prevention Research Institute，Kyoto University，Kyoto611-0011，Japan
* Email：shiyundong@gmail.com

KEYWORDS

Seismic behavior，experiment，thin-walled steel member，connection，local buckling，panel zone.

ABSTRACT

The use of members composed of non-compact or slender elements with large width-thickness ratio in steel gable frames induces different seismic behavior of the end-plate connections compared with those in the ordinary multi-story frames owing to the local buckling. To study the seismic behavior of end-plate connection，five assemblage specimens with end-plate connections and structural members composed of non-compact elements were tested under cyclic loading. Different deformation modes were observed in the test. Serious local buckling of column happened when the connection was designed much stronger than the column，and relatively lower ductile behavior and energy dissipation capacity were available. It was found that local buckling of panel zone（PZ）under shear did not cause serious strength deterioration，and the PZ could develop considerable ductile deformation and relatively stable energy dissipating ability，which implies that the local buckling of PZ with large width-thickness ratio in single layered steel gabled frame could play effective role in seismic protection if proper design is made. The different seismic behaviors of these two local buckling modes at PZ and column respectively are evaluated by their corresponding failure mechanism. Finally the feasibility of utilizing local buckling of PZ for energy dissipating which is against the current design philosophy for ordinary multi-story frames is discussed.

INTRODUCTION

The end-plate connection is widely used in light-weight steel gabled frames to connect beam and column. A great deal of research has been conducted on the behavior of end-plate connection over the past several years（Tsai[1]；Ghobarah[2]；Guo[3]；Shi[4]）. Previous studies indicated there are several different failure modes for end-plate connection. The failure of bolt is not beneficial to the ductility of the connection （Tsai[1]）and hence it should be avoided. Another two failure modes，namely，the end-plate failure mode

and PZ failure mode are studied intensively. According to Adey[5]，relaxed bolt configuration dissipated more energy and showed good ductility，which implied the benefit of end-plate deformation to seismic behavior. On the other side，research results by Ghobarah[2] and Plumier[6] verified that the PZ was a very ductile element with high post yielding strength that could undergo a large number of strain reversals without signs of distress，and therefore the plastic deformation of PZ under shear provided a reliable energy dissipative mechanism.

The previous research relating to the end-plate connection focused on the behavior of ordinary multi-story steel frames composed of members mainly with compact elements，while usage of the non-compact or slender element in gabled frames is common，which will induce different behaviors to both of the members and connections. The beams and columns with large width-thickness ratio element will locally buckle early，and the buckling shall cause strength deterioration. In that case if the connection is designed too strong as that in special or intermediate moment frame（AISC[7]）there is no reliable component in the gabled frame to efficiently consume energy input by earthquake ground motion. The shear buckling which is prohibited in the ordinary steel frame，produces out-of-plane bending of panel，and this deformation mode actually dissipate part of energy. Though such an energy dissipation mode has been considered unstable compared with shear yielding mode，it has not been thoroughly studied. Moreover，previous research work performed for the end-plate connection used in gabled frames mostly focused on the initial stiffness and ultimate capacity. In order to evaluate the seismic behavior of the end-plate connection in gabled frames，specimens with end-plate connections connecting beam and column composed of non-compact elements were tested under cyclic loads. Special consideration was placed in the study for the inelastic deformation of PZ and end-plate.

TEST SPECIMENS

The experiment research program included five beam-to-column connection specimens. The specimens were categorized into two groups，type B1 and B2 as shown in Figure 1，where，the specimens are illustrated by a 90° rotation identical with the status in the test layout. The design details for these two types of specimens are shown in Table 1.

TABLE 1　GEOMETRICAL FEATURES OF SPECIMENS

Specimen ID	Beam section （mm）	Column section （mm）	EW/T[a] of column		Diagonal stiffener	End-plate thickness （mm）	Bolt
			web	flange			
B1-1	H534×120×4×8	H434×134×4×8	137	10.3	Yes	14	M16
B1-2	H534×120×4×8	H434×134×4×8	137	10.3	No	14	M16
B2-1	H600×134×6×8	H466×146×6×8	94	11.1	Yes	18	M20
B2-2	H600×134×6×8	H466×146×6×8	94	11.1	No	18	M20
B2-3	H600×134×6×8	H466×146×6×8	94	11.1	Yes	12	M20

Note：[a]EW/T stands for effective width-thickness ratio. It is defined as for web and $\dfrac{b}{2t_f\sqrt{\dfrac{f_{yf}}{235}}}$ for

flange，where h_w，t_w，b，t_f，f_{yw}，f_{yf} are the web height，web thickness，flange width，flange thickness，yield strength of web and yield strength of flange，respectively.
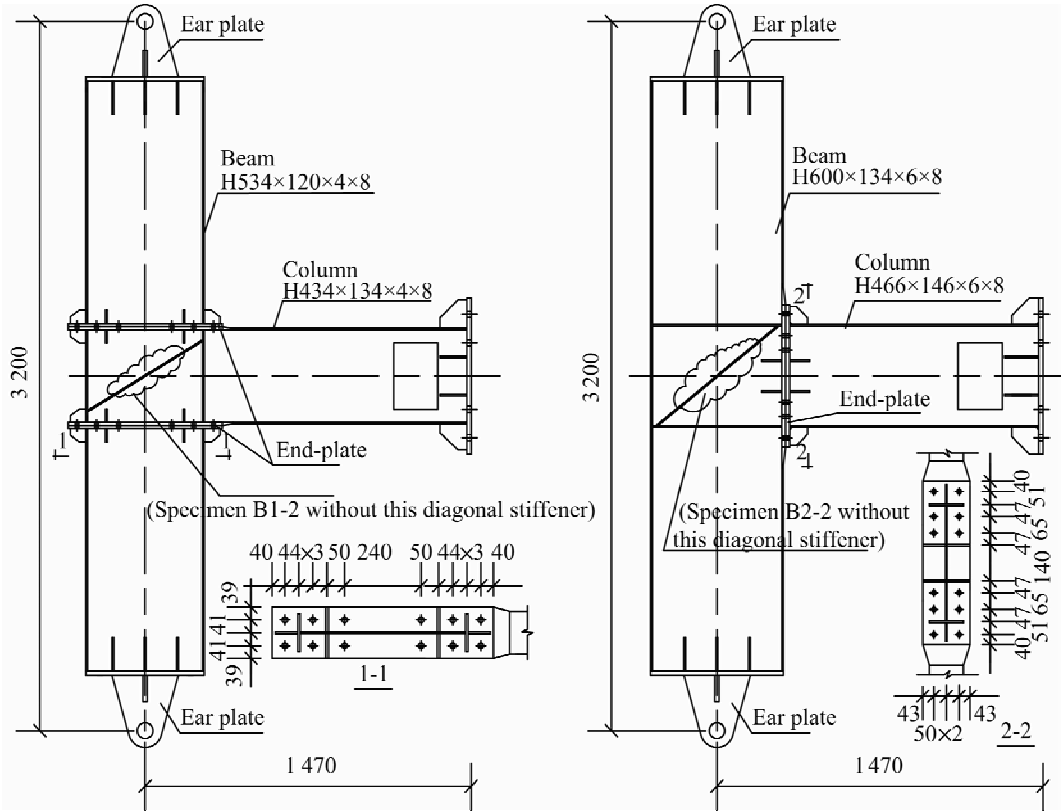
Figure 1   Specimens design

They yield strength f_y and tensile strength f_u of the steel plates were obtained from tensile tests on coupons，while those of bolts were from fabricator's certificate data，as shown in Table 2.

TABLE 2   MECHANICAL PROPERTIES OF MATERIALS

Plate thickness(mm)or bolt size	f_y (MPa)	f_u (MPa)
t4	403	545
t6	368	573
t8	379	545
t12	443	522
t14	447	527
t18	399	564
M16(bolt)	951	1 141
M20(bolt)	950	1 120

TEST PROGRAM

Setup and Loading System

The test setup was designed to accommodate specimens with column in a horizontal position for ease of loading，as shown in Figure 2. The specimen was connected to two steel bearings at two ends with two pins and the steel bearings were fixed to the reaction frame by high strength bolts. The lateral load was

applied to the cantilever end of column by a hydraulic actuator，at a distance of 1 900 mm from the beam centerline. The loading process followed a displacement control program with a step wise increasing deformation of 5 mm at the loading point for one cycle at each step. No axial load was applied to the column because only little axial force exists in actual column member in light-weight gabled frame. To prevent out of plane movement of the specimens，a lateral support system was provided near the column end.
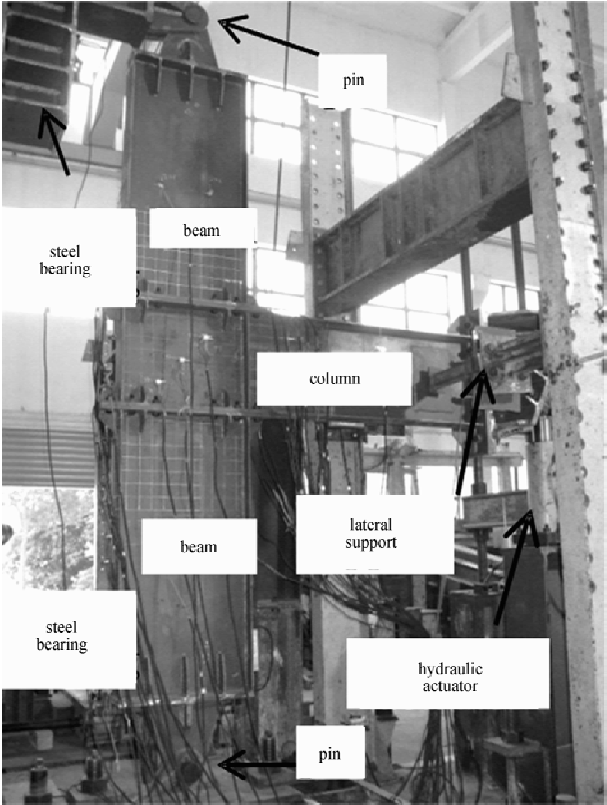
Figure 2　Test setup

Instrumentation

Figure 3 shows the arrangement of displacement sensors on the typical specimens B1-2 and B2-2，and there was only slight change in the other specimens. The displacement of loaded column tip was recorded by two linear variable differential transformers（LVDTs）D1 and D2. LVDTs D7 and D8，were installed diagonally over the PZ，to measure the average shear deformation. The other LVDTs were used to measure the rigid body rotation of the assembly of the specimen by D3-D6，and the gap opening of the end-plates by D9 to D12 in B1 and D9 to D10 in B2. The measured displacement is denoted as δ_{Di}，where the suffix i is corresponding to the LVDTs number. Strain gauges were placed on the column and beam flanges and webs to monitor the occurrence of the local buckling of the column and the internal forces in the beams.

In order to understand the general behavior of the specimen and therefore evaluate the energy dissipating ability of the connection，the concept of sub-assemblage is utilized；those parts of the specimen would develop non-linear deformation in testis used through this paper. The rotation of sub-assembly θ_s can
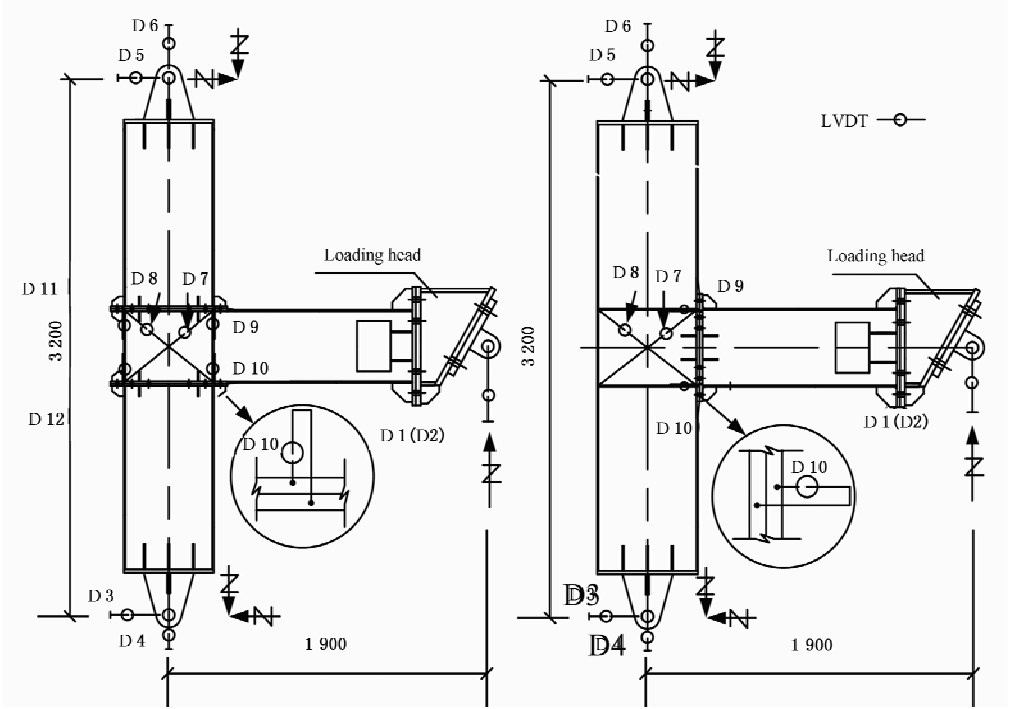
Figure 3   Displacement sensors

approximately be determined by Eqn. 1
Eqn. 1.

$$\theta_s = \Delta_p / L_{lp} \tag{1}$$

Where Δ_p is the column end displacement excluding the elastic deformation caused by column and beam; and L_{lp} is the distance from column end to end-plate.

Test Phenomena

Figure 4 shows three of specimens after failure. For specimen B1-1, column flanges yielded at the 20 mm cycle, and eventually resulted in local buckling of the column web and flange. The measured strain indicated that plastic deformation occurred in the PZ at 20 mm cycle and visible buckling deformation was detected at the same loading cycle. However, the diagonal stiffener prevented the further development of the local buckling in the PZ. Without the diagonal stiffener, the PZ of specimen B1-2 yielded completely
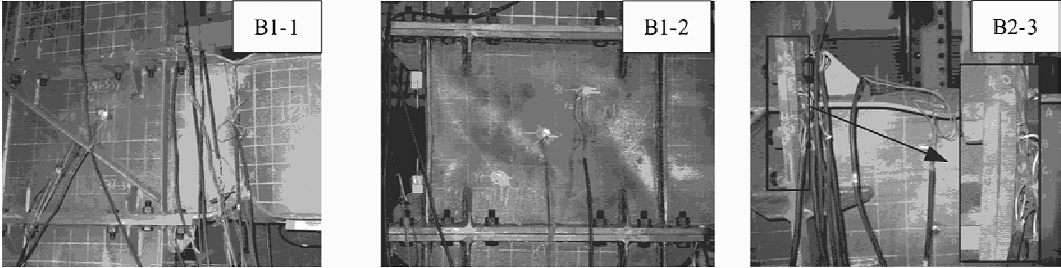
Figure 4   Specimens after failure

at the 15 mm cycle and resulted in visible buckling of the PZ at the same cycle. During the test the convex wave of buckling deformation of PZ changed its direction from one side to another periodically with the reverse of shear force，accompanying with loud sound. Further loading after the buckle of PZ resulted in the yielding of column at 20 mm cycle，and local buckling of both column flange and web at the 25 mm cycle. The test on B1-2 shows that the PZ was able to sustain high loading demands even after shear buckling happened. No evident deformation of the gap between end-plate and column flange was detected for type B1.

For specimen type B2，due to the relatively small width-thickness ratio，the PZ contributed almost nothing to inelastic deformation and energy dissipation. The end-plate connected to column end in type B2 subjected to relatively large bending moment compared with type B1. The maximum gap between the end-plate and the beam flange was about 2 mm for specimen B2-1 and B2-2，and 7 mm for specimen B2-3 because of the large plastic deformation of the thinner end-plate. At the final loading stage of the three specimens，the columns experienced severe local buckling on both flange and web. The difference between B2-1 and B2-2 was the diagonal stiffener in PZ. However，since the width-thickness ratio of the PZ was relatively small and the PZ did not buckle obviously in the test，there was no big difference for the behavior in the two specimens.

To summarize the test results，it is clear that the failure mode for all the tested specimens except B1-2 was dominated by local buckling of the column. For specimen B1-2，the failure mode was a combination of local buckling of column and PZ buckling. Neither failure of the bolt nor weld was observed for all the specimens during the tests.

Moment-rotation Curves

The hysteretic curves of moment vs. sub-assemblage rotation（M-θ_s）of all the specimens are shown in Figure 5，where the moment M is taken as the moment at the neighboring beam flange. The area under the curve for each specimen represents the energy dissipated by the sub-assemblage of the whole specimen，respectively. As marked in the Figure，panel zone buckling happened only in specimen B1-2 and all the specimens exhibited column buckling（both flange and web）behavior before reaching to the maximum capacity. Due to the buckling behavior of the column the strength deterioration occurred for all the specimens.
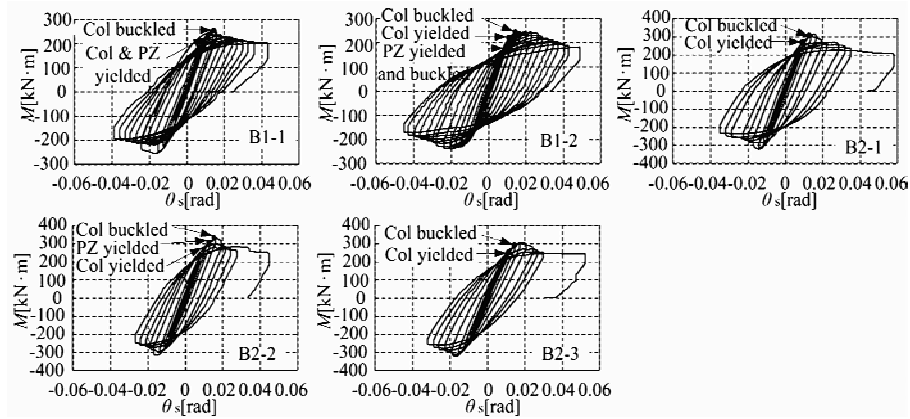

Figure 5   Moment-rotation relationship（Col：column）

Ductility and energy dissipation

The ductility of PZ and sub-assemblage can be quantified by the index, μ, defined as Eqn. 2 from the M-$\theta(\theta_s)$ relationship.

Eqn. 2.

$$\mu = \theta_m / \theta_y \tag{2}$$

where θ_m relates the ultimate rotation corresponding to the load decreasing to 85% of the maximum in each experiment, while θ_y is the yield rotation calculated from the yield capacity and the initial stiffness. The calculated ductility properties are shown in Table 3 and 4. It is found that the PZ of specimen B1-2 exhibited relatively large rotation capacity and ductility, even the PZ was subjected to serious buckling. For the specimens except B1-2, the ductility indices of sub-assemblage are similar. Specimen B1-2 had a higher sub-assemblage rotation capacity, ductility index than other specimens. It is believed that the inelastic behavior of the PZ ensures a more ductile behavior of this specimen.

TABLE 3   PZ DUCTILITY

Specimen ID	θ_y^+ (rad)	θ_y^- (rad)	θ_m^+ (rad)	θ_m^- (rad)	μ^+	μ^-
B1-2	0.002 8	0.002 9	0.017	0.014	6.26	4.72

TABLE 4   SUB-ASSEMBLAGE DUCTILITY AND CUMULATIVE ENERGY DISSIPATED

Specimen ID	θ_{sy}^+ (rad)	θ_{sy}^- (rad)	θ_{sm}^+ (rad)	θ_{sm}^- (rad)	μ^+	μ^-	Energy
B1-1	0.009	0.009	0.022	0.015	2.6	1.7	9.7
B1-2	0.008	0.008	0.032	0.030	4.1	3.9	44.4
B2-1	0.008	0.009	0.018	0.018	2.2	2.0	9.8
B2-2	0.009	0.008	0.020	0.016	2.3	1.9	16.0
B2-3	0.009	0.010	0.024	0.024	2.6	2.5	16.1

The cumulative energy dissipated by the sub-assemblage before the load decreased to 85% of the maximum was calculated and shown in last column of Table 4. It can be seen that the specimens B1-2 and B2-2 dissipated more energy than that by specimens B1-1 and B2-1, respectively. Specimen B2-3 also dissipated more energy compared with specimen B2-1. This shows that the plastic flexural deformation of the PZ after local buckling and inelastic behavior of the end-plate could improve the energy dissipation capacity of the specimen.

The amount of energy dissipated by PZ and column member in specimen B1-2 corresponding to each loading cycle is given in Figure 6. As shown in the Figure, most of the total energy was dissipated by PZ before the load reaching maximum. Strength deterioration occurred due to the buckling of the column. This proves that the PZ had a stable energy dissipating capacity before strength deterioration. And although the total energy dissipated increased after the column reaching its ultimate strength, the strength decreased seriously.

As aforementioned that the strong joint and week beam design with non-compact or slender elements is not beneficial to gabled frames because of the occurrence of beam or column buckling which introduces fast strength degradation. The tests results showed that the specimens with only the failure mode of local
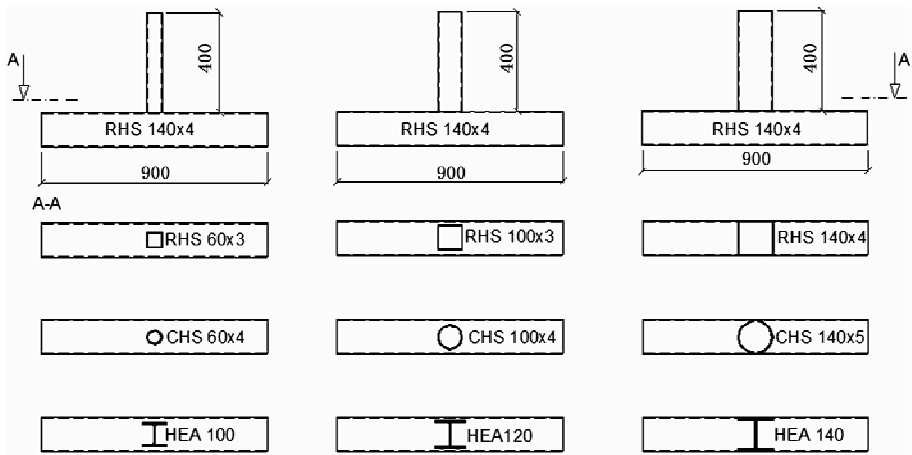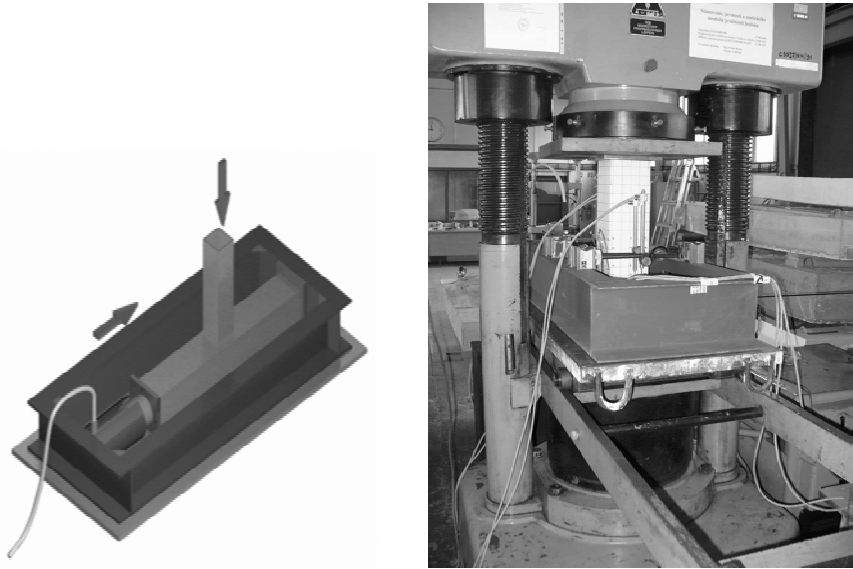
Figure 1   Geometry of test specimens

Figure 2   The loading test assembly

Measurement points on the individual specimens were then selected. Strain gauges were used to measure stress in the specimens and inductive sensors to determine horizontal and vertical deformations. During the strain-gauge measurements attention was focused on the chord member as，based on the calculation model，the joints under investigation collapsed due to the failure of the chord member in particular. Stresses were examined both in the horizontal and vertical walls of the chord and the strain gauges were attached in both longitudinal and transverse directions. Arrangement of strain gauges is shown in Figure 3a. As can be seen from the Figure 3b，deformation was measured mainly in the chord members，specifically in the upper horizontal and vertical walls of the chord member section.
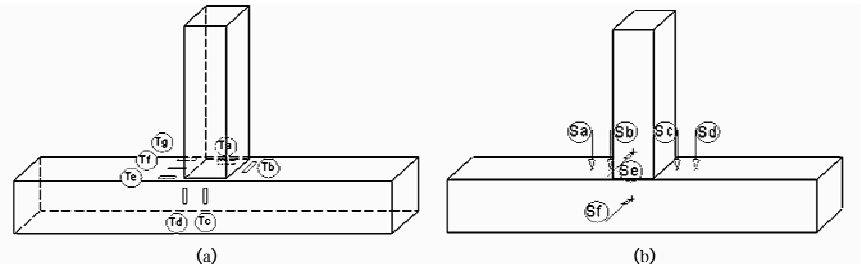
Figure 3   Arrangement of(a) strain gauges, (b) inductive sensors and deformeters

OBTAINED RESULTS

The types of joints selected were observed for both stress and deformation. In the following section of the article, attention will be directed to the deformation of the joints. The following sections provide a very sharp picture of the real behaviour of the individual types of joint. The Figures presented compare both vertical and horizontal experimentally measured deformations of the joints.

Comparison of Deformations in the Joints Consisting of the Identical Type of the Brace Member

The joints with the identical type of the brace member are compared. First, when there is linear deformation, the joint is in the elastic range. Later, as the load is increased, the joint deviate from this linear proportionality and the deformation goes through the elasto-plastic and eventually into its plastic range of action.
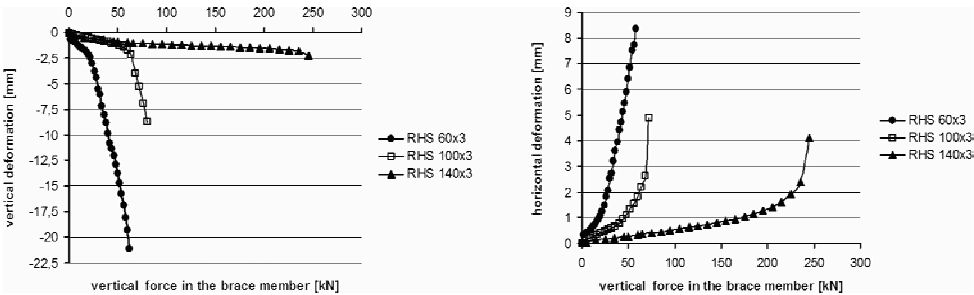
Figure 4   Comparison of the experimentally measured vertical and horizontal deformations in the joints composed of the brace members with rectangular hollow sections
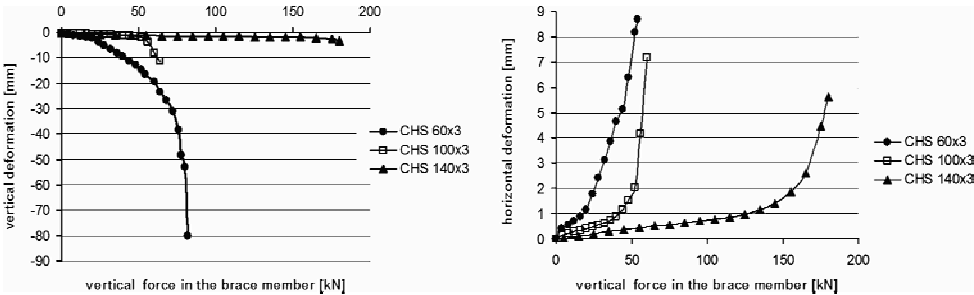
Figure 5   Comparison of the experimentally measured vertical and horizontal deformations in the joints composed of the brace members with circular hollow sections

Of all the types of brace members，the most resistant certainly seem to be those with $b_0 = b_1$ ($\beta = 1$). From the deformation point of view，the joints with a width of 60 mm are the least suitable. These exhibited excessive deformations even under minimal load.
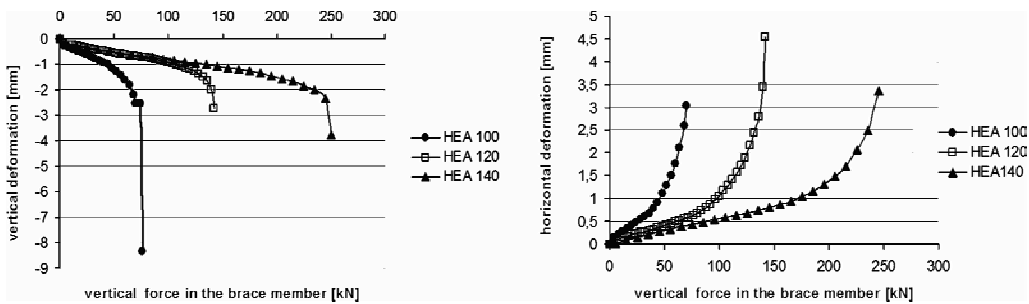
Figure 6   Comparison of the experimentally measured vertical and horizontal deformations in the joints composed of the brace members with open HEA-sections

Comparison of Deformations in the Joints with the Same Widths of Chord and Brace Members

The stiffness of the joint does not depend only on its dimensions but also on the type of the brace member used. The comparisons are presented in the form of the following Figures 7 to 10.

In the first type of joint ($\beta = 1$)，the stability of the chord web（wall）was crucial for the overall resistance of the joint. Figure 7 presents the distribution of values of vertical and horizontal deformation. Significant deformation of the vertical chord web（wall）occurred even under a relatively light vertical load. The joint collapsed completely with the gradual increase in load due to the buckling of the vertical web（wall）of the horizontal chord member. When the resistance of rectangular，circular and open sections was compared，the rectangular sections proved to be the stiffest.
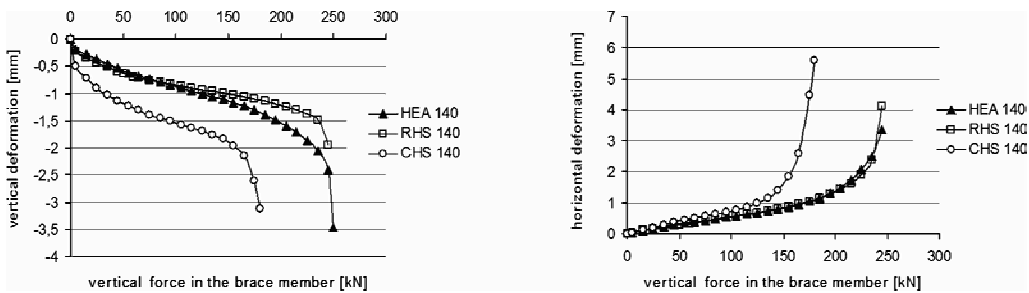
Figure 7   Vertical and horizontal deformation of the T-joint with $\beta=1.00$，depending on the type of brace member used

As can be seen from the Figure 8，the buckling effect of the chord web（wall）on the overall resistance of the joint can be observed also in the joints with $\beta = 0.714$. The overall resistance of the joint was influenced by the loss of stability of the vertical web（wall）although the difference between the vertical and horizontal deformation was less significant than in the first case. When comparing the types of brace member used，the rectangular section appeared to be the most resistant of all. However，the difference between the rectangular and open HEA-section was minimal regarding vertical and horizontal deformation.
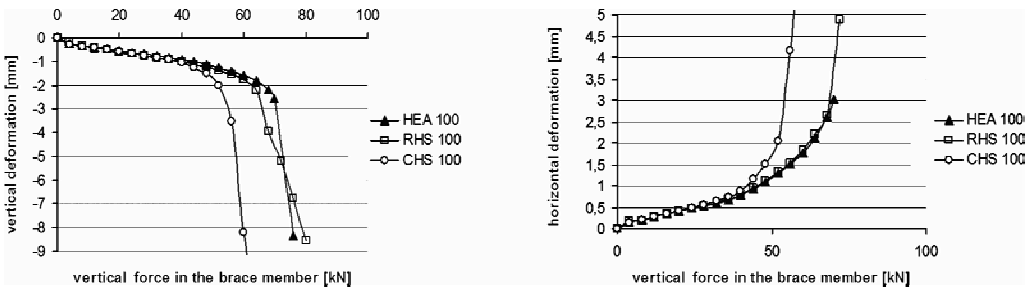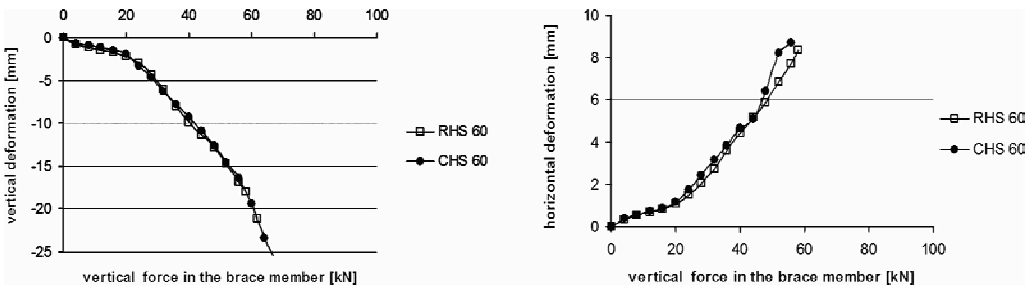
Figure 8   **Vertical and horizontal deformation of the T-joint with $\beta=0.714$ depending on the type of brace member used**

In the third type of joint（Figure 9）with the most slender brace members，the overall resistance of the joint was to a great extent affected by the stiffness of the horizontal chord web（wall）. The difference between the horizontal and vertical deformation in this type of joint is the biggest and the vertical deformation the greatest. The influence of the type of the brace member used on the overall resistance of such joints is virtually negligible. Due to the limited possibilities of the HEA rolling programme，only circular and rectangular hollow sections were compared. For $\beta = 0.714$ the behaviour of open sections was identical to that of rectangular sections and，obviously，it does not change for lower β-parameters.

Figure 9   **Vertical and horizontal deformation of the T-joint with $\beta=0.428$ depending on the type of brace member used**
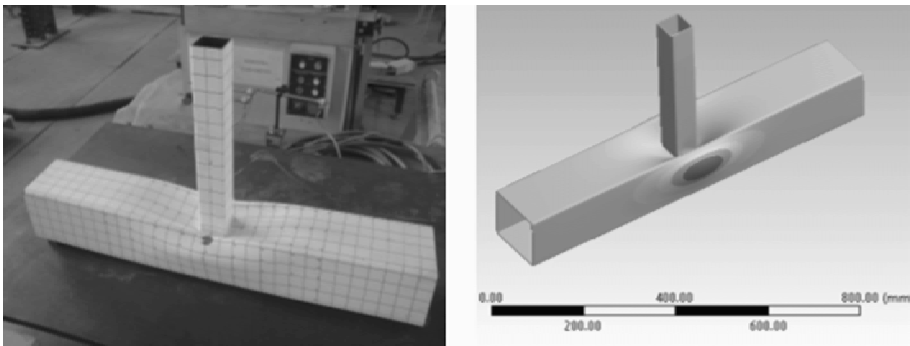
Figure 10   **Comparison of the actual deformation of the specimen and**
the deformation modelled using the finite element method

CONCLUSIONS

The scientific research results and evaluations presented characterize the correlations regarding the global

resistance of joints in lattice structures in the light of the latest scientific knowledge that should be responsibly taken into consideration in their reliable and cost-effective design. The article presented points to the significance and topicality of the issue of investigating the joints in lattice structures. The priority of the research was to acquire knowledge of the real behaviour of the joints and supplement it with more effective methods for the design of joints composed of rectangular and circular hollow sections，and open HEA-sections.

From the results obtained some patterns of behaviour of T-joints may be identified. With respect to the geometry and type of section，it can be concluded that the resistance of a joint with $\beta = 1.00$ is greatly influenced by the type of brace member. This influence sharply diminishes with the decreasing value of a β-parameter. With very low β-parameters，the influence of the type of brace member becomes virtually negligible and unimportant.

The conclusions presented in this article represent only part of a number of results obtained in the experiments. The authors would like to continue in the analysis of such joints，while the main emphasis should be placed on the verification of the obtained results using an appropriate finite model for the joints in question.

ACKNOWLEDGMENT

REFERENCES

［1］Kvočák，V. and Beke，P.，"Experimental analysis of "T"-joints created from various types of sections"，In Selected Scientific Papers：Journal of Civil Engineering，2008，3(2)，pp.51-60.

［2］Kvočák，V. and Beke，P.，"Experimental verification of welded hollow section joints"，In Zeszyty naukowe Politechniki Rzeszowskiej ：Budownictwo i inzynieria Srodowiska，2008，256(50)，pp.185-192.

［3］Beke，P.，"Analýza zváraných styčníkov z pravouhlých dutých prierezov［Analysis of welded joint composed of rectangular hollow section］"，Dissertation work. Košice，2009，135 p.

［4］Packer，J. A.，Wardenier，J.，Kurobabne，Y.，Dutta，D. and Yeomans. N. "Design Guide for Rectangular Hollow Section Joints under Predominantly Static Loading"，Verlag TUV Rheiland，1992.

［5］Beke，P. and Kvočák，V.，"Analysis of joints created from various types of sections"，In Eurosteel 2008：5th European Conference on Steel and Composite Structures：Proceeding：3rd to 5th September 2008 Graz，Austria. Brussels：ECCS European Convention for Constructional Steelwork，2008，pp.531-536.

［6］Freitas，A. M. S.，Mendes，F.C. and Freitas，M. S. R.，"Finite Elements Analyses of Welded T-Joints"，In Proceedings from 5th European Conference on Steel and Composite Structures，Eurosteel，2008，Graz，2008，pp.555-560.

［7］Kala，Z.，Karmazínová，M.，Melcher，J.，Puklický，L. and Omishore，A.，"Sensitivity analysis of steel-concrete structural members"，In Proceedings of the 9th International Conference on Steel-Concrete Composite and Hybrid Structures "ASCCS 2009" held in Leeds，Research Publishing Services，Singapore，2009，pp.305-310.

［8］Karmazínová，M.，Melcher，J. J. and Röder，"Load-carrying capacity of steel-concrete compression members composed of high-strength materials"，In Proceedings of the 9th International Conference on Steel-Concrete Composite and Hybrid Structures，Research Publishing Services，Singapore，2009，pp.239-244.

FRACTURE BEHAVIOR ANALYSES OF WELDED FLANGE-BOLTED WED CONNECTION OF STEEL STRUCTURE

* Y. P. Sun and Z. L. Teng

School of Civil Engineering Lanzhou University of Technology，Lanzhou，730050，China
* Email：tengzunli@126.com

KEYWORDS

Welded flange-bolded wed connection，fracture toughness，artificial crack，stress intensity factor.

ABSTRACT

Welded flange-bolded wed（WFBW）connections are a common form in steel structure，many times in high intensity seismic displayed the good seismic performance in previous years. However，in the 1994 Northridge earthquake and 1995 Kobe earthquake，brittle fracture still occurred in junction of beam flange and column in the（WFBW）connections，So this is very necessary to use fracture mechanics viewpoint to research fracture toughness of the weld root. In this paper ABAQUS is used to establish three dimensional finite element（3D）model of WFBW，fracture behavior of "artificial crack" of the weld root is analyzed，the stress intensity factor（K_I）as a fracture mechanics parameters to calculate fracture behavior in the beam flange weld root. Results show that stress intensity factor varies cross the beam flange width，and is largest in the middle of the flange. When selecting the same initial flaw length，the stress intensity factors of bottom flange weld root was significantly higher than in the top flange weld root. The K_I increases nearly linear with the increase of the initial flaw length. Comparison of 2D and 3D models，when the same initial flaw length，calculation of K_I/σ_n by the three-dimensional model approximately as 1.5 times as that by two-dimensional model.

INTRODUTION

Although 2011 Japan Earthquake proved that seismic performance of steel buildings better than other systems，at the beam-column joints brittle fracture were still discovered. Fracture toughness properties of the welded joint are obtained Wang Yuanqing[1] with the two-dimensional finite element method. Zhang Li[2] studied loading rate and pre-strain effect on the structure mechanics performance and the fracture toughness. Liu Hongbo[3-4] proved that the beam flange width has primary effect on the ratio of equivalent stress intensity factor to average. Yao Guochun[5] calculated the stress distribution of beam-column joints and the stress intensity factor around the crack tip when different concentrate loads are applied at the beam end. Sun Yuping[6] analyzed beam-column section and Young's modulus influence on the maximum energy release rate（Ge）around the crack tip.

In this paper ABAQUS is used to establish three dimensional finite element model of （WFBW） connection. When selecting different initial flaw length （a），Calculation of the stress intensity factor around the crack tip of the weld root，which influenced by initial flaw length and varies across the beam flange width are studied. In the same time the stress intensity factor in the beam bottom flange and in the beam top flange are compared.

DETERMINATION OF STRESS INTENSITY FACTOR

Stress intensity factor K is a parameter to describe the stress field around the crack tip intensity level. As shown in Figure 1，the origin of coordinates is crack tip，in the very near crack tip stress expression：
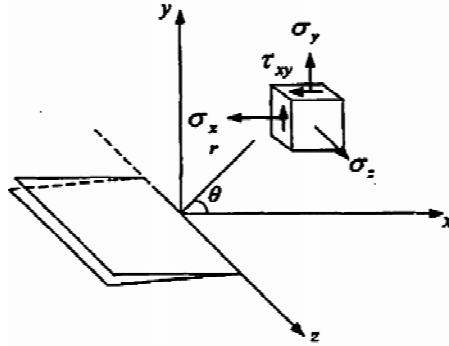
Figure 1   coordinate system and stress components at Crack tip

$$\sigma_x = \frac{K_I}{\sqrt{2\pi r}}\cos\frac{\theta}{2}\left(1 - \sin\frac{\theta}{2} \cdot \sin\frac{3\theta}{2}\right)$$

$$\sigma_y = \frac{K_I}{\sqrt{2\pi r}}\cos\frac{\theta}{2}\left(1 + \sin\frac{\theta}{2} \cdot \sin\frac{3\theta}{2}\right)$$

$$\tau_{xy} = \frac{K_I}{\sqrt{2\pi r}}\sin\frac{\theta}{2} \cdot \cos\frac{\theta}{2} \cdot \cos\frac{3\theta}{2}$$

$$\mu = \frac{K_I}{8G}\sqrt{\frac{2r}{\pi}}\left[(2\chi - 1)\cos\frac{\theta}{2} - \cos\frac{3\theta}{2}\right] \quad \upsilon = \frac{K_I}{8G}\sqrt{\frac{2r}{\pi}}\left[(2\chi + 1)\sin\frac{\theta}{2} - \sin\frac{3\theta}{2}\right]$$

Where G is shear modulus，υ is Poisson's ratio，in the crack extension line （the Direction of υ，$\theta = 0$） :

$$\sigma_x = \sigma_y = \frac{K_I}{\sqrt{2\pi\gamma}} \quad \tau_{xy} = 0 \Rightarrow K_I = \sigma\sqrt{2\pi\gamma}$$

Stress intensity factor $K_I = Y\sigma\sqrt{\pi a}$，where Irepresents tear-type crack，Y is the shape factor.

The Numerical Simulation of WFBW with Initial Flaw

The WFBW connections in this paper recommended by "Code for seismic design of buildings （GB 50011—2010）"，welded bean section is H400×150×8×12 mm and welded column section is H450×250×12×16 mm. The elastic modulus and Poisson's ratio are assumed as $E = 2.06×10^5$ MPa，$\upsilon = 0.3$ both for Q235 base metal and E4303 weld metal. The web was connected through a bolted shear tab with supplementary welding，and the flanges were joined using field groove welds. The mechanical properties of base metal

EXPERIMENTAL STUDY ON BENDING CAPACITY OF MULTIPLANAR RHS-TO-CHS TT-JOINTS IN SPACE TRUSSES

* L. W. Tong[1]，Y. Y. Hu[1]，Y. Y. Chen[1]，Z. M. Yin[2]

[1] Department of Building Engineering，Tongji University，Shanghai，200092，China
[2] Shanghai Huajian Institute of Architectural Design and Research，China
* Email：tonglw@tongji.edu.cn

KEYWORDS

Welded TT-joints，hollow sections，experiment，bending capacity，failure mode.

ABSTRACT

The space tubular trusses made of rectangular or square hollow section（RHS or SHS）braces and circular hollow section（CHS）chords are new application in civil engineering. There is no idea and design guideline for the bending capacity of the multiplanar tubular joint. The behavior of multiplanar welded TT-joins with two RHS braces and a CHS chord under bending moments on the braces in the plane and out of plane was investigated experimentally in the paper. The detained experimental setup is presented. Three test specimens with different geometric parameters were organized. Special self-balanced equipment was design in order to apply bending moment to the braces of the TT-joints. During the tests，a lot of strain gauges were installed at both the CHS chord and the RHS brace close to the circumference of the weld connecting the brace to the chord. The failure modes and ultimate bending capacity of these joints were observed and analyzed.

It is concluded from the current experiments that the joints underwent CHS chord plastification，RHS brace local buckling and RHS weld failure under in-plane bending，whereas CHS chord plastification under out-of-plane bending. The in-plane bending capacity of the joints was within a range of the elastic bending moment and plastic moment of the RHS brace，but the out-of-plane bending capacity of the joints was less than the elastic bending moment of the RHS brace. So the in-plane bending capacity was higher than the out-of plane bending capacity.

INTRODUCTION

With many advantages of steel hollow sections such as symmetric cross-section，high bending and torsional capacity，low wind and wave resistance and low maintenance cost，tubular truss structures are widely used in modern architectural and civil engineering along the world[1, 2]. The investigation on behaviour of welded truss joints made of circular，or rectangular or square hollow section members（CHS，or RHS or

SHS) under static and fatigue loading has been performed well in the world during the past thirty years and then the relevant research results have been introduced into some design specifications[3~7]. However, these researches generally focused on the joints subjected to axial loading, or on the joints with the same shape of hollow section for brace and chord members or on the joints with CHS brace and RHS chord.

The tubular trusses made of RHS braces and CHS chords are new application being seldom used in structural engineering. There is no idea and design guideline for the kind of welded RHS-to-CHS joints. Hu and Tong, *et al* investigated the bending rigidity of multiplanar RHS-to-CHS TT-joints used in Vierendeel Trusses (see Figure 1)[8]. The current paper discusses the bending capacity of this kind of joints based on experimental study under bending moments on the braces in the plane and out of plane respectively.
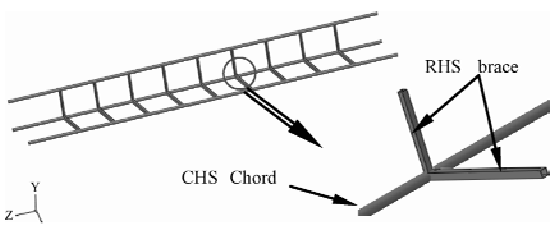
Figure 1   Vierendeel Truss and RHS-to-CHS TT-Joint

EXPERIMENTAL SETUP

Experimental Specimens

Full size tests were conducted on three typical TT-joints A, B and C, which were made from Q345 steel. Table 1 gives their sizes and non-dimensional geometric parameters of the specimens. Three specimens have the same chord dimension and angle between two braces out of plan. The dimensions of two braces are the same for the specimens B and C, but different for the specimen A. The constructional details of specimens are shown in Figure 2. Table 2 gives the strength of steel used for these specimens.

TABLE 1   DIMENSION OF TT-JOINT SPECIMENS AND BENDING CASE

Specimen	Chord (mm)		Brace (mm)	β_{IP}	β_{OP}	γ	τ	Overlap	Bending case
A	Φ203×8	b1	□ 120×6	0.591		12.688	0.750	Yes	In-plane
		b2	□ 180×150×8	0.887	0.739				In-plane
B	Φ203×8	b1	□ 120×6	0.591				No	Out-of-plane
		b2	□ 120×6						Out-of-plane
C	Φ203×8	b1	□ 150× 6	0.739				Yes	In-plane
		b2	□ 150× 6						In-plane

Note: β_{IP} = RHS brace height h / CHS chord diameter D, β_{OP} = RHS brace width b / CHS chord diameter D
γ = CHS chord diameter D / (2 * thickness T), τ = RHS brace thickness t / CHS chord thickness T

TABLE 2   STEEL STRENGTH OF SPECIMENS

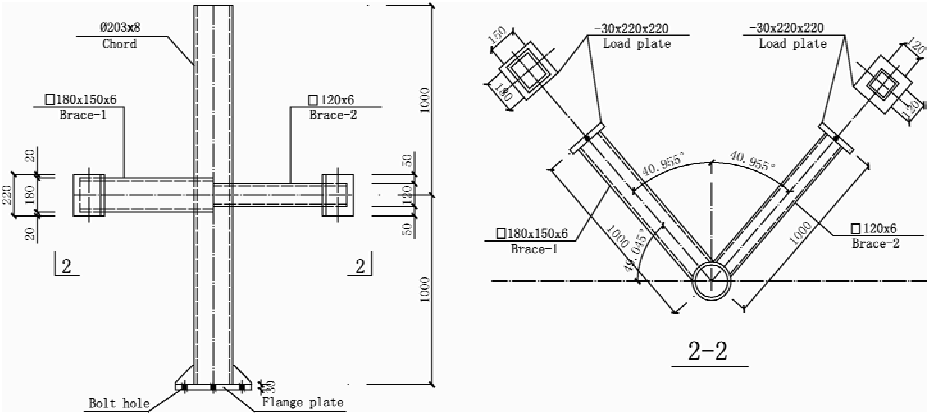| Dimension(mm)	Yield strength，f_y(N/mm^2)	Ultimate strength，f_u(N/mm^2)
Φ203×8	359	547
☐ 180×150×8	368	644
☐ 120×6	369	581
☐ 150× 6	429	638

Figure 2   Details of specimens

Loading Framework

A special self-balancing loading framework which had sufficient strength and rigidity（see Figure 3）was designed in order to apply lateral loads in different directions to the ends of braces，and then produce in-plane and out-of-plane bending moments respectively. Specimens were connected to the framework by high-strength bolts. During the tests，a lot of strain gauges were installed at both the CHS chord and the RHS brace close to the circumference of the weld connecting the brace to the chord.
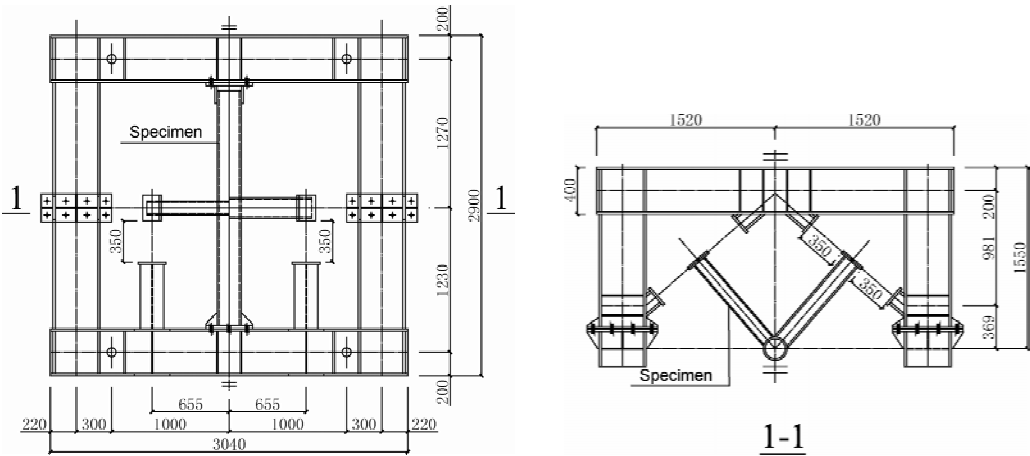
（a）In-plane bending   （b）Out-of-plane bending

Figure 3   Self-balancing loading framework

Bending Cases

Table 1 presents the bending moments applied to each specimen. The so-called in-plane and out-of-plane are defined as follow: *In-plane* is the plane where a bending moment produced by a concentrated force is in the plane formed between the axes of a chord and a brace as shown in Figure 3a. Out-of-plane is the plane perpendicular to the in-plane as shown in Figure 3b.

EXPERIMENTAL RESULTS AND DISCUSSION

Bending Capacity

Figure 4～Figure 6 illustrates M-Δ curve of Specimen A, B and C. In the Figures, Bending Moment, M, equals to the lateral shear force V (applied on the end of braces vertically) multiplied by brace length (the distance from brace end to the centerline of chord), where Δ means the lateral displacement of brace end.

For the comparison between two kinds of bending capacity in the brace, the definition of an edge-fiber yield bending moment (M_e) and a full-cross-section plastic bending moment (M_p) is given as follows:

$$M_e = f_y \cdot W_e \tag{1}$$

$$M_p = f_y \cdot W_p \tag{2}$$

Where: W_e— elastic modulus of section, W_p— plastic modulus of section, f_y— yield strength, see steel strength in Table 2.

Bending capacities of three experimental joints, M_e and M_p of all braces are shown in Table 3. Figure 4 illustrated M-Δ curve of Specimen A under in-plane loading. As the two braces had different dimensions, the section elastic modulus ratio is: $W_{b1} : W_{b2} \approx 2 : 5$. In order to make the two braces achieve ultimate bending capacity at the same time, loading jack with ranges of 200 kN and 500 kN were loaded synchronously on the two braces with loading ration of 2 : 5. It was found that the in-plane bending capacities $M_{A, IP}$ of specimen A was larger than corresponding M_e and smaller than corresponding M_p. The M-Δ curve began to develop plastically before the load reached M_e.

For specimen B, the two braces had the same dimensions, So synchronous out-of-plane loading with ratio 1 : 1 was applied on the braces. As shown in Figure 5, the ultimate out-of-plane bending capacity $M_{B, OP}$ of specimen B was smaller than not only M_p but also M_e. In addition, specimen A and B had brace with dimension □120×6. It was obvious that the in-plane bending capacity $M_{B, IP}$ (48.8 kN • m) was larger than out-of-plane $M_{B, OP}$ (24.8 kN • m).

As shown in Figure 6, specimen C had two same braces and the in-plane bending capacity M_{CIP} was larger than M_e but less than M_p.
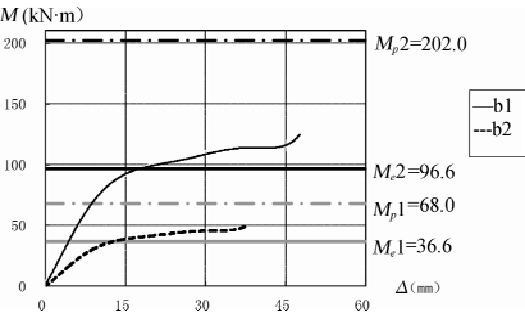
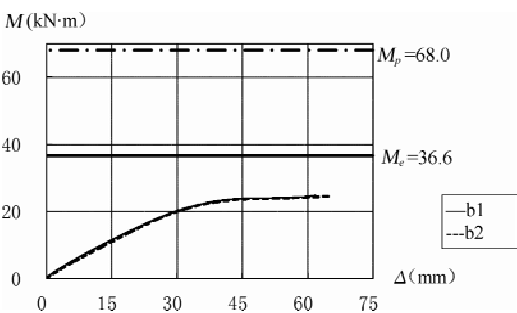**Figure 4　*M-Δ* curve of specimen**

A under in-plane loading

Figure 5　*M-Δ* curve of specimen B
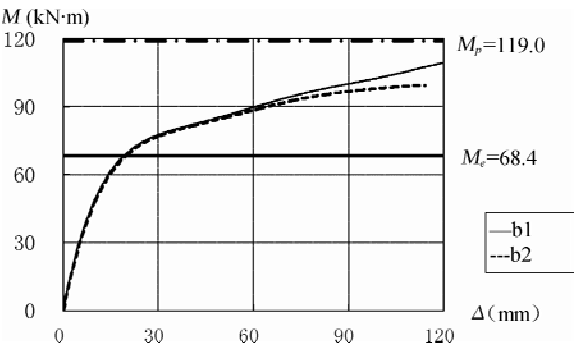
of out-of-plane loading

Figure 6　*M-Δ* curve of specimen C of in-plane loading

TABLE 3　BENDING CAPACITY OF SPECIMENS（KN・M）

Specimen	Dimension(mm)	M_e	M_p	Loading case	Ultimate bending capacity
A	□120×6	36.6	68.0	In-plane	48.8
	□180×150×8	96.6	202.2	In-plane	122.0
B	□120×6	36.6	68.0	Out-of-plane	24.8
C	□150×6	68.4	119.0	In-plane	99.3

Failure Modes

With various load and geometric parameters，hollow section joints may have different possible failure modes[2]：（1）Brace Yielding（BY），（2）Brace Local Buckling（BLB），（3）Chord Plastification（CP），（4）Chord Punching Shear（CPS），（5）Chord Shear（CS），（6）Chord Local Buckling（CLB），（8）Weld Filure（WF）.

Figure 7 ～ Figure 9 showed the failure modes of the three specimens when they lost their loading capacities. As is shown in Figure 7，the chord of specimen A changed its shape from a circle into an ellipse，which meant chord plastication（CP）failure happened. Besides，significant concave and convex deformation occurred on the compressive side wall of brace near the joint，which means local buckling failure occurred in the brace wall. Therefore，the specimen A had the failure mode combined with chord

plastification and brace local buckling（CP ＋ BLB）.

(a) Chord plastification　　　　　　　　　(b) Brace local buckling

Figure 7　Failure mode of specimen A

As is shown in Figure 8，the chord of specimen B changed its shape from a circle into an ellipse like specimen A，which means chord plastification（CP）failure happened.

As for specimen C，during in-plane loading a crack took place at the weld toe of the tension side of brace b2（see Figure 9a）when the bending moment of the end of two braces achieved 99. 4 kN · m. Then，the jack applied on the brace b2 stopped loading and the jack on the brace b1 continued loading. When the load on the brace 1 reached M1 = 110. 4 kNm，another crack occurred at the weld toe of the tension side of brace b1 which caused the experiment ended. It is found that the shape of the chord changed from a circle into an ellipse，which means chord plastification happened（see Figure 9b）. At same time，local buckling failure occurred at the tension side of the brace wall. So the specimen C had the failure mode combined with weld failure，chord plastification and brace local buckling（WF＋CP＋BLB）.

Chord became ellipse
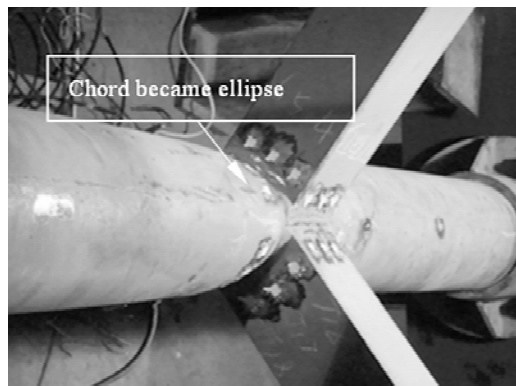
Figure 8　Failure mode of specimen B
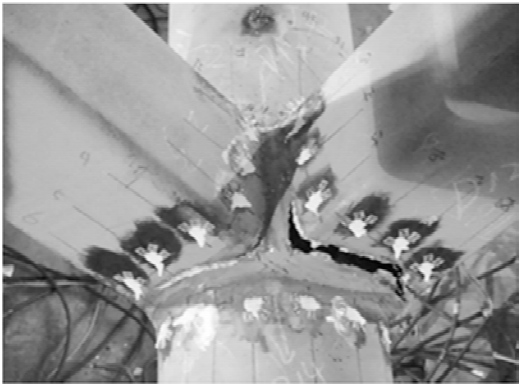
（a）Weld toe cracking

（b）Chord plastification

（c）Brace local buckling

Figure 9　Failure mode of specimen C

CONCLUSIONS

Based on the bending capacity tests of multiplanar welded RHS-to-CHS TT-joints subjected to loading in the brace，the following conclusions were drawn：

（1）Three kinds of failure modes were found in the TT-joints，namely chord plastification，brace local buckling and brace weld failure. The joints under in-plane bending in the brace had a combined failure mode of chord plastification，brace local buckling and weld failure，whereas under out-of-plane bending on the brace had a failure mode of chord plastification.

（2）The in-plane bending capacity of TT-joints，M_{IP}，was larger than the edge-fiber yield bending moment M_e in the brace but less than the full-cross-section plastic bending moment M_p in the brace，whereas the out-of-plane bending capacity，M_{OP}，was smaller than not only M_p but also M_e.

（3）The out-of-plane bending capacity of TT-joints M_{OP} was smaller than the in-plane bending capacity M_{IP}.

REFERENCES

［1］Chen，Y. Y. and Chen，Y. J.，"Research Developments in Unstiffened Steel Tubular Joints"，Journal of Building Structure，2002，7(32). (in Chinese)

［2］Wardenier，J.，"Hollow Sections in Structural Applications"，CIDECT，2000.

［3］Kurobane，Y.，Makino，Y. and Ochi，K.，"Ultimate Resistance of Unstiffened Tubular Joints"，Journal of the Structural Engineering，1984，110(2)，pp. 385-400.

［4］Vegte，G. J.，Koning，C. H. M. and Puthli，R. S.，"The Static Strength and Stiffness of Multiplanar Tubular Steel X-Joints"，International Journal of Offshore and Polar Engineering，1991，1(1).

［5］Wardenier，J.，Kurobane，Y.，Packer，J. A.，van Vegte，G. J. and Zhao，X. L.，"Design Guide for Circular Hollow Section Joints under Predominantly Static Loading，Second Edition"，CIDECT，2010.

［6］Packer，J. A.，Wardenier，J.，Zhao，X. L.，van Vegte，G. J. and Kurobane，Y.，"Design Guide for Rectangular Hollow Section Joints under Predominantly Static Loading，Second Edition"，CIDECT，2010.

［7］Zhao，X. L.，Herion，S.，Packer，J. A.，Puthli，R.，Sedlacek，G.，Wardenier，J.，Weynand，K.，Wingerde，A. and Yeomans，N. 2000，"Design Guide for Circular and Rectangular Hollow Section Joints under Fatigue Loading"，Verlag TUV Rheinland，Koln，Germany.

［8］Hu，Y. Y.，Tong，L. W.，etc. "Study on Bending Rigidity of Welded TT-joints between RHS Brace and CHS Chord"，Symposium on International Association for Shell and Spatial Structures，Shanghai，2010.

CONSTITUTIVE RELATION OF END PLATE CONNECTIONS BASED ON CORRELATION AND SENSITIVITY

J. R. Pan[1]，* Z. Wang[1]，L. Q. Zheng[1]，C. Gong[2]

[1] State Key Laboratory of Subtropical Building Science，South China University of Technology，Wushan Road 381，Guangzhou，510640，China

[2] Shenzhen Watson Architecture and Engineering Design Consultants Ltd.，Nanshan District，Shenzhen，518054，China

* Email：wangzhan@scut.edu.cn

KEYWORDS

End plate connection，semi-rigid，constitutive relation，correlation，sensitivity.

ABSTRACT

Studies agree that semi-rigid behavior of joint should be considered in frame analysis and design. Replacing the traditional methods，the structural sensitivity analysis of constitutive relation was carried on based on the correlations and probabilities of design variables for extended end plate connections with stiffeners. 4 specimens of beam to column with various configurations were tested under monotonic loads. The loading capacity and the rotation deformation have been measured. The initial rotation rigidity，the maximum bending moment，the ultimate load and so on essential characteristic parameters have been obtained. With a new way，an elastic moment-rotation model was put forward within considering the correlations of geometrical parameters. From the mathematical expression can be seen that parameters how sensitive to the relative rotation，positive or negative correlation with the relative rotation，and the parameters and their power exponents have obvious physical meaning. Proposed analysis method on constitutive relation of the semi-rigid end-plate connection based on correlation analysis and probability sensitivity analysis was suitable for steel frames and concrete-filled steel tubular frames in the structural analysis and design.

INTRODUCTION

In the traditional analysis of semi-rigid steel frame joints，whether routine test analysis，finite element analysis，or analytic calculation，were based on the assumption that the design variables of joint are determined completely. Single design variable's change was considered separately to effect on the joints' response，while the effects of relationship between all variables were ignored. Many researchers put forward some moment-rotation models of different connections. Most of the models are obtained by curve-fitting and statistically regressed with the test data，and many human factors are contained. In

certain conditions，the moment-rotation curves are fitting to the experimental data，but the defined model parameters have little physical meaning or are inconvenient for engineering design by reason of the complexity of the parameters definition，even some error would appear for some formulas in the calculation，such as the negative stiffness，which is impossible in the actual project. Therefore，it is very necessary to replacing the traditional methods of analysis，consider the relationship in design variables and put forward a new research method of constitutive relation for the steel frame joints.

THE DESIGN AND MANUFACTURE OF SPECIMENS

The specimen of end plate connections with stiffeners was taken from a typical element between the points of contra flexure of beam to column of conventional multi-storey steel frame structures under lateral loads. There were four specimens，numbered D1，D2，D3，and D4. The friction-type high-strength bolts，hardness of 10.9，were M20，M22 and M24. In addition to high-strength bolts，the other components were manufactured with the steel Q235. The main parameters and dimensions of the specimens are shown in Table 1. The end plate stiffener was a triangle，and the two right-angle sides were 100mm in length. The anti-slip friction coefficient of the contact surface between end plate and column flange was 0.44. The torque method was adopted to fasten the high-strength bolts in reference[1]. The pretension forces of the high-strength bolts M20，M22 and M24 were 170kN，210kN，250kN respectively.

TABLE 1　THE MAIN PARAMETERS OF THE SPECIMENS（mm）

N	Column section	Beam section	End plate thickness	Bolt diameter	Pitch of bolts	End plate stiffener thickness
D1	$250 \times 175 \times 7 \times 21$	$200 \times 150 \times 6 \times 9$	22	22	60	6
D2	$300 \times 200 \times 8 \times 12$	$250 \times 175 \times 7 \times 11$	16	20	45	8
D3	$350 \times 250 \times 9 \times 14$	$300 \times 200 \times 8 \times 12$	20	24	55	9
D4	$400 \times 300 \times 10 \times 16$	$400 \times 200 \times 8 \times 13$	18	24	50	10

Note：the pitch of bolts is the distance of the first row of bolts to the up flange of the beam.

EXPERIMENT AND FINITE ELEMENT ANALYSIS

Characteristics for the Structural Steels

The average characteristics for the structural steels of the end plate connections with stiffness is set out in Table 2. In this table the values for the Young modulus，E，the static yield and tensile stresses，f_y and f_u，the strain at yield point，ε_y are given.

TABLE 2　CHARACTERRISTIC VALUES FOR THE STRUCTURAL STEELS

Components	Thickness of section(mm)	f_y(MPa)	ε_y (10^{-6})	E（MPa）	f_u(MPa)
Beam and column	6	328	1 654	198 320	383
	8	325	1 613	201 435	380
	10	323	1 595	202 489	376
	12	320	1 574	203 321	373
	16	316	1 534	205 984	370

continued

Components	Thickness of section(mm)	f_y (MPa)	ε_y (10^{-6})	E (MPa)	f_u (MPa)
	18	312	1 512	206 350	368
Beam and column	20	308	1 482	207 890	365
	22	306	1 469	208 349	363
Bolt	—	995	4 830	200 000	1 160

Loading Devices

The loading devices are shown in Figure 1. The jack was used to load concentrated monotonic loading of the beam free end. The upper and lower ends of the column were fixed. The column was loaded by the certain axial load.
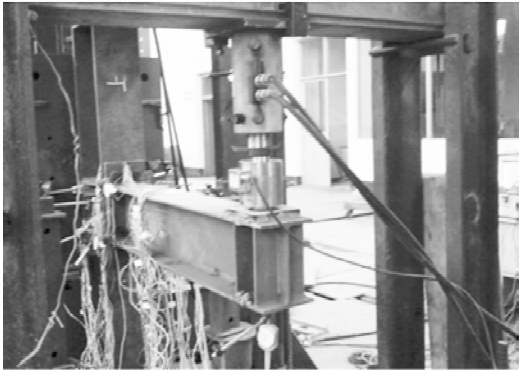
| Figure 1   Loading devices | Figure 2   Finite element model |
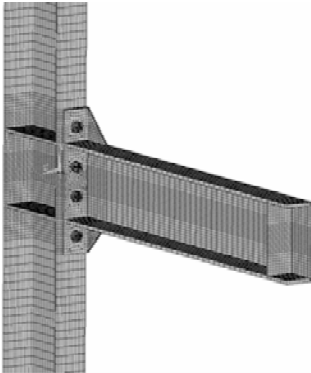
Finite Element Analysis

A 1/2 three-dimension finite element model of the extended end plate connections with stiffeners had been used in the study, shown in Figure 2. The structure was modeled by solid element SOLID 95 (3‑D 20‑node structural solid in ANSYS software). Contact pair (TARGE170 and CONTA174) was used to simulate the contact between the extended end plate and the column flange. The pretension force of bolts was applied by PRETS179.

Comparisons between Experiment and Finite Element Analysis

The failure behavior of extended end plate connections with stiffeners is shown in Figure 3. The deformation of finite element model (left chart) is similar to the experimental result (right chart). From Figure 3 can be seen that, the end plate was pulled away from the column flange, the column flange and high-strength bolts had bending deformations, and at a results the joint was failed with T-shaped failure mode.

The strain，stress，yield load，ultimate load，the initial rotational stiffness and the total deformation obtained from finite element analysis had been compared with the experimental results. The measured
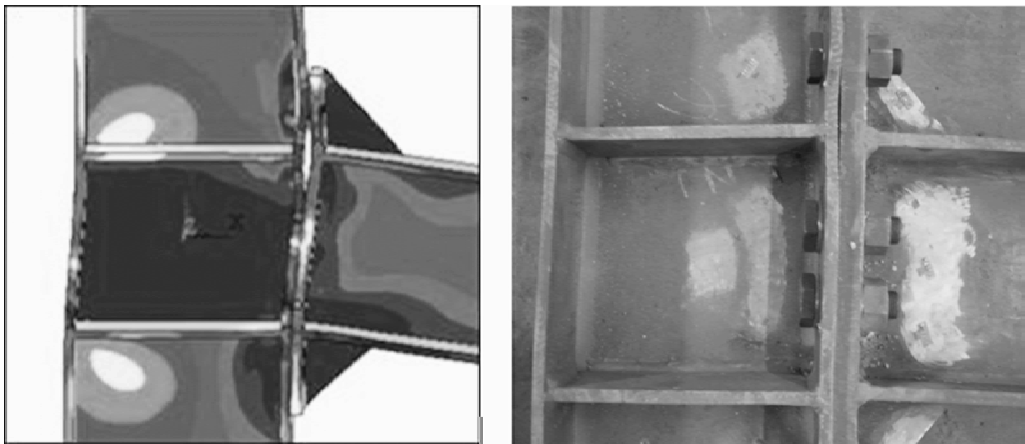
Figure 3　Comparison between FEM（left）and experiment（right）

results for 4 specimens are shown in Table 3. From the Table 3 can be seen that，the differences of initial rotational stiffness are 3%～5% between finite element simulation and experiment，the maximum error of yield load is 5%，and the error value of ultimate load range from 4% to 6%. Close agreement between the finite element and experimental results can be observed. Therefore，the finite element model of extend end plate connections with stiffeners was valid and accurate，although there are still some differences between experimental results and the finite element analysis.

TABLE 3　CAPACITY RESULTS

Number	Analysis	Yield load（kN）	Ultimate load（kN）	The initial rotational stiffness（kN·m·rad^{-1}）
	Exp	60	100	22 459.4
D1	FEM	58	94	23 305.7
	FEM/Exp	0.96	0.94	1.04
	Exp	108	162	29 615.8
D2	FEM	104	156	30 665.1
	FEM/Exp	0.96	0.96	1.03
	Exp	165	235	52 332.9
D3	FEM	158	220	55 108.3
	FEM/Exp	0.95	0.94	1.05
	Exp	332	440	81 000.1
D4	FEM	300	400	83 510.2
	FEM/Exp	0.96	0.95	1.03

PROBABILISTIC SENSITIVITY ANALYSIS

According to the reference[2]，the correlation coefficient is 0.845 between the thickness of H-shaped beam flange，T，and web thickness，TW. Considering the coefficient，using ANSYS PDS finite element probabilistic design method，the probabilistic sensitivity analysis for the extended end plate connections with stiffeners was taken out by adopting Monte Carlo simulation techniques.

The sensitivities of input parameters（geometrical parameters）to maximum displacement of beam free

end（YD1）are shown in Figure 4. From Figure 4 we can see，the distance between the outer rows of bolts to the beam horizontal axis（HBOTTOM_BOLT）is the most sensitive to the YD1. The second is the height of the beam section（B_H），and the third is the end plate thickness（DB_T）. The load applied to the beam free end（F_BEAM）and the column flange thickness（C_T_2）have a little effect on YD1. Other input parameters can be regarded as non-sensitive to YD1. In addition to above analysis，we can also see that a positive correlation between HBOTTOM_BOLT and YD1，a negative correlation between B_H and DB_T. It can be determined that the closer from the outer rows of bolts to the top flange，the displacement（YD1）will be smaller，and the stiffness of the beam to column joint will be greater.

The sensitivities of input parameters to the relative rotation of beam to column（ROTA）are shown in Figure 5. From Figure 5 can be seen that，HBOTTOM_BOLT，DB_T，C_T_2，and F_BEAM have the greater sensitive to ROTA. Otherwise the thickness of column web（C_T_1），the height of column section（C_H），the thickness of beam flange（B_T_2），the thickness of beam web（B_T_1），and the thickness of the stiffener set in the end plate（DBL_T）have the smaller sensitive.
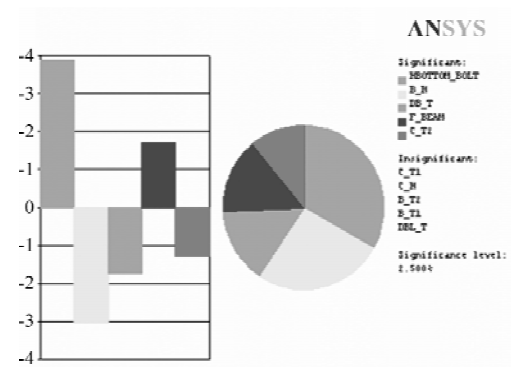
Figure 4　Sensitivity plots for displacement
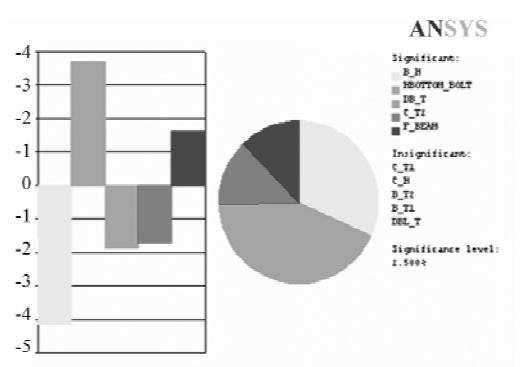
Figure 5　Sensitivity plots for rotation

RELATIVE MOMENT-ROTATION MODEL

The sensitivity coefficients of the input parameters to the rotation（ROTA）are listed in Table 4. According to the reference[2]，the sensitivity coefficient corresponding to the load（F_BEAM）as a standard，is determined 1.000. The other coefficient values are listed in the third column in the Table 4 according to the respective ratios.

TABLE 4　INTEGRATED DATA

Parameter	ROTA	Standardized score	$C_1(\times 10^{-4})$	Initial value	E_0	Mean $\overline{E}_0$
C-T2（t_{fc}）	-0.170	-1.056	-1.63	12 mm	355 094	
C-T1（t_{wc}）	-0.023	-0.143	-0.34	8 mm	345 770	
C-H（h_c）	-0.039	-0.242	-0.02	294 mm	360 994	
B-H（h_b）	-0.415	-2.578	-0.20	244 mm	347 508	
B-T2（t_{fb}）	-0.008	-0.050	-0.08	11 mm	373 666	
B-T1（t_{wc}）	-0.050	-0.311	-0.97	6 mm	351 377	351 747
DBL-T（t_{dbl}）	-0.020	-0.124	-0.23	10 mm	354 646	
DB-T（t_{db}）	-0.188	-1.168	-1.35	16 mm	355 653	
HB-T（h_{up}）	0.357	2.220	0.26	182 mm	318 620	
F-BEAM	0.161	1.000	0.000 743	25 000 N	354 138	

According to correlations and regression lines of scatter plots between geometrical parameters and rotation of the joint，let this field data as input parameters in the formula corresponding power exponent of the model，a special expression between geometrical parameters and relative rotation of beam to column is suggested in the following，Eqn. 1.

Eqn 1.

$$\theta = \frac{h_{up}^{2.22} M}{E_0 t_{fc}^{1.056} t_{wc}^{0.143} h_c^{0.242} h_b^{2.578} t_{fb}^{0.05} t_{wb}^{0.311} t_{dbl}^{0.124} t_{db}^{1.168}} \tag{1}$$

Where，θ is the relative rotation between beam and column（rad），h_{up} is the distance between the outer rows of bolts to the beam horizontal axis（mm），M is the beam bending moment（ N • mm ），t_{fc} is the thickness of column flange（mm），t_{wc} is the thickness of column web（mm），h_c is the height of column section（mm），h_b is the height of beam section（mm），t_{fb} is the thickness of beam flange（mm），t_{wb} is the thickness of beam web（mm），t_{dbl} is the thickness of stiffener（mm），t_{db} is the thickness of the end plate（mm）.

E_0，is a composite constant，determined by derivative of any parameter from Eqn. 1. For example，partial derivative of parameter h_{up} from Eqn. 1 is Eqn. 2. The value $C_1 = -0.000\,026$ is slope coefficient of the scatter plot between ROTA and h_{up}. Solving Eqn. 2，get $E_0 = 318\,620$. Many different E_0 were attained with C_1 differently，listed in Table 4. At last，$\overline{E}_0$，the mean value of E_0，was selected as the constant of Eqn. 1. The elastic moment-rotation model was validated by experimental results of the extended end plate connections with stiffeners.

Eqn. 2

$$\frac{\partial \theta}{\partial h_{up}} = \frac{\partial}{\partial h_{up}} \left(\frac{h_{up}^{2.22} M}{E_0 t_{fc}^{1.056} t_{wc}^{0.143} h_c^{0.242} h_b^{2.578} t_{fb}^{0.05} t_{wb}^{0.311} t_{dbl}^{0.124} t_{db}^{1.168}} \right) = C_1^{h_{up}} \tag{2}$$

CONTRAST ANALYSIS

Take the specific parameters of the specimen into Eqn. 1，which can get the initial rotational stiffness of the specimen by the moment-rotation model. The calculated results were compared with the experimental results，as shown in Table. 5. From the Table 5 can be seen the differences of the initial rotational stiffness range from 2% to 6% between calculated results and experimental results. In the range of allowable error，it is acceptable，and the moment-rotation model for the end plate connections with stiffeners was verified.

TABLE 5 COMPARISONS OF INITIAL ROTATIONAL STIFFNESS

Number	Calculated results (kN • m • rad^{-1})	Experimental results (kN • m • rad^{-1})	Ratio
D1	22 065.3	22 459.4	0.98
D2	30 768.4	29 615.8	1.03
D3	55 839.1	52 332.9	1.06
D4	83 791.2	81 000.1	1.03

SUMMARY

Correlation analysis，probabilistic sensitivity analysis and constitutive relation analysis of extended end plate connections with stiffeners were carried out in this paper.

In many geometrical parameters，the distance from the outer rows of bolts to the beam horizontal axis（HBOTTOM_BOLT）was most sensitive to the maximum deflection of beam free end and the rotation of beam to column.

The elastic relative moment-rotation model of the extended end plate connections with stiffeners was put forward for flexible working stage，which has been verified well compared with experimental results. The parameters powers exponents of the model have notable physical meanings indicating sensitive to relative rotation of beam to column，which can be easily applied to engineering design.

ACKNOWLEDGEMENTS

REFERENCES

［1］JGJ82-91，"Code for design，construction and acceptance of high strength bolting for steel structure"，China Architecture Building Press，1992.

［2］Pan，J. R.，"Analytical method on semi-rigid joint of framework based on correlations"，Shantou University，2009.

［3］Shi，G.，Shi，Y. J.，Wang，Y. Q.，Li，S. F. and Chen，H.，"Experimental study of semirigid end-plate connections in multi-story steel frames"，Journal of Tsinghua University (Science and Technology)，2004，44(3)，pp391-394.

［4］GB 50017-2003，"Code for design of steel structure"，China Planning Press，2003.

［5］Boyi，Studio，"Classic of advanced analysis technology and example explanation for ANSYS. 9. 0"，China Water Power Press，2005.

ANALYSIS OF SEMI-RIGID BOLTLESS BEAM-TO-COLUMN CONNECTORS IN STEEL STORAGE RACKS

Z. Y. Wu, * B. Cheng and Y. Zhang

School of Civil Engineering, Harbin Institute of Technology, Harbin, 150090, China
* Email: chengbo198508@126.com

KEYWORDS

ABSTRACT

Storage racks are three-dimensional load bearing structures for the storage and retrieval of goods in warehouses. Compared to traditional steel structures, steel storage racks have two main differences: the continuous perforated cold-formed steel columns and semi-rigid boltless hook-in connectors. The connector, welded to each end of the beam, has hooks or other devices which engage in slots in the column. The connectors from different manufacturers have different geometry and performance, so it is difficult to develop a generalized analytical method. In this study, three series of tests were conducted on a commercially available connector. The objective of tests is to study the stiffness and ultimate strength of the connector subjected to bending, shear or tensile force. Both moment-rotation curves from bending tests and load-displacement curves from shear or tensile tests are highly non-linear. The finite shell element models that simulate the experimental behaviour closely were developed using ANSYS finite element software. According to the test failure phenomena that the hooks in tension side cut in the columns web, a simplified calculation model has been developed, using the springs to replace the effect of hooks. Based on the model, the formulas, calculating the moment resistance and initial rotational stiffness of connectors, have been proposed. The comparison between experimental results and solutions obtained from the formulas show that the accuracy of the calculation model is acceptable. Thus the calculation model can be used to estimate the connector performance when there is no test data.

INTRODUCTION

Steel storage racks are widely used to store goods on pallets in industry. They play an important role in the process of moving the products from the producer to the end user. In the market, there are many different types of racks such as selective pallet racks, drive-in racks, cantilever racks, narrow aisle racks, gravity flow racks and so on. A typical selective pallet rack, the most common type of racks, is shown in Figure 1. Two columns and their bracings constitute column frames which are the vertical load carrying

element. Horizontal shelf beams link adjacent column frames and lie in the direction perpendicular to the plane of column frames. Goods，which are stored on the wooden or plastic pallets，are placed by forklift truck on the beams. In the storage racks，semi-rigid boltless hook-in connectors are used. On the beam-end-plates welded to the end of beams，there are tabs which are engaged into the slots of the column at optional heights determined by the size of goods. In the racks which have no bracing members in the plane of beams，beam-to-column connectors are the only source of stiffness required for the rack stability.
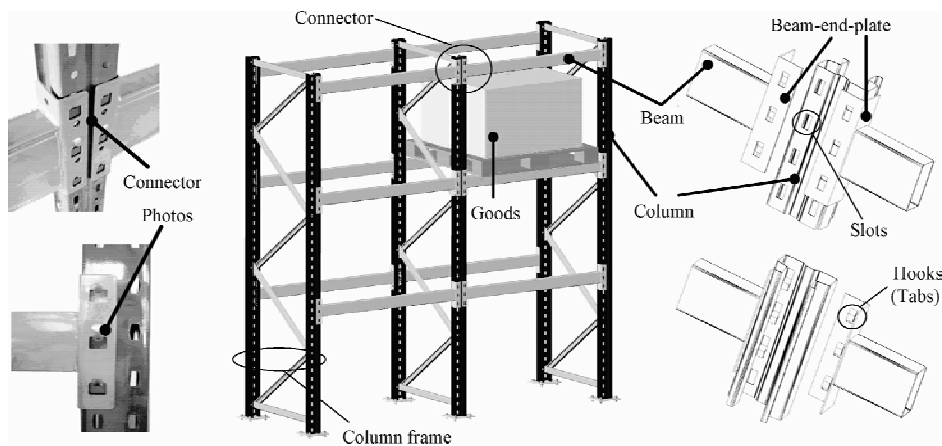
Figure 1　A typical selective pallet storage rack

The previous work on beam-to-column connectors focused on studying the moment-rotation behaviour of them. Because of the diversity and complexity of connectors，the experimental evaluation and numerical analysis are favourable methods. Markazi et al.[1] carried out tests on four different types of connectors to estimate the parameters governing the behaviour of connectors. Bernuzzi and Castiglioni[2] conducted an experimental analysis to investigate the behaviour of beam-to-column joints under cyclic reversal loading. Markazi et al.[3] presented a finite element analysis of a boltless connector and investigated the effects of different boundary conditions of the finite element model. Bajoria and Talikoti[4] tested the flexibility of connectors using two different test methods and found that both methods were available to study the connectors. Gilbert and Rasmussen[5] did cyclic tests on a bolted moment connection used in storage racks. The bolted connector studied by authors was different from the common boltless ones，but it still had a significant amount of looseness. Prabha et al.[6] conducted eighteen experiments on pallet rack connections and proposed simple analytical models to predict the moment rotation behaviour of these connections.

The review of existing literature reveals that most research work is concentrated on the flexural behaviour of connectors. Although the flexural behaviour has a great effect on the stability of racks，it is also important and necessary to study shear and tensile performances of connectors. More over，few scholars do the research work on developing generalized analytical models of connectors. However，the analytical model of calculating the rotational behaviour of connectors is useful for designers in the design work.

In this study，three series of tests of the connectors were carried out. Besides bending tests which are familiar in the previous investigations，tensile tests and shear tests were also conducted to study comprehensive performances of the connector. The finite element models that simulate the experimental behaviour well were also developed. The commercial software ANSYS was used in the simulation. In the

last section，a simplified calculation model，calculating the moment resistance and initial rotational stiffness of connectors，has been proposed. The solutions obtained from the simplified model have been compared with experimental results from this paper and other literature.

EXPERIMENTAL INVESTIGATION

The connectors，which were purchased from market，were fabricated from cold-formed steel. The cross section details of the components are shown in Figure 2. The column has two different thicknesses（1. 75 mm and 2. 20 mm），however the thickness of the beam and beam-end-plate for all specimens are the same. A total of 18 specimens were divided into three series，and the specimen label can be seen in Table 1. For example in the specimen T-T1. 75–1，"T" indicates the tensile test，"T1. 75" represents the thickness of the column as 1. 75mm and the "1" represents it is the number one of three identical specimens. The material properties of the beam and column were determined by tension tests and the results are listed in Table 2.
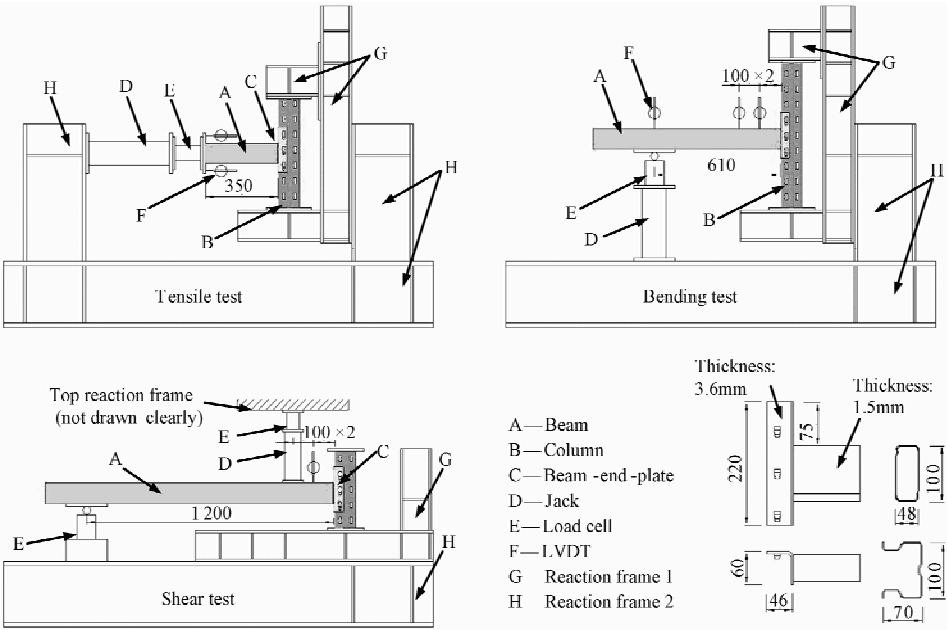
Figure 2　Schematic diagram of the test set-up

The schematic diagrams of tests are also shown in Figure 2，and the tensile test set-up arrangement is shown in Figure 3. In the tensile test，both ends of the column were fixed on the reaction frame 2. Through a load cell，the free end of short beam was connected to a hydraulic jack which can apply the pulling force. Two linear variable differential transducers（LVDTs）were used to obtain the horizontal displacement of the beam. In the bending test，the lengths of the beam and column were longer than those in the tensile test. The load was applied by a screw jack，and a load cell was also used to monitor the applied load. One LVDT was placed at the position of the jack，and the other two LVDTs were placed in the vicinity of the connector to get rotation of the beam. In the shear test，the length of beam was the longest in the all three types of tests. The free end of the beam was supported on a roller to simulate the simply supported condition. A screw jack was placed near the connector. Between the jack

and connector，one LVDT was positioned to monitor the vertical displacement of connector.

From the recorded data of tests，the load-displacement curves and moment-rotation curves of the connections are plotted in Figure 4. All the tests curves are highly non-linear. The initial stiffness and failure load of the connectors are tabulated in Table 1. Because of the difference of initial imperfections in the specimens，results from the identical specimens are different. The failure phenomena of tests were the cutting of the tabs into the column webs or the tearing of tabs. In the tensile test，all the three tabs cut into the column web（Figure 5a）. In the shear test，the tabs were damaged and slipped out of the column web slots（Figure 5b）. In the bending test，only the tab in tension side cut into the column web（Figure 5c）.

TABLE 1   TEST RESULTS OF BEAM-TO-COLUMN CONNECTORS

Tensile test specimen	Initial tensile stiffness (kN/mm)	Ultimate tensile strength (kN)	Shear test specimen	Initial shear stiffness (kN/mm)	Ultimate shear strength (kN)	Bending test specimen	Initial rotational stiffness (kNm/rad)	Ultimate moment capacity (kNm)
T-T1.75-1	15.55	27.15	V-T1.75-1	3.40	15.22	B-T1.75-1	93.50	1.90
T-T1.75-2	14.77	26.95	V-T1.75-2	3.53	17.51	B-T1.75-2	67.27	2.35
T-T1.75-3	13.05	31.70	V -T1.75-3	1.57	16.47	B-T1.75-3	53.61	2.04
Average	14.46	28.60	Average	2.83	16.40	Average	71.46	2.10
T-T2.20-1	9.95	30.38	V-T2.20-1	3.68	17.09	B-T2.20-1	89.04	2.06
T-T2.20-2	16.01	32.55	V-T2.20-2	4.07	15.31	B-T2.20-2	173.60	3.04
T-T2.20-3	14.51	33.01	V-T2.20-3	3.51	13.50	B-T2.20-3	91.06	1.92
Average	13.49	31.98	Average	3.57	15.30	Average	117.9	2.34

TABLE 2   MATERIAL PROPERTIES FOR MEMBERS

Member	Thickness （mm）	Yield strength （MPa）	Ultimate strength （MPa）	Young's modulus （$\times 10^5$ MPa）	Poisson's ratio
Column 1	1.75	289	384	2.0	0.28
Column 2	2.2	359	446	1.9	0.27
Beam	1.5	243	360	1.8	0.30
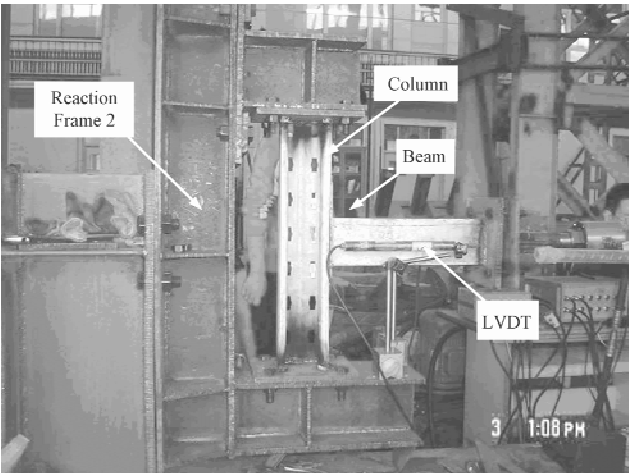
Figure 3   The tensile test set-up arrangement
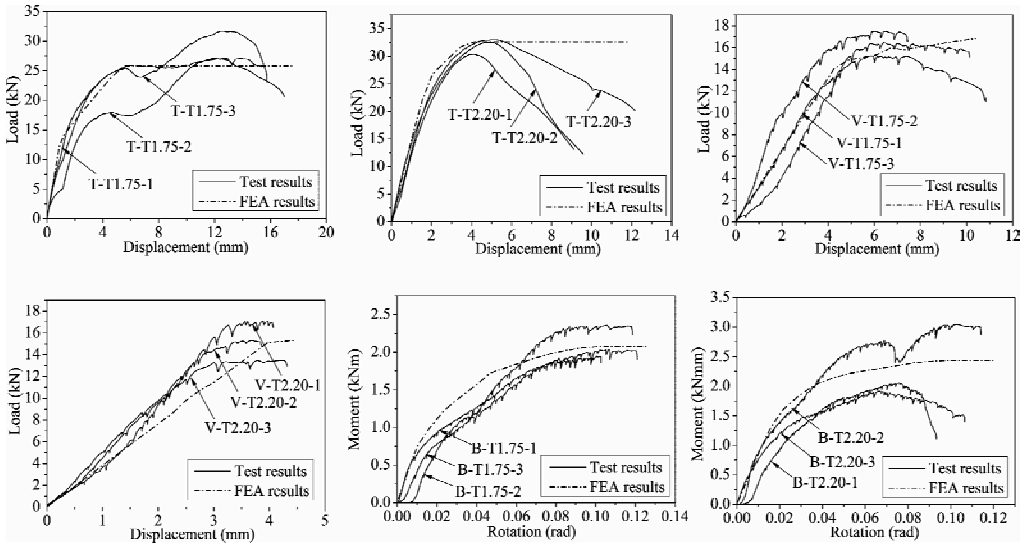
Figure 4   Comparison of FEA and experimental curves for tensile, shear and bending tests
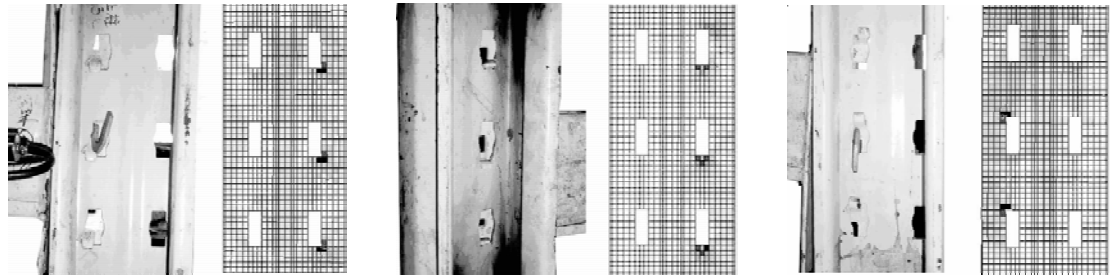
(a) Tensile test   (b) Shear test   (c) Bending test

Figure 5   Failure phenomena of the tabs in the tests and von Mises stress patterns in FEA

FINITE ELEMENT ANALYSIS

The finite element software of ANSYS version 10.0 was used to develop a finite element model, which aimed to simulate the experimental behaviour of connectors. The column, beam and beam-end-plate are modelled using the element SHELL181, which is a four-node shell element with six degrees of freedom at each node. The size of element in column and beam-end-plate is approximately 5mm × 5mm. The coupon test results in Table 2 are used in modelling. Stress-strain relationship of steel is described by a bilinear stress-strain curve.

There are two types of contacts in the connector: surface-to-surface contact and node-to-node contact. The surface-to-surface contact between the column and beam-end-plate is modelled using contact elements TARGE170 and CONTA174. Since it is difficult to model the node-to-node contact between the column web slots and the tabs, the nonlinear axial spring element COMBIN39 is used. The details of the finite element model are shown in Figure 6. The coordinates of nodes in column slots lower edges and beam-end-plate tabs are identical. These nodes form twelve node pairs, which are linked by COMBIN39. The

spring element can only carry compressive load. Take the example of node pairs 1~4, horizontal spring elements are used in node pairs 1 and 4, but vertical spring elements are used in all node pairs. Force-deflection relation of horizontal spring elements is tri-linear, however force-deflection relation of vertical spring elements is bilinear. The values of F_i and D_i in force-deflection relations are chosen to make the models simulate the experimental behaviour of the connector best.

The comparison of FEA and experimental curves for all three series of tests are shown in Figure 4. Most of the curves from FEA fit well with the experimental ones. The von Mises stress patterns of column web are shown in Figure 5. The stress of the web sections, where the tearing happens in the test, is high. To a large extent, the FEA model is capable of predicting the experimental behaviour of connectors.
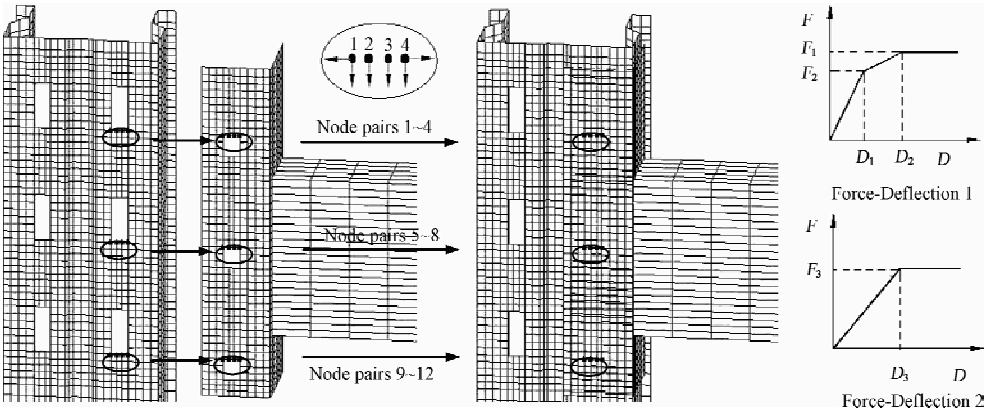
Figure 6   Finite element model of the connector

SIMPLIFIED CALCULATION MODEL

A simplified calculation model, using the springs replace the effect of tabs, has been proposed (Figure 7). In the model, it is assumed that the beam-end-plates bend around the stiffness calculated point or the moment calculated point and the part of plates above the points are rigid. In the tensile test, the average initial tensile stiffness and ultimate tensile strength of specimen T-T2.20 are 13.5 kN/mm and 32.0 kN. As there are three tabs, the initial tensile stiffness and ultimate tensile strength of one tab are approximately 4.5 kN/mm and 10.6 kN. Based on these results, the tensile stiffness K_s and ultimate tensile strength F_s of the tab in the calculation model are calculated as,

$$K_s = 0.65 \times 4.5 \times (t_1/3.6)^{0.5} \times (t_2/2.2)^{0.5} \times (3/n)^{1.6} \tag{1}$$

$$F_s = 1.3 \times 10.6 \times (t_1/3.6)^{0.5} \times (t_2/2.2)^{0.5} \times (3/n)^{0.5} \tag{2}$$

where t_1 is the thickness of the beam-end-plate; t_2 is the thickness of the column; n is the number of the tabs; 0.65 and 1.3 are adjusting coefficients.

The distance x_1 from the stiffness calculated point to the lower edge of beam-end plate and the distance x_2 from the moment calculated point to the lower edge of beam-end plate are calculated as,

$$x_1 = 0.3 \times (h_p - h_b - f) \tag{3}$$

$$x_2 = 0.7 \times (h_p - h_b - f) \tag{4}$$

A — Stiffness calculated point
B — Moment calculated point
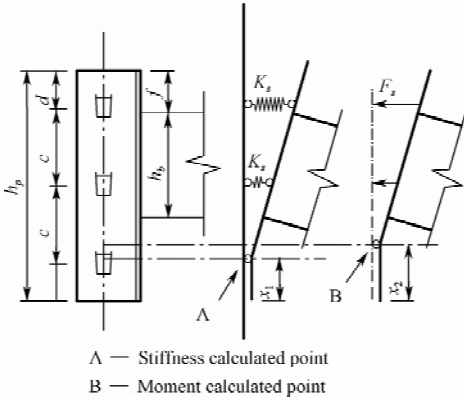
Figure 7 Simplified calculation model
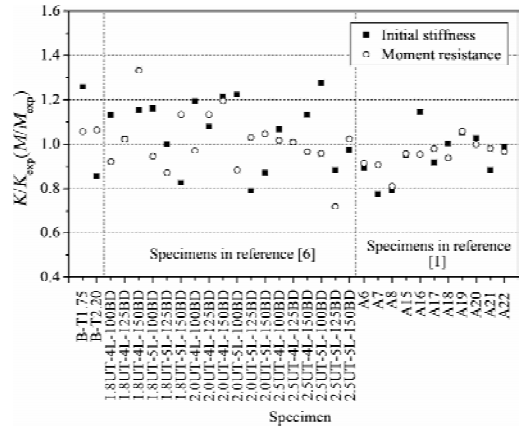
Figure 8 Results of K/K_{exp} and M/M_{exp}

Assuming the tensile stiffness of all the tabs in the connector is K_s, the initial rotational stiffness K of the connector are calculated as,

$$K = K_s \times (h_p - x_1 - d)^2 + K_s \times (h_p - x_1 - d - c)^2 \tag{5}$$

It is assumed the largest tensile strength of the tabs is F_s, when the connector fails. The ultimate moment capacity M of the connector are calculated as,

$$M = F_s \times (h_p - x_2 - d) + F_s \times (h_p - x_2 - d - c)^2 / (h_p - x_2 - d) \tag{6}$$

Some notations in the Eqns (3)~(6) are defined in Figure 7. The Eqns (5)~(6) are only useful for the connector with three tabs. When the number of the tabs is not three, the Eqns (5)~(6) need some changes following the similar calculation model. Markazi et al.[1] and Prabha et al.[6] also conducted bending tests on the connectors. The experimental results, initial rotational stiffness K_{exp} and ultimate moment capacity M_{exp}, are chosen to verify the calculation model. The results of K/K_{exp} and M/M_{xp} are given in Figure 8. For most of the ratios are in the range of 0.7–1.3, the calculation model is useful to predict the connector performance in the design stage.

CONCLUSIONS

The experimental investigation, finite element analysis and simplified calculation model study of a beam-to-column connector in steel storage racks have been presented. The main conclusions are summarized as follows:

1. The failure phenomena of all the three series of tests is that, the tabs cut into the web of columns or the tabs themselves are damaged. The load-displacement curves and moment-rotation curves of the connection are highly non-linear.

2. The comparison between experimental results and the FEA predictions prove the finite element analysis is generally a reliable tool to get behaviour of connectors.

3. An analytical model has been proposed, focusing on the effect of hooks on the behaviour of the connector. After calculating the tensile stiffness and ultimate tensile strength of the tab, the initial

rotational stiffness and ultimate moment capacity of the connector can been gotten. This model prediction has a close fit with the experimental results.

REFERENCES

［1］Markazi，F.D.，Beale，R.G. and Godley，M.H.R.，"Experimental analysis of semi-rigid boltless connectors"，Thin-Walled Structures，1997，28(1)，pp.57-87.

［2］Bernuzzi，C. and Castiglioni，C.A.，"Experimental analysis on the cyclic behaviour of beam to column joints in steel storage pallet racks"，Thin-Walled Structures，2001，39，pp.841-859.

［3］Markazi，F.D.，Beale，R.G. and Godley，M.H.R.，"Numerical modeling of semi-rigid boltless connectors"，Computers and Structures，2001，79，pp.2391-2402.

［4］Bajoria，K.M. and Talikoti，R.S.，"Determination of flexibility of beam-to-column connectors used in thin walled cold- formed steel pallet racking systems"，Thin-Walled Structures，2006，44，pp.372-380.

［5］Gilbert，B.P. and Rasmussen，K.J.R.，"Bolted moment connections in drive-in and drive-through steel storage racks"，Journal of Constructional Steel Research，2010，66，pp.755-766.

［6］Prabha，P.，Marimuthu，V.，Saravanan，M. and Jayachandran，S.A.，"Evaluation of connection flexibility in cold formed steel racks"，Journal of Constructional Steel Research，2010，66，pp.863-872.

DEVELOPMENT AND EXPERIMENTAL TESTING OF STEEL POST-TENSIONED CONNECTIONS WITH INNOVATIVE SEISMIC ENERGY DISSIPATERS

[*] G. Vasdravellis[1], T. L. Karavasilis[2], B. Uy[1]

[1] Institute for Infrastructure Engineering，University of Western Sydney，Australia
[2] School of Engineering，University of Warwick，Coventry，UK
[*] Email：g. vasdravellis@uws. edu. au

KEYWORDS

Self-centering frames，steel connections，experiments，cyclic loading，seismic response，hysteresis.

ABSTRACT

A new self-centering beam-to-column connection is proposed. The connection uses post-tensioned high-strength steel bars to provide self-centering capability and carefully designed energy-dissipation elements （EDs） that consist of steel cylindrical pins with hourglass shape. The proposed EDs：1）have superior energy dissipation and fracture capacity；2）are placed between the upper and the bottom flanges of the beam so that they do not interfere with the composite slab；and 3）can be very easily replaced if damaged. A simplified performance-based procedure was used to design the proposed connection. The connection performance was experimentally validated under quasi-static cyclic loading. The specimens were imposed to drift levels beyond the expected design ones in order to identify all possible failure modes. The experimental results show that the proposed connection exhibits stable self-centering behavior by eliminating residual drifts，sufficient energy dissipation capacity，and strength and stiffness comparable to those of a conventional moment connection. In addition，repeatable tests on a connection specimen were conducted along with replacing damaged EDs. These repeatable tests show that the proposed connection can be very easily repaired after a major earthquake without disturbing building use or occupation. In particular，the proposed EDs were easily replaced without using bolting or welding. A simplified analytical procedure using plastic analysis and simple mechanics was found to predict the connection behavior with sufficient accuracy.

INTRODUCTION

Conventional ductile steel moment-resisting frames （MRFs） are currently designed to form a global plastic mechanism under strong earthquakes through the development of plastic hinges at the end of beams and at the base of the columns （Eurocode 8 2004）. This design approach provides well known advantages such as acceptable behaviour able to protect human life，economy，low base shear force and controlled total floor

accelerations. However，plastic hinges in structural members involve significant cyclic inelastic deformations and local buckling which result in difficult to inspect and repair damage as well as residual drifts. Therefore，conventional steel MRFs result in socio-economical losses such as damage repair costs and loss of building use or occupation after a major seismic event. In addition，they may result in building demolition due to the complications associated with repairing large residual drifts. Research efforts developed self-centering steel moment resisting frames（SC-MRFs）with post-tensioned（PT）connections （Garlock et al. 2007）. SC-MRFs have the potential to eliminate inelastic deformations and residual drifts under strong earthquakes as the result of several features：softening force-drift behaviour due to separations（gap openings）developed in beam-to-column connections；re-centering capability due to elastic pre-tensioning elements（e. g. ，high strength steel bars）providing clamping forces to connect beam and columns；and energy dissipation capacity due to energy dissipation elements（EDs）which are activated when gaps open. When properly designed，these EDs can be easily inspected and replaced. In this paper，a new SC beam-to-column connection typology is proposed. The connection uses PT high-strength steel bars to provide self-centering capability and new EDs consisting of yielding web hourglass pins（WHPs）which can be very easily replaced if damaged. The connection performance is experimentally validated under quasi-static cyclic loading conditions. The experimental results show that the proposed connection exhibits stable self-centering behaviour and energy dissipation. The connection specimens are imposed to drift levels far beyond the expected design ones to identify all possible failure modes.

SC-PT CONNECTION WITH WEB HOURGLASS PINS

Structural Details

The proposed SC PT connection was designed to provide stable self-centering capability and increased energy dissipation with the aid of high strength steel bars and WHPs which do not interfere with the floor slab and are very easy to replace. Figure 1 shows a 3D representation of the proposed connection. The Figure represents the actual configuration of an exterior connection of a steel SC-MRF. Two high strength steel bars located at the mid-depth of the beam，one at each side of the web，are anchored to the exterior column flange and pass through holes drilled on the column flanges. The bars are post-tensioned and hence，clamp the beam to the column while providing self-centering capability. WHPs consist of two pairs of steel pins which are inserted in aligned holes drilled on the web of the beam and on strong supporting plates. The pairs of WHPs are symmetrically placed（close to the top and bottom beam flange） to provide increased lever arm and hence，increased internal moment resistance under cyclic connection rotations. The WHPs are designed to have an hourglass shape to provide enhanced energy dissipation and
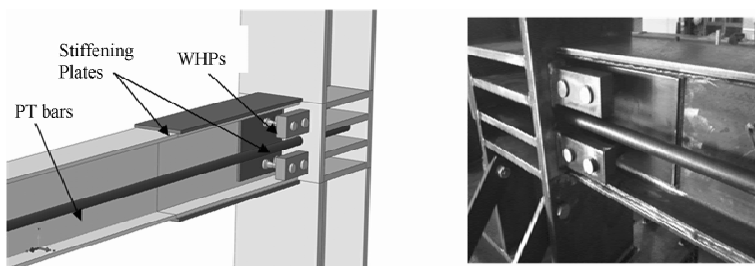

Figure 1   Left：3D representation of the proposed self-centering PT connection and
Right：a photo of the connection in the Lab.

fracture capacity (Kobori et al. 1992). Both sides of the beam web are reinforced with steel plates which increase the contact surface between the WHPs and the web. In this way, possible ovalization of the sides of the holes drilled on the web and the reinforcing plates under the high WHP bearing forces will be negligible and connection pinching behaviour can be avoided. The strong supporting plates are welded on the column flange. The connection also includes beam flange reinforcing plates to avoid excessive early yielding in the beam flanges under the high PT bars forces. In addition, the panel zone is strengthened with horizontal stiffeners and continuity plates along the web of the column.

DESIGN OF PROTOTYPE SC PT CONNECTION WITH WHPS

The design focuses on the exterior connection of the 4th floor of a prototype steel building (Vasdravellis et al. 2011). This connection is designed as a self-centering PT connection with WHPs using the methodology presented in Garlock et al. (2007). This methodology uses two major performance objectives and associated structural limit states, namely: (1) Immediate Occupancy (IO) under the design basis earthquake (DBE) by avoiding damage in beams and columns while permitting gap opening (it is assumed that damaged WHPs can be replaced without disturbing building occupation); and (2) Collapse Prevention (CP) under the maximum considered earthquake (MCE) by avoiding PT bar yielding and beam local buckling while permitting minor yielding in beams and columns. The MCE has intensity equal to 150% the intensity of the DBE. The above performance objectives proposed in Garlock et al. (2007) may result in sudden loss of strength and stiffness due to undesirable failures related to beam local buckling or tendon yielding when the connection is deformed beyond the MCE drift limit. In this work, the details proposed by Kim & Christopoulos (2009a) are employed to avoid local buckling and form a ductile plastic hinge at the end of the flange reinforcing plate for drifts equal or higher than the MCE drifts. This design approach is slightly different than the one presented in Kim and Christopoulos (2009b) where the ductile plastic hinge is formed for drifts equal or higher than the DBE drifts. The design of the connection is based on story drifts equal to 0.64% under the FOE (Frequently Occurring Earthquake), 1.6% under the DBE and 2.4% under the MCE. These drifts are significantly lower than those used in previous works based on the IBC 2% drift limit under the DBE due to the strict serviceability drift limits imposed by the EC8 under the FOE. The FOE has intensity equal to 40% the intensity of the DBE. PT bars are designed to avoid yielding for $\theta_r \leqslant 0.07$ rad. This value eliminates the possibility of strand yielding since beam shortens (and the stress in the PT bar is reduced) due to the plastic hinge formation for drifts higher than the 2.4% MCE drift.

WHP COMPONENT TESTING

Component tests on the WHPs were conducted in order to assess their energy dissipation capacity and ductility under cyclic loading. Two pins were tested in order to reproduce the behaviour of the WHPs in the proposed SC connection typology. The supporting plates were welded on a fixed plate and the plate simulating the web of the beam was attached to the actuator applying the load. The thicknesses of the plates were equal to the thicknesses of the corresponding components in the connection tests described later. The induced displacement history was chosen to be consistent with that used for the connection tests, i.e., the required displacement of the pins due to the imposed connection rotation in the actual tests was calculated and applied as the component testing displacement history. The WHPs were designed in order to guarantee a stable and ductile hysteretic behaviour and to maximize the energy dissipation capacity during a seismic event. The hourglass geometry of the pins was calibrated in order to be

consistent with the bending-moment diagram. In this way，a more efficient energy dissipation capability is ensured. Moreover，probable associated pinching effects are avoided. Figure 2. a shows the WHPs at ultimate deformation levels during the component tests. This deformation corresponds to a connection rotation of about 0. 06 rad. The pins were capable of sustaining repeated large inelastic cycles without fracturing prior to an imposed displacement corresponding to 7% drift. Figure 2(b) plots the force-displacement cyclic relationship achieved by the WHPs. The pins provided a force equal to 160 kN. It is evident that the developed geometry resulted in a highly-dissipative system with good hysteretic behaviour and high ductility levels.

| (a) Ultimate deformation | (b) Hysteretic force-displacement loop of the WHPs |
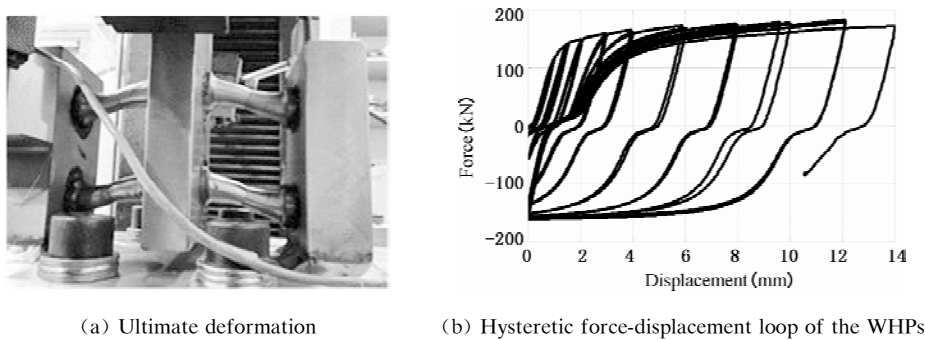
Figure 2

LARGE-SCALE CONNECTION TESTS

Test Setup

The test setup is schematically shown in Figure 3. The 250UB37 beam was connected to a strong 310UC158 column. Two additional steel members were welded to the column to form a truss system in order to minimize the column deformations (the 310UC158 horizontal member and the 200UC52 diagonal member). The whole system was bolted on the strong floor. The imposed displacement history was applied vertically by a 2 000 kN-capacity and 250 mm-stroke hydraulic actuator. The actuator was positioned at a distance of 1800mm from the beam-column face and thus was able to impose a joint rotation equal to 7%，much larger than the target rotation of 2.4%，corresponding to the MCE level.
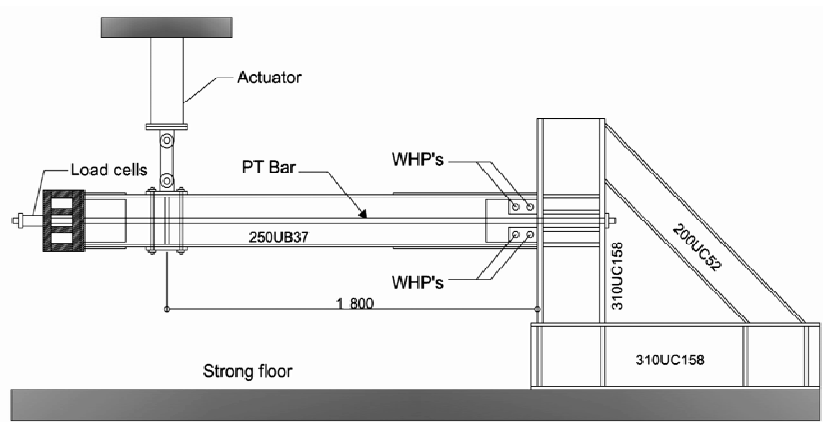
Figure 3   The test setup

Specimens

Two specimens representing the proposed SC post-tensioned connection were designed according to the procedure described in Section 4. Due to laboratory limitations, the specimens were designed at a 0.6 scale with respect to the original dimensions of the prototype building. The resulting beam and column sizes and relevant details of the connections are summarized in Table 1.

TABLE 1　SPECIMEN DETAILS

Specimen	SC-WHP1	SC-WHP2
Beam section	250UB37	250UB37
Column section	310UC158	310UC158
Initial post-tension（kN）	500	500
Length of reinforcing plates（mm）	700	700
Longitudinal stiffeners	NO	YES

The two specimens were identical except that four longitudinal stiffeners were welded on the web and four 27 mm-holes were drilled on the flanges of the second specimen, according to Kim & Christopoulos (2009a). The details of this configuration are shown in Figure 4. The purpose of this configuration is to eliminate local buckling effects on the beam web or flanges. Instead, a plastic hinge is intended to be formed at the end of the reinforcing plate. In this way, sudden failures and local instabilities are avoided and a ductile ultimate failure mode under large inelastic drifts is ensured.
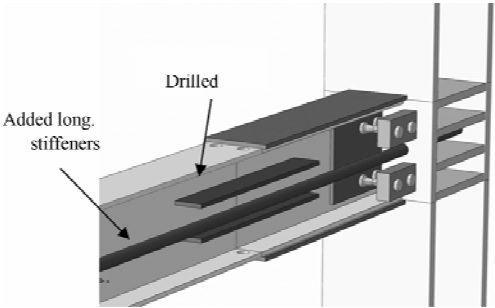
Figure 4　Details of the second specimen

Material Properties

The beam and column were made of F_y = 300 MPa steel, while the yield strength of the reinforcing plates, stiffeners and pin-supporting plates was F_y = 350 MPa. The post-tensioned bars were made of high-strength steel, with nominal yield strength equal to 930 MPa and a fracture stress limit equal to 1 060 MPa. The pins were made of 1 020 grade carbon steel with nominal yield strength of 500 MPa. This type of steel was chosen in order to achieve the required strength provided by the WHPs to the connection, while keeping the sizes of the pins relatively small. Also, this specific material was the most suitable for fabricating the hourglass shape of the WHPs.

Experimental Results

The specimens were loaded under displacement-controlled conditions, according to the AISC loading

protocol（AISC 2005）. The cyclic hysteretic response of the two specimens is shown in Figure 5 in terms of the respective moment-rotation loops. It is shown that the specimens had a full self-centering capacity up to rotations equal to 0.05 rad. In fact，no damage in any part except the WHPs was observed up to this rotation levels. This rotation is considerably larger than the specified target rotation of 0.035 rad，which is set as the required rotation capacity of a connection for Ductility Class High（DCH）structural design concept in Eurocode 8. Nevertheless，the connections were loaded to excessive drift levels in order to identify all possible failure modes. A final cycle of 10% drift（or joint rotation）was imposed for this purpose. It can be seen from Figure 5 that after the last large imposed displacement the connection lost its self-centering capability and a permanent deformation was present at the end. The failure modes were different in the two specimens. The failure mode of specimen SC-WHP1 was the local buckling of the beam which took place immediately after the end of the reinforcing plates on the beam flanges. The buckling initiated at the web and propagated to the flanges. This failure caused a significant drop in the stiffness of the connection. The specimen SC-WHP2 had a different failure mode than the first one. The reinforced with the longitudinal stiffeners web did not show any evidence of local buckling，and the behaviour was stable and ductile. However，a failure has occurred due to local buckling of the beam flanges at the contact regions with the column. It has to be noted that the design procedure adopted for the detailing of the specimens，and especially that for the determination of the length of the reinforcing plates on the beam flanges，is rather conservative，as it was proved by the experimental behaviour. In fact，local buckling in specimen SC-WHP1 has occurred at considerably larger drift levels than those intended by the design procedure.

(a) SC-WHP1　　　　　　　　　　　　　　　(b) SC-WHP2
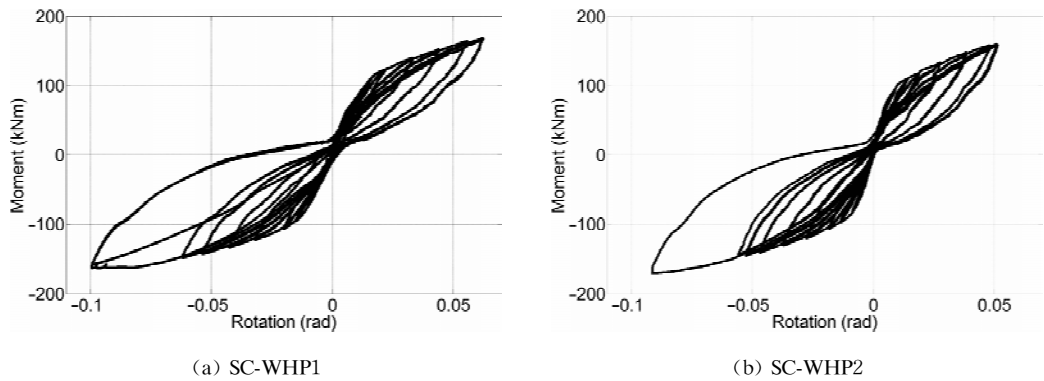
Figure 5　Moment-rotation hysteresis loop for specimens

PRELIMINARY FINITE ELEMENT ANALYSIS

A three-dimensional solid finite element model was constructed for the simulation of the behavior of the proposed connection. Preliminary results of this study are given in the present section. The geometry of the tests was reproduced in full detail. Figure 5(a) summarizes the element types used in the model. Tie interactions were employed to simulate the welded surfaces，e. g. the WHP supporting plates on the column flange，all the stiffeners on the beam and column，and the anchor block on the tip of the beam. Contact interactions were specified between the beam and the column，the PT bars and the column holes，and the WHPs and the supporting plates holes. A friction coefficient equal to 0.4 was specified for the beam-column interface，while no friction was specified for all other interactions. The stress-strain relationships obtained from the material tests were converted into piece-wise linear true stress-plastic

strain curves, as required for the material input, and used to define the constitutive relationships for the WHPs and the structural steel, while nominal values provided by the manufacturer were used for the material of the PT bars. The vertical load was applied as an imposed displacement at a distance equal to 1 800 mm from the connection face. Figure 5(b) plots the force versus percentage drift hysteretic curve obtained from the FEM analyses and compares the results with the experimental outcome for the first tested configuration, e.g. specimen SC-WHP1. The model can capture well the overall cyclic behavior of the connections. The predicted values for the decompression moment and the gap opening moment are in very good agreement with the corresponding experimental ones, while the initial and post-elastic stiffnesses are almost identical. Finally, the model captured well the failure mode of the tested specimen, which resulted in a residual drift of about 3% after the last imposed displacement cycle of 9% drift.
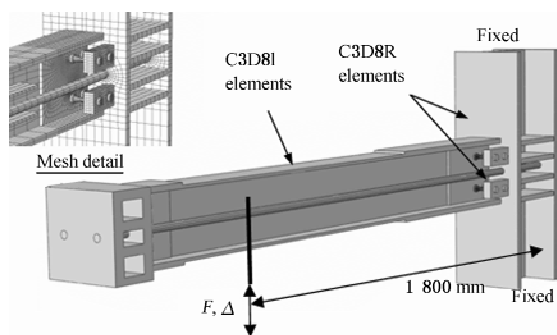
(a) Finite element model details   (b) comparison of experimental and numerical responses.
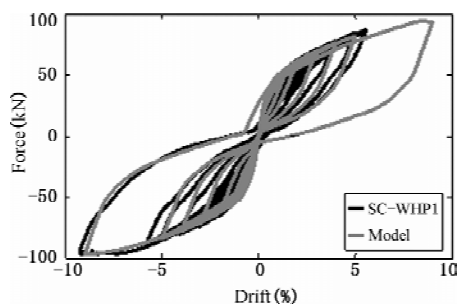
Figure 6

SUMMARY and CONCLUSIONS

Two specimens representing a new steel post-tensioned connection were designed and tested under cyclic quasi-static loading. The proposed connection configuration is equipped with a set of hourglass-shaped steel pins acting as energy dissipaters under earthquake loading. The specimens were loaded to drift levels far beyond the expected design ones in order to identify all possible failure modes. The connections performed well showing full self-centering capacity up to drift levels equal to 6%. Under the design earthquake drift levels, damage was mainly concentrated to the energy dissipation pins which can be easily replaced after a seismic event. In large drifts, the failure modes were mainly the local buckling of the beam web and flanges immediately after the end of the reinforcing plates and the local yielding in the beam due to bearing forces at the contact regions with the column flange. The experiments demonstrated the adequacy of the adopted detailing method to avoid local buckling failure at large drift levels. A nonlinear finite element model was developed and found to be capable to capture the cyclic hysteresis of the first specimen and the observed ultimate failure modes.

REFERENCES

［1］AISC 2005. Structural provisions for structural steel buildings. Chicago, Illinois.
［2］Eurocode 8, Design of structures for earthquake resistance, 2004.
［3］Garlock M., Sause, R. and Ricles, J., "Behaviour and design of post-tensioned steel frame systems," J Struct

Eng(ASCE)，2007，133(3)，pp.389－399.

［4］Kim，H.J. and Christopoulos，C.，Numerical models and ductile ultimate deformation response of post-tensioned self-centering moment connections，Earthquake Eng Struct Dyn，2009，38(1)，pp.1－21.

［5］Kim，H.J. and Christopoulos，C.，Seismic design procedure and seismic response of post-tensioned self-centering steel frames，Earthquake Eng Struct Dyn，2009，38(5)，pp.355－376.

［6］Kobori T.，Miura，Y.，Fukuzawa，E.，Yamada T.，Arita T.，Takenaka Y.，Miyagawa N.，Tanaka N. and Fukumoto T.，Development and application of hysteresis steel dampers，Proc. Earthquake Engineering，Tenth World Conference. Rotterdam：Balkem，1992.

［7］Vasdravellis，G.，Karavasilis，T. L. and Uy，B.，Design and experimental validation of steel post-tensioned connections with web hourglass pins，J Struct Eng （ASCE）. Under review，2011.

EXPERIMENTAL STUDY ON THE INFLUENCE OF STIFFENING RING ON BEARING CAPACITY OF TUBE-PLATE JOINT

X. B. Wei[1], Y. L. Peng[1], * J. F. Yang[2], H. B. Li[1]

[1.] Henan Electric Power Survey & Design Institute，Zhengzhou，450007，China
[2] School of Civil Engineering，Xi'an University of Architecture & Technology，Xi'an，710055，China
* Email：yjf9807@126.com

KEYWORDS

Stiffening ring，tube-plate joint，bearing capacity.

ABSTRACT

Tube-plate joint is a frequently-used joint type in steel-tube tower，but now，the theoretical investigation and experimental investigation on tube-plate joint are absent both at home and abroad. In this paper，the influence of different stiffening ring on joint bearing capacity was researched by carrying full-scaled test of tube-plate joint. The results indicate that the influence of different stiffening ring on joint bearing capability is significant. The design bearing capacity of 1/4-stiffening ring joint is close to 20% lower than that of 1/2-stiffening ring joint，and the design bearing capacity of none-stiffening ring joint is up to 40% lower than that of 1/2-stiffening ring joint. For ultimate bearing capacity，the degrees of decline are near 20% and 40% respectively. Therefore，the stiffening ring is recommended when tube-plate joint is designed in order to using least steel to gain maximal bearing capacity.

TEST DESIGN

Specimen Design

Nine specimens were designed to carry out full-scaled model test，in order to research the influence of different stiffening ring on the bending bearing capacity. The main tube is $\Phi 480 \times 12$，the primary plate length is 400 mm，all the components of the joint，including primary plates，subsidiary plates and stiffening rings，are welded together. The steel material is all Q345B，the specimen with 1/2 stiffening rings are showing in Figure 1. The specimen with 1/4 stiffening rings and the specimen without stiffening rings are the same but for stiffening rings，all the specimens are listed in table 1.

Test Device

Test device is showing in Figure 2. The column foot was connected on the support foundation rigidly. The

support foundation is H600×890(800) × 22×28 and the steel material is Q345B.
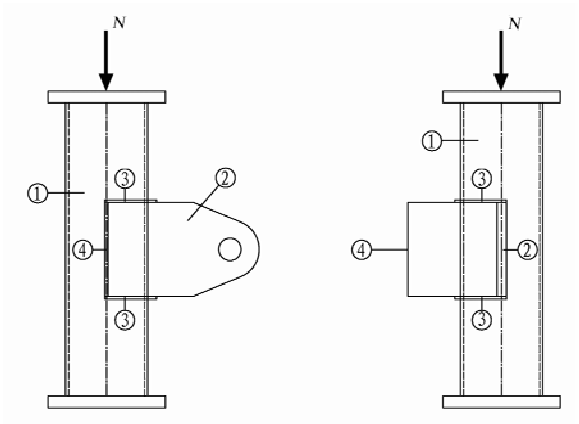
Figure 1　Specimen with 1/2 stiffening rings

TABLE 1　COMPONENTS OF ALL SPECIMEN

Stiffening ring type	Specimen number	Stiffening ring ③	Primary plate thickness ②	Subsidiary plate ④
1/2	1	1/2−5×60	20 mm	−12×200×400 (2)
	2	1/2−5×60	25 mm	−12×200×400 (2)
	3	1/2−5×60	28 mm	−12×200×400 (2)
1/4	4	1/4−5×60	20 mm	−12×200×400 (1)
	5	1/4−5×60	25 mm	−12×200×400 (1)
	6	1/4−5×60	28 mm	−12×200×400 (1)
none	7	—	20 mm	—
	8	—	25 mm	—
	9	—	28 mm	—
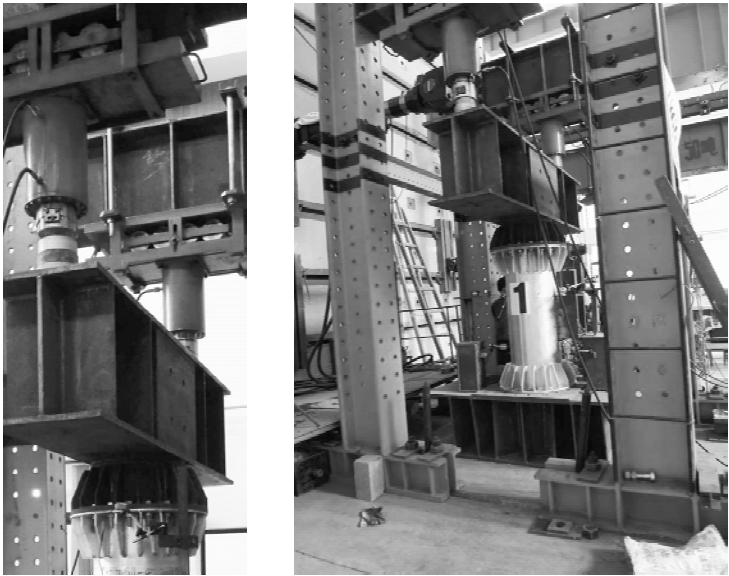
Figure 2　Test device

Load Step

Before formal loading，preliminary loading was carried out. In formal loading，the first step was to apply axial load $N = 1\ 800$ kN on the main tube only，and then kept for ten minutes. In this process，the height of the lever was monitored so as to insure the axial load unchangeable. The second step was to apply load on the primary plate until the specimen failed. The magnitude of this load was monitored by sensor.

Displacement Observation

The displacement of all measure points on the specimens was recorded by displacement gauge during testing. The arrangement of displacement gauges on the specimens with $1/2$ stiffening rings is showing in Figure 3. The arrangement of displacement gauges on the other specimens is homoplastically.
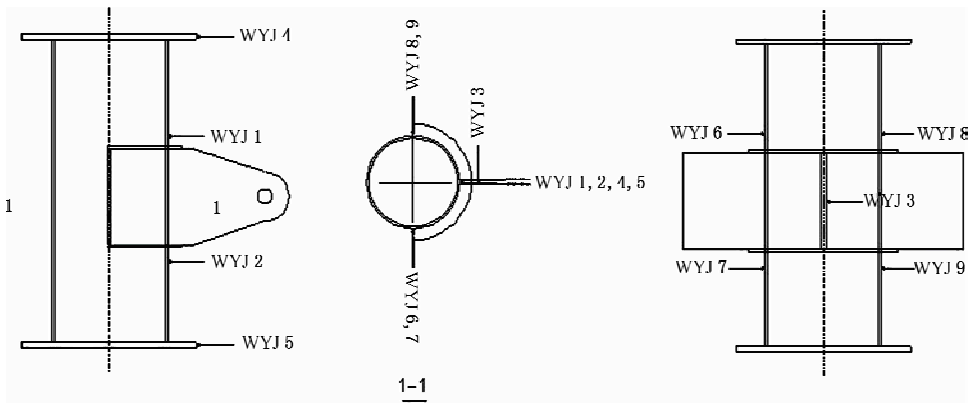
Figure 3   Arrangement of displacement gauges

The displacement gauge 1(WYJ1) was used to measure the displacement of the upper junction of main tube and primary plate，and the displacement gauge 2(WYJ2) was used to measure the displacement of the lower junction of main tube and primary plate. The lateral displacement of the primary plate was measured by the displacement gauge 3(WYJ3). The displacement gauge 4(WYJ4) and displacement gauge 5(WYJ5) were used to measure the displacement on the top and bottom of the specimen respectively. The displacement gauge 6，7，8，9(WYJ6，7，8，9) were used to measure the displacement of the junction of main tube and subsidiary plate.

THE DETERMINING PRINCIPLE OF THE ULTIMATE BEARING CAPACITY FOR THE JOINTS

The failure criterion of joints can be divided into three classes，（1）ultimate load criterion：connection fail or crack，（2）ultimate deformation criterion：deformation beyond allowable value，（3）initial crack criterion：appearing macro crack that can be seen by naked eyes.

The initial crack criterion usually cannot easily be controlled and also cannot be convenient to making a standard. The tubular joints often have excess plastic deformation that do not suit for bearing before they carry the ultimate load，so the ultimate load criterion is also not suitable. Now it is generally accepted internationally that the ultimate deformation criterion is taken as the failure criterion of joints. That is to

say，the joints fail when there is excess deformation on the main tubules. So，the ultimate bearing capacity for the simple joints is the maximum axial force on the end of the branch tubules when there is excess deformation on the main tubules[1].

In this paper，the ultimate deformation criterion is adopted. If there appears the ultimate load before the deformation reaches $3\% D_0$ (D_0 is the diameter of the main tube)，the ultimate load is taken as the ultimate bearing capacity. If there does not appear the ultimate load when the deformation reaches $3\% D_0$，then the load when the deformation is $3\% D_0$ is taken as the ultimate bearing capacity[2]. The Load-displacement curve is given in Figure 4[3]. Except for ultimate bearing capacity of the joint，there is design bearing capacity of the joint，which is the load when the deformation is $1\% D_0$.

(a) $\Delta_{max} < 3\% D_0$ (b) $\Delta_{max} > 3\% D_0$
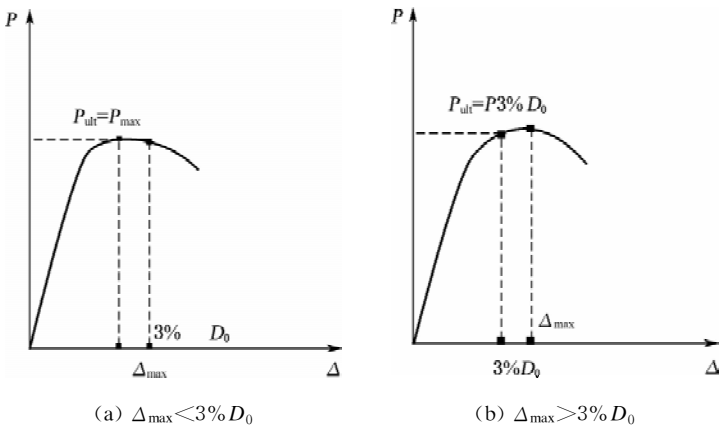
Figure 4   Load-displacement curves

TEST RESULTS AND ANALYSIS

Nine specimens were divided into three groups according to the thickness of the primary plate. The concave deformation on the upper junction of main tube and primary plate is showing in Figure 5.
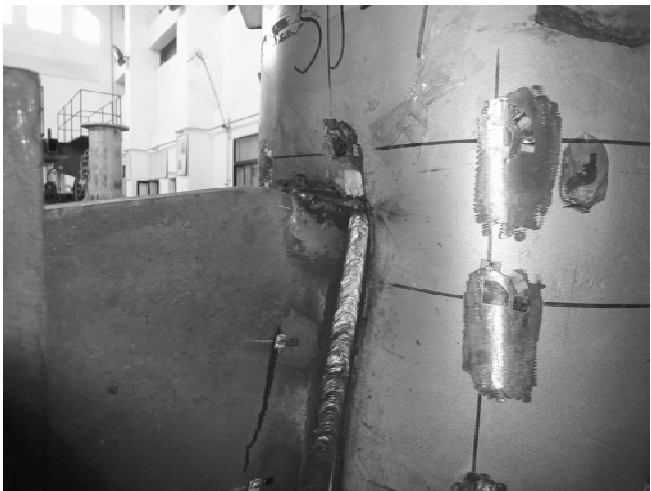
Figure 5   Concave deformation on the upper junction of main tube

Comparison of The Group 1（Specimen 1，4，7）

The thicknesses of the primary plate in this group were all 20 mm；the difference was that specimen 1 was fitted with 1/2 stiffening rings，specimen 4 was fitted with 1/4 stiffening rings，and specimen 7 was fitted without stiffening rings. The load-displacement（WYJ1）curves of these specimens in this group are showing in Figure 6.
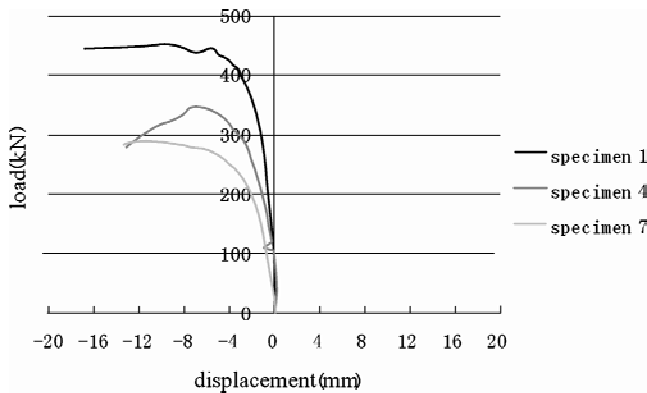
Figure 6   Load-displacement（WYJ1）curves of specimen 1，4，and 7

Test results of specimen 1，4，7 were listed in table 2.

TABLE 2   TEST RESULTS OF SPECIMEN 1，4，7

Specimen number	Design bearing capacity and the corresponding deformation		Ultimate bearing capacity and the corresponding deformation	
	Deformation/mm	Load/kN	Deformation/mm	Load/kN
1	4.8	433.28	8.65	453.55
4	4.8	329.70	7.115	348.39
7	4.8	261.61	12.105	289.03

From the test results，it is easily found that the design bearing capacity of specimen 1 is bigger than specimen 4 by 103.58 kN，and specimen 4 is bigger than specimen 7 by 68.09 kN.
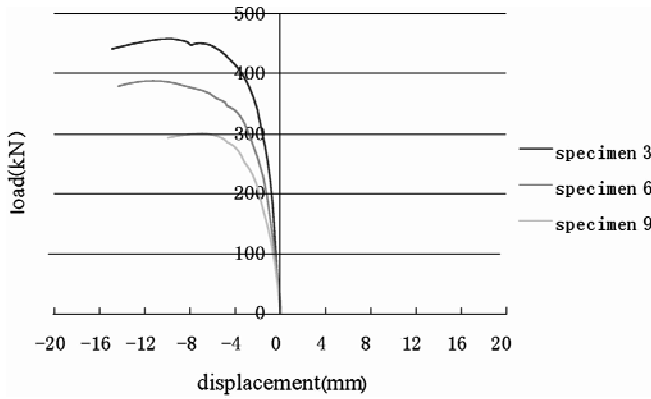
For the ultimate bearing capacity，specimen 1 is bigger than specimen 4 by 105.16 kN，and specimen 4 is bigger than specimen 7 by 59.36 kN.

Comparison of The Group 2（Specimen 2，5，8）

The thicknesses of the primary plate in this group were all 25 mm；the difference was that specimen 2 was fitted with 1/2 stiffening rings，specimen 5 was fitted with 1/4 stiffening rings，and specimen 8 was fitted without stiffening rings. The load-displacement（WYJ1）curves of these specimens in this group are showing in Figure 7.
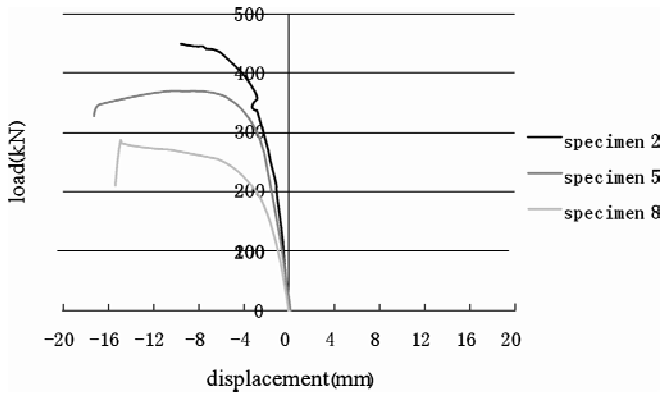
Figure 7   Load-displacement（WYJ1）curves of specimen 2，5，and 8

Test results of specimen 2，5，8 were listed in table 3.

TABLE 3   TEST RESULTS OF SPECIMEN 2，5，8

Specimen number	Design bearing capacity and the corresponding deformation		Ultimate bearing capacity and the corresponding deformation	
	Deformation/mm	Load/kN	Deformation/mm	Load/kN
2	4.8	413.26	9.485	449.03
5	4.8	350.10	10.31	369.68
8	4.8	239.06	14.4	280.40

From the test results，it is easily found that the design bearing capacity of specimen 2 is bigger than specimen 5 by 63.16 kN，and specimen 5 is bigger than specimen 8 by 111.04 kN.
For the ultimate bearing capacity，specimen 2 is bigger than specimen 5 by 79.35 kN，and specimen 5 is bigger than specimen 5 by 89.28 kN.

Comparison of the Group 3（Specimen 3，6，9）

The thicknesses of the primary plate in this group were all 28 mm；the difference was that specimen 3 was fitted with 1/2 stiffening rings，specimen 6 was fitted with 1/4 stiffening rings，and specimen 9 was fitted without stiffening rings. The load-displacement（WYJ1）curves of these specimens in this group are showing in Figure 8.

Test results of specimen 3，6，9 were listed in table 4.

TABLE 4   TEST RESULTS OF SPECIMEN 3，6，9

Specimen number	Design bearing capacity and the corresponding deformation		Ultimate bearing capacity and the corresponding deformation	
	Deformation/mm	Load/kN	Deformation/mm	Load/kN
3	4.8	427.28	9.765	455.48
6	4.8	346.26	12.135	385.81
9	4.8	285.89	6.86	299.35

From the test results，it is easily found that the design bearing capacity of specimen 3 is bigger than specimen 6 by 81.02 kN，and specimen 6 is bigger than specimen 9 by 60.37 kN.

Figure 8   Load-displacement (WYJ1) curves of specimen 3, 6, and 9

For the ultimate bearing capacity, specimen 3 is bigger than specimen 6 by 69.67 kN, and specimen 6 is bigger than specimen 9 by 86.46 kN.

CONCLUSIONS AND SUGGESTIONS

In this test, the width of all stiffening rings is 60 mm and the thickness is 5 mm. It is observed that the different shape of stiffening ring has significant influence on the bearing capacity of specimens. Setting stiffening ring can enhance the bearing capacity, because the stiffening ring can restrict the local deformation of the tube wall, reduce the stress concentration, extend the plastic region, and increase the lateral rigidity of the plate in some degree.

ACKNOWLEDGEMENTS

REFERENCES

[1] Wang, X. Y., "Research of Large—Size Steel Tubular K-joints", Southeast University, 2001, pp. 56.
[2] Wu, Z. Y. and Zhang, Y. C., "A formula of inclined yield line for T-type RHS joints under axial force", Civil Engineering Journal, 2002, 35(4), pp. 20 − 24. (in Chinese)
[3] Zhao, X. L., "Deformation limit and ultimate strength of welded T-joints in cold-formed RHS sections", Journal of Constructional Steel Research, 2000, 53, pp. 149 − 165.

FEM-ANALYSIS OF BEAM-COLUMN RIGID JOINTS TRANSFERRING FORCES OUTSIDE BOX COLUMNS

* Z. G. Xu[1] , D. R. Cheng[1] , C. G. Deng[2]

[1] Faculty of Civil Engineering，Guangzhou University，WaiHuanXi Road 230 of Mega-center，Guangzhou，510006，China
[2] Faculty of structural engineering，Tongji University，Siping Road 1239，Shanghai，200092，China
* Email：xuzhonggen@263. net

KEYWORDS

Beam-column joint，plates to transfer force，stress，strain，carrying capacity，load-displacement curve，retrofitting，inventing patent.

ABSTRACT

After finishing a retrofitting project，we got a inventing patent of a new kind of beam-column rigid joints （Patent number：ZL 2007 1 0028454. X）. In this paper，3D FEA-models were built up for the specimen of beam-column rigid joints transferring forces outside box columns without inner diaphragms. Displacement variation and the distribution of stress of the new beam-column joints under static loads are calculated. The joint failure mechanism is analyzed. In addition，by comparing of joints with the adding plates or not，and several beam-column rigid joints transferring forces outside steel columns are calculated. To compare the ultimate bearing capacities of joints of different axial compressive forces of columns，different thickness and width of adding plates on the ultimate strength are considered. The research indicates that the main distribution of stresses are not concentrated on beam-column joints，and the main stress transfer to adding plates and beam-flanges，and the stresses of beam-column joints are small. In the same static loads，the steel columns of beam-column rigid joints transferring forces outside steel column have no displacement. So the adding plates make stresses of the connection zone to be less，and to transfer forces outside steel columns. In addition，the ultimate bearing capacities of beam-column rigid joints transferring forces outside steel column are obviously higher than relating traditional beam-column rigid joints without inner diaphragms. The results show that thickness or width of adding plates can be taken as to equal to thickness or width of beam-flanges. If the thickness or width of the adding plates is too small，the transferring forces outside steel columns are small and their bearing capacities are small，and easy to destroy. When thickness or width of plates is greater than thickness or width of beam-flanges，the effect of adding plates is not obvious. This kind of joints can be used to some retrofit projects.

INTRODUCTION

Being connections of elements and key points of forces transforming，beam-column joints are important

parts of steel structures. The cost of beam-column joints represents 30% of a steel structure, so research on beam-column joints is of great importance.

In North-Ridge Earthquake (U. S.)[1], which took place at January 17, 1994, and Kobe Earthquake (Japan), which took place at January 17, 1995, there are many beam-column joints damaged. After that, the mechanics characters of beam-column joints and seismic performances of structures are paid more attention to. In order to avoid beam-columns joints being damaged, an effective method is to make the plastic hinges to take place out of the beam-column joints by reinforcing ends of beams or weakening cross section of beams[2–5]. That is to improve the performance of steel moment resistant frame connections, by improving strength of joints with cover plates or adding webs, or by reducing bending capabilities of beams connecting to the joints with weakened flanges or webs.

After a retrofitting project, a new type of beam-column joints by transforming forces outside the box columns is introduced in this paper[6]. There are no inner diaphragms in the box column of this type of joint. Adding plates are welded to connect beam flanges and are used to transforming forces of these flanges.

CHARACTERISTICS OF A NEW TYPE OF BEAM-COLUMN JOINTS WITHOUT INNER DIAPHRAGM

A new type of beam-column joint[6], with plates connecting the upper flanges of neighboring horizontal beams or the lower flanges of neighboring horizontal beams, is introduced. In a retrofitting project, in fact it is a new building, when the multi-story steel frame was almost built up, a box column was found to be set one meter higher than required level. On its roof, this column was standing out for one meter. At beginning, the workers do not know why. They all thought the column was too long. But later they found that the column was set at wrong level from its basement. That is, every beam was connected at wrong places of the column, without inner diaphragms to connect flanges of beams. In order to solve this problem, we found this type of beam-column joint and we have finished retrofitting the building.

As shown in Figure 1, around the box column 1, there are four horizontal beams 2. There are some adding plates 3a connecting the upper flanges of neighboring horizontal beams and some adding plates 3b connecting the down flanges of neighboring horizontal beams. The section of horizontal beams is H-section. The adding plates are welded to the upper flanges of the beams or to the down flanges of the beams.
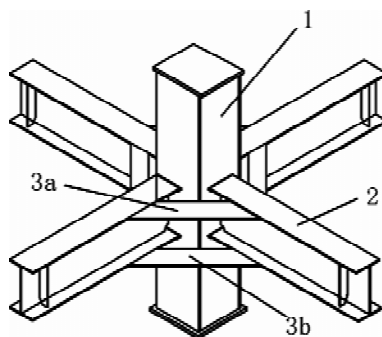
Figure 1　Three dimensional view of the new beam-column joint without inner diaphragm[2]

FINITE ELEMENT ANALYSIS

Design of the Test Member

Regulation of joint zone[7]

According to Chinese regulations，web stability check of joint zone is as Eqn. 1.

$$t_p \geqslant (h_b + h_c)/90 \tag{1}$$

Yielding carrying capacity of joint zone is as Eqn. 2.

$$\frac{\psi(M_{pb1} + M_{pb2})}{V_p} \leqslant \frac{4}{3} f_v \tag{2}$$

Where，t_p is the thickness of the joint zone. h_b is height of the beam section. h_c is height of the web height of the column. Ψ is reduction factor. M_{pb1} and M_{pb2} are full plastic bending capacity of the beams at both side of the joint zone. V_p is the volume of the joint zone. f_v is design value of shear strength of the joint zone.

Maximum carrying capacity of a joint

Maximum carrying capacity of a joint is checked as Eqn. 3 and Eqn. 4.

$$M_u \geqslant 1.2M_p \tag{3}$$

$$V_u \geqslant 1.3(2M_p/l_n) \text{ and } V_u \geqslant 0.58h_w t_w f_{ay} \tag{4}$$

Where，M_u is ultimate bending capacity of a beam with its upper flange and lower flange by full penetration slope welding. V_u is ultimate shearing capacity of a beam web. M_p is the full plastic bending capacity of a beam. l_n is the net span of a beam. h_w is web height of the beam. t_w is the web thickness of the beam. f_{ay} is yielding strength.

Regulation of re-enforcement of columns and weakening of beams

Under seismic action，in order not to let the columns be damaged earlier than beams，and let plastic hinges to be formed at beams，and keep the column in elastic stag，Chinese seismic code regulates as Eqn. 5.

$$\sum W_{pc}(f_{yc} - N/A_c) \geqslant \eta \sum W_{pb} f_{yb} \tag{5}$$

Where，η is column re-enforcing factor. W_{pc} and W_{pb} are plastic section modulus of column and beam respectively. f_{yb} and f_{yc} are yielding strength of beam and column respectively. N is axial force of the column. A_c is cross section area of the column.

Joint's Parameters

Several joints are designed according to a real project. These joints are made with H-beams and box columns by Q235 steel. Width and thickness of the force-transforming plates are same with those of beam flanges. There are no inner diaphragms in the box columns. Size of beam is H250×125×6×9，and four

beams in a joint are with the same cross section. Size of the column is $200 \times 200 \times 8$. The material is taken as ideal isotropic elastic-plastic material.

Joint's Material Mechanics Model

The material is taken as Q235. Considering geometric and material mechanics non-linearity，multi-line isotropic strengthened model is used. Its elastic modular is taken as 2.06×10^5 MPa and its Poisson's ratio is taken as 0.3.

Selection of Joint Elements and Netting

With ANSYS program，when a joint model is being built，solid element SOLID45 with 8 nodes is chose for elements far apart the joint and solid element SOLID95 with 20 nodes is chose for elements of joints and beam ends. Elements of force-transforming plates are also use SOLID95. Joint elements netting is shown in Figure 2.
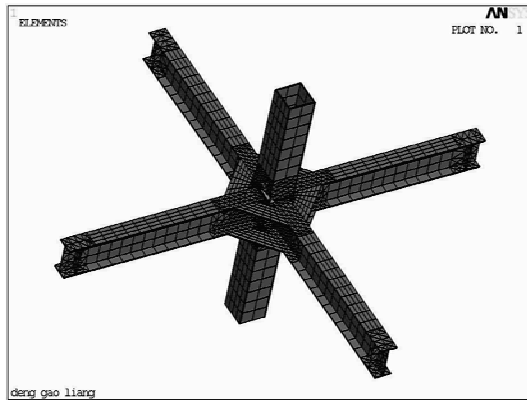
Figure 2   Finite elements netting of the joint

Restraint and Loading

When adding restraint to the model，lower end of the joint was added restraints along X，Y and Z direction. On top of the joint，restraints were added along X and Y direction. Side restraints were added to the four beams to prevent out of plan buckling. Concentrated forces were added on top of four beams where stiffeners located. Axial force was added uniformly and vertically on top of the column.

ANALYSIS OF FINITE ELEMENT METHOD

Comparison of Joints with and without Force-transforming Plates

In order to show performance difference of the joints with and without force-transforming plates，with models described above，calculation was carried out. Load-displacement curves are shown in Figure 3.

Obviously，stiffness，strength，yielding stress and ultimate carrying capacity of the joint with force-transforming plates are increased greatly. For joint with force-transforming plates，when the load is
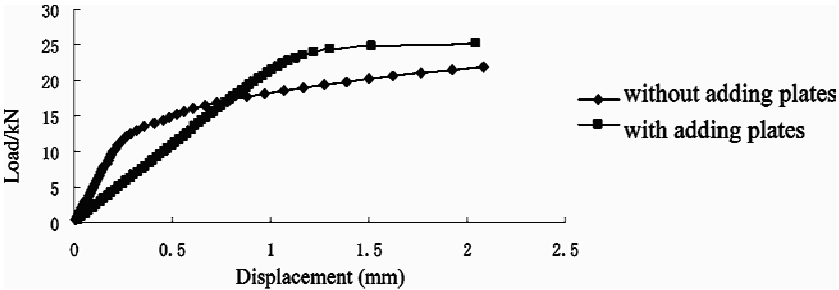
Figure 3   Load-displacement curve of the reference point of the joint

increased from 0 to 23.52 kN，the joint is maintained in linear elastic area. When the load is more than 23.52 kN，plastic deformation takes place，and its displacement increases quickly，until the load gets to its highest point 25.2 kN，that is its ultimate carrying capacity. But for the joint without force-transforming plates，its yielding load is only 12.6 kN，which decreased for 46.4%.

Stress distributions of the joints without and with force-transforming plates are shown in Figure 4 and Figure 5 respectively.
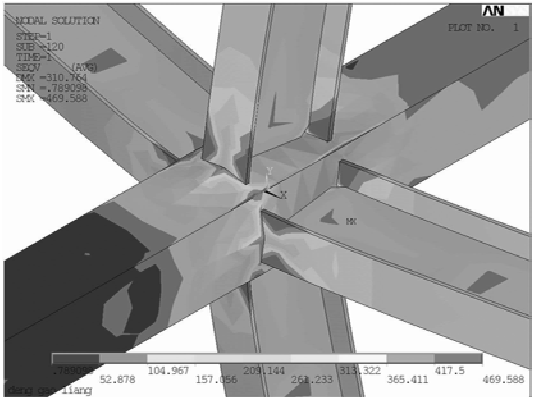
Figure 4   Distribution of Von-Mises stress of the joint without inner diaphragm
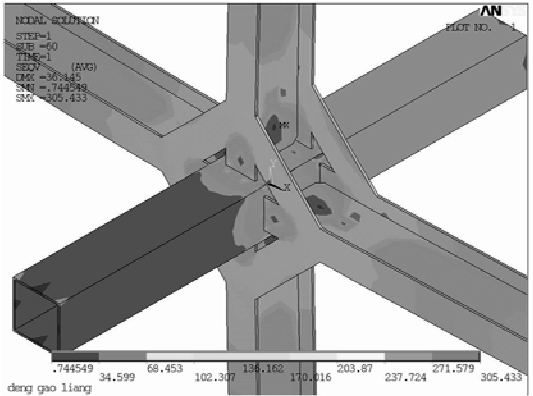
Figure 5   Distribution of Von-Mises stress of the joint transferring force outside column

It is shown in the Figure 4 that because of great tension and shearing coming from horizontal beams，walls of steel columns deformed seriously and damaged with its stresses concentrated mostly on the connection parts. As shown in Figure 5，because of force-transforming plates，stresses distribution of joint zone are improved obviously，with smaller stresses and more even distributed. And the main stresses of the joint are no long concentrated at connection parts of the beams and column，but changed to force-transforming plates and connection parts of the beams and the pates. Stresses of connection parts of beams and column are much smaller. Under the same loading condition，walls of the steel column have no side deformation. So the force-transforming plates can improve stresses condition of the joint zone，and force-transforming outside the column is realized.

In order to show more clearly stresses distributions of different parts，three paths（Path 1 is in the middle of right beam flange，path 2 is the left end of right beam flange，path 3 is the left end of the right beam web）are defined on the test member as shown in Figure 6. Under vertical load of 24. 9 kN，stress distributions along these three paths are shown in Figure 7，Figure 8 and Figure 9 respectively.
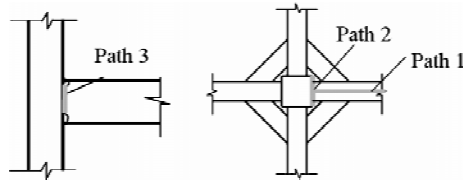
Figure 6   Three paths of the joint
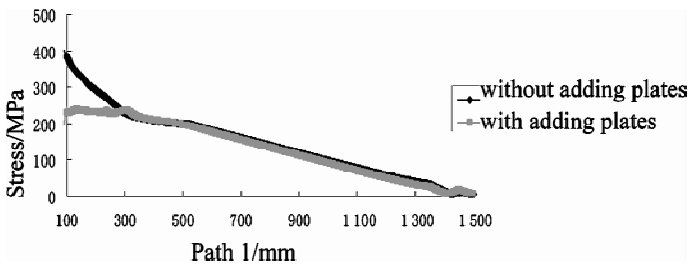
Figure 7   Von -Mises stress distribution of path 1
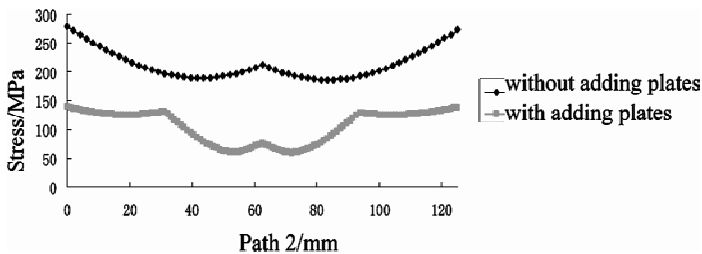
Figure 8   Von -Mises stress distribution of path 2

We can see from Figure 7，Figure 8 and Figure 9 that after reinforced by welding force-transforming plates，stresses distribution of joint zone is changed，and stresses at connection of beams and column are greatly reduced. Along path 2 which is transverse to the beam，stresses are symmetrically distributed，and the maximum stresses are at two ends. Beam ends' stresses of joint without force-transforming plates are
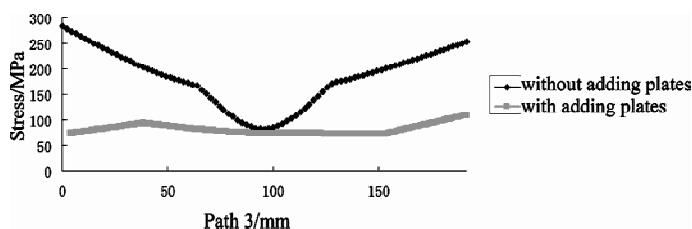
Figure 9   Von -Mises stress distribution of path 3

already got to its yielding stress，but those of joint with force-transforming plates are only 40%. Along path 3 which is along web height direction of a beam，stresses are smaller in the middle and greater at two ends. For joint with force-transforming plates，stresses are distributed more evenly without so great concentration. So with the force-transforming plates，stresses distribution is changed and the joint's carrying capacity is increased.

CONCLUSION

With a finite-element-method program ANSYS，beam-column welding joints with and without force-transforming plates under different columns' axial forces are analyzed，then following conclusions can be drawn.

（1）The main distribution of stresses are not concentrated on beam-column joints，and the main stress transfer to adding plates and beam-flanges，and the stresses of beam-column joints are small. In the same static loads，the steel columns of beam-column rigid joints transferring forces outside steel column have no displacement. In the same static loads，the steel columns of beam-column rigid joints transferring forces outside steel column have no displacement. So the adding plates make stresses of the connection zone to be less，and to transfer forces outside steel columns.

（2）In addition，the ultimate bearing capacities of beam-column rigid joints transferring forces outside steel column are obviously higher than relating traditional beam-column rigid joints without inner diaphragms.

（3）Thickness or width of adding plates can be taken as to equal to thickness or width of beam-flanges. If the thickness or width of the adding plates is too small，the transferring forces outside steel columns are small and their bearing capacities are small，and easy to destroy. When thickness or width of plates is greater than thickness or width of beam-flanges，the effect of adding plates is not obvious.

（4）This kind of joints can be used to some retrofit projects.

REFERENCES

［1］FEMA－355D. "State of the art report on connection performance of steel moment frames subject to earthquake ground shaking". Prepared by the SAC Joint Venture for the Federal Emergency Agency，Washington DC，2000. pp. 355–434.

［2］Dai，S. B.，Liu，W. J. and Huang J.，"Experimental research on working behavior of dog-bone style rigid

connection joints". Journal of Wuhan University of Technology，2004，26(12)：56-58.(in Chinese)

［3］Zhang，X. and Ricles，J. "Seismic behavior of reduced beam section moment connections to deep columns"，Journal of Structural Engineering，2006，132(3)：358-367.

［4］Chen，J. and Su M. Z.，"Experimental study on steel moment resistant frame connections with welded flange plates"，Journal of Building Structures，2007，28(3)：1-7.(in Chinese)

［5］Xie，X. D.，Yang N. and Yang Q. S.，"Parameter analysis of steel reduced web connection"，Industrial construction，2006，36(5)：79.（in Chinese）

［6］Xu，Z. G. and Wang，X. T.，"A steel frame beam-column joint of rectangular steel tube column". China：ZL 2007 1 0028454. X(Invent Patent).(in Chinese)

［7］GB 50011—2010，"Code for Seismic Design of Building". Beijing：China Architecture and Building Press，2010.（in Chinese）

TRANSMISSION OF WARPING THROGH JOINTS OF STEEL FRAMES

* S. Shayan，K. J. R. Rasmussen and H. Zhang

School of Civil Engineering，University of Sydney，Sydney，NSW 2006，Australia
* Email：shabnam. shayan@sydney. edu. au

KEYWORDS

Warping，thin-walled structures，warping spring，substructure，finite element analysis.

ABSTRACT

Thin-walled steel moment frames are often used in construction and engineering practice. Since these frames are composed from open section members with low torsional stiffness，the members are likely to experience warping deformations. At joints，warping displacements in one member may redistribute and produce warping and twisting in other attached members. This behaviour can be accurately captured at the expense of substantial computational effort by discretising the entire frame using shell finite elements. However，for one-dimensional beam finite elements，the development of a suitable model to incorporate the effects of warping restraint and partial transmission through the joint is a complex task.

A simple theory is developed in this paper which considers the effect of warping continuity through the joint of thin-walled steel frames when using beam finite element analysis. The suggested model can readily be implemented into conventional types of analysis without the need to modify the stiffness matrix or employ shell finite element analysis，which requires greater computational effort. Using a condensed stiffness matrix generated by the substructuring technique，warping springs are introduced to represent the condition of partial warping restraint at intersections between members. The general theory of static condensation，which is the basis of substructuring，is briefly described in this study. For validation purposes，the performance of the proposed model is demonstrated by a number of numerical examples. Excellent agreement is achieved between the results of beam finite element analysis using the suggested joint model and accurate shell finite element analysis.

INTRODUCTION

A brief overview of the literature on the transmission of warping through joints of thin-walled steel frames shows that all suggested models need substantial numerical or computational effort（Krenk and Damkilde[1]，Tong et al.[2] and Masarira[3]）. Due to the complexity of current models，the partial transmission of warping through the joint is ignored in most design cases. Even if a designer wanted to consider transmission of warping through joints，available commercial finite element softwares are limited

to either completely prevent warping or allow warping to occur freely at joints when using beam finite element analysis（B-FEA）. At this point in time，there is no FE software available that allows the seventh degree of freedom（warping）to be partially prevented. The only option to model warping accurately is using shell element which is not a desired method for complex structures due to its high computational cost.

The present study is concerned with developing a new method for modelling joints including warping effects，benefiting from the accuracy of 3D finite element modelling and from the computational efficiency of using 1D beam elements. A new joint model is developed with the help of the substructuring technique and linear springs. The joint accepts warping deformations from adjoining loaded members and redistributes the deformation to all connected beams and columns. In fact，the suggested joint model acts as a flexible interface between members and provides partial warping restraint by means of springs. The model is general and can be applied to any kind of joint in thin-walled structural frames.

SUBSTRUCTURING AND STATIC CONDENSATION

Substructuring is a technique commonly used to overcome the difficulty of working with large dimensional problems. The basic idea of substructuring analysis is that only certain degrees of freedom are retained while others are eliminated by static condensation. In partitioned matrix form，the equation between forces and displacements can be written as

$$\begin{bmatrix} \mathbf{K}_{rr} & \mathbf{K}_{re} \\ \mathbf{K}_{er} & \mathbf{K}_{ee} \end{bmatrix} \begin{bmatrix} \mathbf{u}_r \\ \mathbf{u}_e \end{bmatrix} = \begin{bmatrix} \mathbf{F}_r \\ \mathbf{F}_e \end{bmatrix} \tag{1}$$

in which $\mathbf{u}_r$，$\mathbf{u}_e$，$\mathbf{F}_r$ and $\mathbf{F}_e$ are displacements and forces of retained and eliminated DOFs respectively and $\mathbf{K}$'s are stiffness sub-matrices. Solving the second set of Eqn. 1 with respect to the eliminated DOFs（$\mathbf{u}_e$）the expression of Eqn. 2 may be obtained：

$$\mathbf{u}_e = \mathbf{K}_{ee}^{-1}(\mathbf{F}_e - \mathbf{K}_{er}\,\mathbf{u}_r) \tag{2}$$

The condensed equilibrium equation can be written by substituting Eqn. 2 into the first set of Eqn. 1：

$$(\mathbf{K}_{rr} - \mathbf{K}_{re}\mathbf{K}_{ee}^{-1}\mathbf{K}_{er})\mathbf{u}_r = (\mathbf{F}_r - \mathbf{K}_{re}\mathbf{K}_{ee}^{-1}\mathbf{F}_e) \tag{3}$$

After application of static condensation only the retained degrees of freedom are present in stiffness equations（Han[4]）.

JOINT MODEL

ABAQUS[5] is used in this study for creating numerical models. The beam finite element（B31OS）has 7 DOFs of which the seventh is warping. The joint is modelled by S4R shell elements as a substructure in the same way that any structural model may be created. The warping deformation must then be mapped into joint deformations by a series of constraint equations which tie the longitudinal displacement of one corner node to the longitudinal displacements of other corner nodes on the same face so as to represent a warping displacement in the direction of the attached beam（Figure 1（a））. For sections composed of three plate elements（e. g. I-sections），this requires three constraint equations for each face. For each connected face，one degree of freedom，which is chosen as the longitudinal displacement of a corner node （e. g. node H in Figure 1（a）），is retained. The number of degrees of freedom retained in the substructuring process depends on the number of adjoining beams and columns. A warping deformation of

the beam will cause a compatible deformation at each corner of the connected face of the joint, as shown in Figure 1(b). The joint itself is analysed using the ABAQUS * SUBSTRUCTURE GENERATE command. Currently, substructure modelling is not supported by ABAQUS/CAE[5]; thus a PERL script was written to generate the joint model.
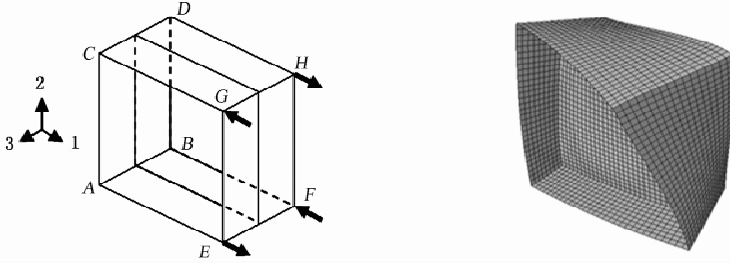

Figure 1   (a) Displacements to generate a single warping degree of freedom,
(b) Joint deformations due to applied warping

For the particular corner joint consisting of one beam and one column, the condensed stiffness matrix has four components: one for the warping degree of freedom of the vertical face connected to the beam (K_{BB}), another one for the warping degree of freedom of the horizontal face attached to the column (K_{CC}) and two off-diagonal components to represent interaction between those warping degrees of freedom (K_{BC} and K_{CB}). The general form of the stiffness matrix for the substructure after condensation is:

$$\boldsymbol{K}_{ss} = \begin{bmatrix} K_{BB} & K_{BC} \\ K_{CB} & K_{CC} \end{bmatrix} \quad \text{where } K_{BC} = K_{CB} \tag{4}$$

As the retained degrees of freedom are longitudinal displacements, their multiplication by the stiffness matrix produces forces while the corresponding terms for the warping DOFs are bimoments. Thus the relation between forces ($\boldsymbol{F}$) and longitudinal displacements ($\boldsymbol{u}$) (Eqn. 5) needs to be converted to a relation between bimoments ($\boldsymbol{B}$) and warping deformations ($\boldsymbol{\varphi}'$) (Eqn. 6), in which $\boldsymbol{K}_{sp}$ is the spring stiffness matrix.

$$\boldsymbol{F} = \boldsymbol{K}_{ss}\boldsymbol{u} \tag{5}$$

$$\boldsymbol{B} = \boldsymbol{K}_{sp}\boldsymbol{\varphi}' \tag{6}$$

Bearing in mind that a warping deformation may be produced by applying four axial forces to the flange tips (see Figure 1), the bimoment matrix may be expressed by Eqn. 7:

$$\boldsymbol{B} = \boldsymbol{F}bh \tag{7}$$

where b is the flange width and h the section height. The warping displacement matrix ($\boldsymbol{\varphi}'$) can also be defined as:

$$\boldsymbol{\varphi}' = \boldsymbol{u}/\overline{w} \tag{8}$$

in which $\overline{w}$ is the sectorial coordinate of the flange tips. Substituting Eqns 5 and 6 into Eqns 7 and 8 results in:

$$\boldsymbol{K}_{sp} = \begin{bmatrix} \overline{K}_{BB} & \overline{K}_{BC} \\ \overline{K}_{CB} & \overline{K}_{CC} \end{bmatrix} = \boldsymbol{K}_{ss}(bh\,\overline{w}) \tag{9}$$

where $\overline{K}$'s are stiffness terms. Once the converted stiffness matrix is formulated, it can be applied to the beam finite element model. Ordinarily, this would be achieved using spring elements. However, in

ABAQUS[5], spring elements can only be linked to translations and rotations (i.e. the first six degrees of freedom), while there is no direct way of relating spring elements to the warping degree of freedom. Therefore, an indirect method of connecting springs to the seventh DOF is proposed. The model consists of using a combination of a spring and a linear constraint equation for each member connected to the joint. For the particular corner joint shown in Figure 1, two springs and two constraint equations are needed. The relation between warping and bimoment in the corner joint takes the form,

$$\boldsymbol{K}_{sp}\boldsymbol{\varphi}' = \begin{bmatrix} \overline{K}_{BB} & \overline{K}_{BC} \\ \overline{K}_{CB} & \overline{K}_{CC} \end{bmatrix} \begin{Bmatrix} \varphi'_B \\ \varphi'_C \end{Bmatrix} = \begin{Bmatrix} B_B \\ B_C \end{Bmatrix} \tag{10}$$

where (φ'_B, φ'_C) and (B_B, B_C) are warping and bimoments respectively of beams and columns. To obtain the required linear constraint equations, the first diagonal stiffness term is considered as a fixed value ($\overline{K}_{BB}$) and the other terms are written as a fraction of that term. For example, for the present case $\overline{K}_{BB}$ is used as the fixed value and the stiffness matrix is changed to

$$\boldsymbol{K}_{sp} = \begin{bmatrix} \overline{K}_{BB} & a_1 \overline{K}_{BB} \\ a_2 \overline{K}_{BB} & a_3 \overline{K}_{BB} \end{bmatrix} \tag{11}$$

Substituting the new matrix into Eqn. 10 gives:

$$\begin{cases} \overline{K}_{BB}(\varphi'_B + a_1 \varphi'_C) = B_B \\ \overline{K}_{BB}(a_2 \varphi'_B + a_3 \varphi'_C) = B_C \end{cases} \tag{12}$$

where $\overline{K}_{BB}$ represents stiffness, (B_B and B_C) are bimoments and the terms in round brackets are warping displacements which must be tied to the linear displacements of the springs by using constraint equations in ABAQUS[5] (see Eqn. 13). In Eqn. 13, the terms U_B^7 and U_C^7 are the warping degrees of freedom of the beam and column respectively, while u_b^1 and u_c^2 are linear spring displacements in DOF directions 1 and 2 respectively. It is obvious that the stiffness of all springs should be same and equal to $\overline{K}_{BB}$ (see Figure 2).

$$\begin{cases} U_B^7 + a_1 U_C^7 = u_b^1 \\ a_2 U_B^7 + a_3 U_C^7 = u_c^2 \end{cases} \tag{13}$$

Keeping in mind that the frame should be modelled in such a way that separate nodes are used for the adjoining members at the joint and that these nodes are located at the perimeter of the joint, then, new "dummy" nodes are created near the ends of the adjoining elements and springs are attached to these nodes (Figure 2(a)). The SPRING2 element of the ABAQUS library[5] is used to represent the warping stiffness. While the seventh DOF (warping) is partially transferred using the presented spring model, the other six DOFs are transmitted directly and rigidly between members connected to the joint. That is, the joint is considered to be rigid with respect to rotation and translation (Figure 2(b)).
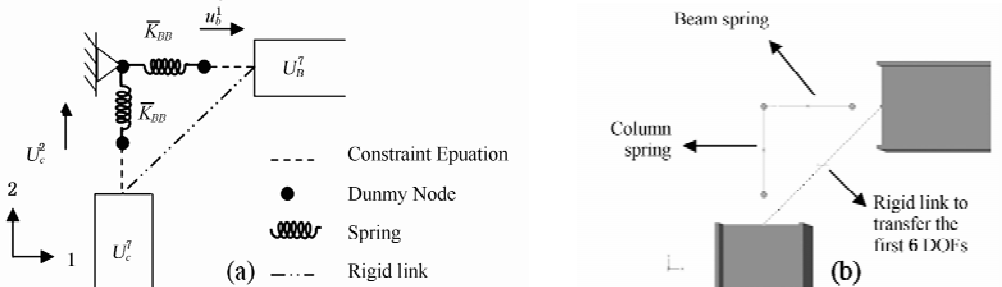
Figure 2   Joint spring model: (a) sketch, (b) ABAQUS

VERIFICATION AND ILLUSTRATIVE EXAMPLES

In order to evaluate the accuracy and capability of the proposed joint model，three thin-walled steel frames have been analysed using the model in conjunction with one-dimensional beam elements and compared with results for the same frames obtained using 3D shell elements. All frames are made of steel I-sections with elastic modulus（*E*）equal to 200 GPa and Poisson's ratio equal to 0.3. All sections are considered to be compact so as to preclude local deformations. The column bases are fully fixed and the joints are laterally restrained to prevent out-of-plane displacements. For this study，three dimensional beam elements with 7 DOFs per node（B31OS）and S8R shell elements are used. The shell finite element analyses are based on discretisations of the flanges and webs into 4 and 6 elements respectively while the length of each element in the beam analyses is taken as 25 mm.

L-Shape Plane Frame

The first study illustrates the buckling and elastic behaviour of the L-shape steel frame shown in Figure 3，which has only one beam and one column meeting at the joint. Three different types of joint have been considered：（a）box joint，（b）box joint with one diagonal stiffener and（c）box joint with two diagonal stiffeners. The beam and column are made from 150UB14 section（http：//www.onesteel.com）and a vertical point load *P* equal to 10 kN is applied to the shear centre at the end of the beam.
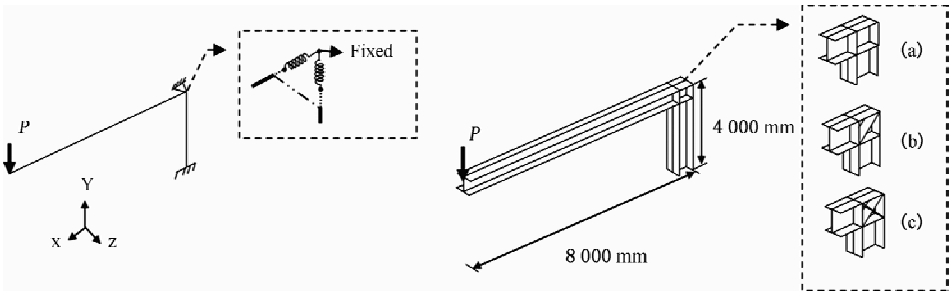
Figure 3　Configuration and dimension of L-shape plane frame

Table 1 shows the spring stiffness and the bimoments in the adjoining members. The spring stiffness increases as stiffeners are added to the joint. The warping transmission is complete and inverse for the box joint（a）and almost prevented for the box joints with one and two diagonal stiffeners（b and c），as confirmed by Basaglia et al.[6].

TABLE 1　SPRING STIFFNESS AND BIMOMENTS

	Spring Stiffness（$\overline{K}_{BB}$）	Beam Bimoment（N・mm²）	Column Bimoment（N・mm²）
Joint（a）	1.09E+13	5 510	4 473
Joint（b）	1.71E+13	11 875	1 081
Joint（c）	2.36E+13	12 179	1 340

The critical buckling loads obtained using beam（B-FEA）and shell（S-FEA）element based analyses for the three different joint configurations are summarised in Table 2. The maximum discrepancy is 1.8%，indicating good accuracy. It is worth noticing that the joint configuration influences the critical buckling load and that by adding two stiffeners to the joint，the buckling load is increased by 12% compared to the

frame with box-joint. Figure 4 further illustrate an excellent agreement between the load-deflection curves of the L-shape frame with box-joint using beam and shell element first order elastic analyses.
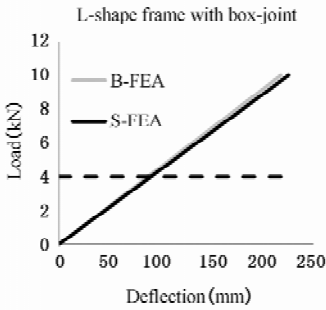
Figure 4　First order elastic analysis

TABLE 2　CRITICAL BUKLING LOAD（kN）

Joint configuration	Joint（a）	Joint（b）	Joint（c）
B-FEA	3.97	4.47	4.52
S-FEA	3.92	4.39	4.52
Error（%）	1.26	1.8	0

Plane Portal Frame with an Overhanging Member

A portal frame with an overhanging member has been studied. In addition to the corner joint considered in the previous example，the frame features an intermediate joint which connects three members. This example has been chosen to show that the method is general and does not depend on the number of adjoining members. The frame configuration and joint types can be seen in Figure 5. Once again，an excellent agreement is achieved between the critical buckling loads obtained from the beam and shell element analyses（Table 3）. The largest error is 2.3% which relates to the box joint with one diagonal stiffener. Similar to the previous example，changing the joint configuration from a box joint to box joints with one and two diagonal stiffener increases the critical buckling load by 11.5% and 12% respectively.
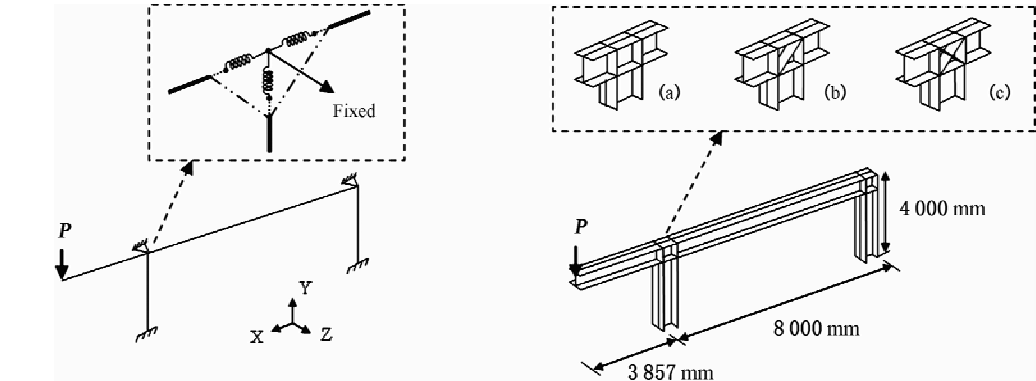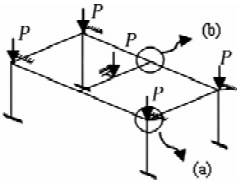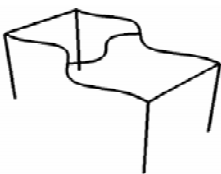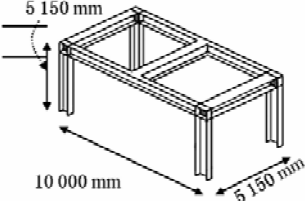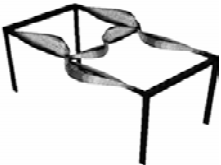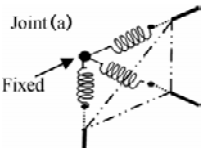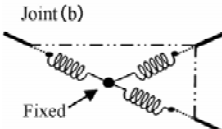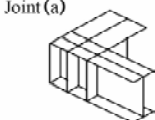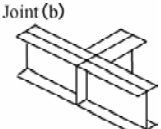
Figure 5　Configuration and dimension of plane portal frame with an overhanging member

TABLE 3　CRITICAL BUKLING LOAD（kN）

Joint configuration	Joint（a）	Joint（b）	Joint（c）
B-FEA	7.28	8.19	8.27
S-FEA	7.25	8	8.25
Error（%）	0.41	2.3	0.24

Space Frame

The space frame presented in Table 4 has been analysed using beam and shell finite elements to show that the proposed method can be extended to 3D models. All members have the same I-300×8 cross-section with a width of 150 mm，height of 300 mm and thickness of 8 mm except the two end beams for which the flange width is 300 mm. Five equal point loads P are applied at the top of the columns and the mid-span of the transverse beam at the centre. The frame features two types of joint：(a) beam-column joint and（b）beam-beam joint. Warping through the joints can be modelled by the use of three springs and three constraint equations in the beam finite element analysis. Table 4 shows the frame configuration，critical buckling shape and joint types for both B-FEA and S-FEA. The difference between the critical buckling loads obtained using the two types of analysis is 2.13%. The beams incur significant flexural-torsional buckling deformations which cause pronounced warping of the joints，so the performance of the joint model is well tested by this example.

TABLE 4 CONFIGURATION, BUCKLING SHAPE AND JOINT TYPE OF SPACE FRAME

B-FEA	S-FEA
Critical buckling load = 350.30 kN	Critical buckling load = 342.83 kN

CONCLUSION

This paper outlines an accurate new joint model for use in beam finite element analysis considering the effect of warping and its transmission between connected members. The suggested model can be easily implemented into frame type analyses without the need for modifying stiffness matrices or using complete shell finite element discretisation which requires greater computational effort. The introduction of warping springs provides a simple and accurate estimate of the joint warping stiffness in one-dimensional beam finite element analysis. The model is general and applicable to any type of joint. Three different frames have been analysed to evaluate the performance and capability of the proposed joint model. Excellent agreement has been achieved comparing the critical elastic buckling loads of these frames with values obtained using shell finite element analysis.

REFERENCES

［1］Krenk，S. and Damkilde，L.，"Warping of Joints in I-Beam Assemblages"，Journal of Engineering Mechanics，

1991，117(11)，pp.2457-2474.

［2］Tong，G.S.，Yan，X.X. and Zhang，L.，"Warping and bimoment transmission through diagonally stiffened beam-to-column joints"，Journal of Constructional Steel Research，2005，61(6)，pp.749-763.

［3］Masarira，A.，"The effect of joints on the stability behaviour of steel frame beams"，Journal of Constructional Steel Research，2002，58(10)，pp.1375-1390.

［4］Han，T.Y. and Abel，J.F.，"Substructure condensation using modified decomposition"，International Journal for Numerical Methods in Engineering，1984，20，pp.1959-1964.

［5］ABAQUS，Inc. ABAQUS. Ver. 6.8. analysis user's manual，2009.

［6］Basaglia，C.，Camotim，D. and Silvestre，N.，"Kinematic models to simulate the torsion warping transmission at thin-walled steel frame joints"，Proceeding of the 4th International Conference of Steel & Composite Structures，Sydney，Australia，21-23 July 2010.

ANALYSIS OF INFLUENCING FACTORS FOR BEARING PERFORMANCE OF HIGH STRENGTH BOLTED CONNECTION IN STAINLESS STEEL WHICH CARRIED SHEAR FORCE

* J. Guan[1]，Y.Q. Wang[2]，Y. Zhang[1]，Y.J. Shi[2]

[1] School of Civil Engineering，Beijing Jiaotong University，Beijing，100044，China；
[2] Key Laboratory of Civil Engineering Safety and Durability of China Education Ministry，
Department of Civil Engineering，Tsinghua University，Beijing，100084，China.
* Email：guanjian2105@126.com

KEYWORDS

Stainless steel，bolt connection，bearing performance，finite element analysis，parameter analysis.

ABSTRACT

The application of stainless steel in buildings is a trend in civil engineering because of its corrosion resistance and good processing performance. However，there are few specifications or codes about stainless steel structure design in China，and the design theory and design method lags behind relatively. Stainless steel has obvious nonlinear performance，which should be considered of in the design. Cover plate connection is one of the bolted connections，which is an important form in steel structure. This paper analyzed the influencing factors for bearing performance of the bolted cover plate connection in stainless steel with finite element program ANSYS，and the values from tests and Euro code are compared. Also the effect of the factors for bearing strength of the bolt connection is discussed. Based on the results of the analysis，the bearing performance increased with the increase of the thickness of the plate，the diameter of the bolt and the end distance. When the bolt diameter and the end distance increase to some value，the effect reduces.

INTRODUCTION

Stainless steel started to be used in constructions in early 20th century in Europe. Recently stainless steel has become an important part in construction in Japan，Korea，western countries，etc. As of 2005 in Japan，according to incomplete statistics，the consumption of stainless steel is 300 000 tons，25 percent of the plate consumption. The use of stainless steel in constructions started late in China. However，it is becoming the optimal material in offshore structures because of its excellent corrosion resistance. The bolt connection is an important connection form in steel structures，including the cover plate

connection，T-stub connection，flange connection etc. Cover plate connection is easy to use. The load is transferred by plates in bearing and bolts in shear. The mechanical behaviour of the cover plate connection mobilizes the bolt shear，the bolt-hole bearing and net-section deformation[1]. An research on stainless steel bolted cover plate connections was carried out at the Civil Engineering Laboratory，Blaise Pascal University[2]. There is few research on bolt connections for stainless steel in our country，and there is no relevant structural specification. However，the annual output of stainless steel in China ranked first in the world. Thus more study ought to be needed for the connections for stainless steel. Figure 1 shows two kinds of cover plate bolt connections[1].

(a) Cover plate connection with one shear plane   (b) Cover plate connection with two shear planes
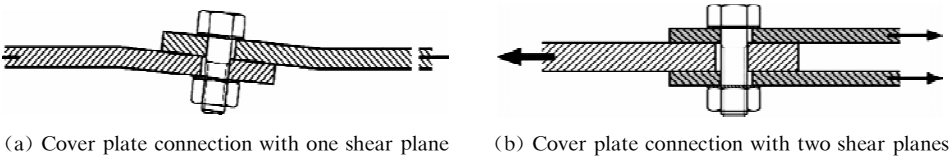
Figure 1   Cover plate bolt connections

In this paper，a finite element model is developed to discuss the bearing performance of the cover plate connection in two shear planes in stainless steel plates，in which the material of the cover plates is Q345 steel and inner plates are made of austenitic stainless steel 316 which is referred in[3] and[4]，including two kinds of thickness：6 mm and 8 mm. What's more，the comparison between austenitic stainless steel 1.440 1 from EN3-1-4 and austenitic stainless steel 316 tested from[3] is carried out in this paper.

FOUNDATION AND VERIFICATION FOR THE FE MODEL

Material Properties

Compared with carbon steel，stainless steel has significant nonlinear stress-strain relationship without a well defined yield stress as shown in Figure 2[5]. Consideration about the nonlinear performance to structures should be taken into the design.

The most widely used model for nonlinear material stress-strain behaviour is Ramberg-Osgood expression，given in Eqn.1，where E_0 is the material Young's modulus，$\sigma_{0.2}$ is the 0.2% proof stress，n is a strain hardening exponent which values 3~10 for stainless steel.

$$\varepsilon = \frac{\sigma}{E_0} + 0.002 \left(\frac{\sigma}{\sigma_{0.2}} \right)^n \tag{1}$$
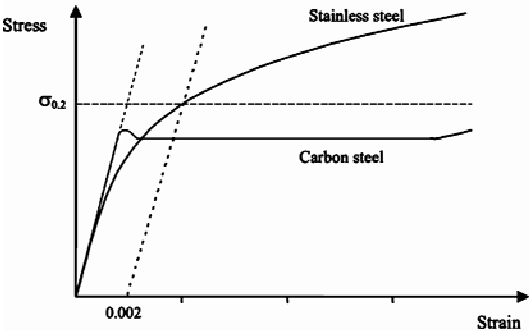
Figure 2   Stress-strain curves for carbon steel and stainless steel

However，Mirambell and Real[6] discovered the Ramberg-Osgood expression inaccuracies with the measured stress-strain data beyond the 0.2% proof stress. Some researchers modified the Ramberg-Osgood expression later. Gardner and Nethercot finally proposed to adopt the stress-strain relationship in Eqn. 2，where $\sigma_{1.0}$ is 1% proof stress，$E_{0.2}$ is the tangent stiffness at the 0.2% proof stress，$n'_{0.2, 1.0}$ is a strain hardening coefficient representing a curve that passes through $\sigma_{0.2}$ and $\sigma_{1.0}$. Besides，Eqn. 3 is proposed in EN3-1-4，where E_y is the tangent modulus of the stress-strain curve at yield strength defined，$E_y = E/(1+0.002nE/f_y)$，ε_u is the ultimate strain，$\varepsilon_u = 1-f_y/f_u$，$m$ is a coefficient calculated as $m = 1+3.5f_y/f_u$. In this paper，Eqn. 3 is adopted as the code value.

$$
\begin{cases}
\varepsilon = \dfrac{\sigma}{E_0} + 0.002 \left(\dfrac{\sigma}{\sigma_{0.2}}\right)^n, \ \sigma < \sigma_{0.2} \\
\varepsilon = \dfrac{(\sigma - \sigma_{0.2})}{E_{0.2}} + \left(0.008 - \dfrac{\sigma_{1.0} - \sigma_{0.2}}{E_{0.2}}\right) \left(\dfrac{\sigma - \sigma_{0.2}}{\sigma_{1.0} - \sigma_{0.2}}\right)^{n'_{0.2, 1.0}}, \ \sigma \geqslant \sigma_{0.2}
\end{cases}
\tag{2}
$$

$$
\begin{cases}
\varepsilon = \dfrac{\sigma}{E_0} + 0.002 \left(\dfrac{\sigma}{\sigma_{0.2}}\right)^n, \ \sigma \leqslant f_y \\
\varepsilon = 0.002 + \dfrac{f_y}{E} + \dfrac{\sigma - f_y}{E_y} + \varepsilon_u \left(\dfrac{\sigma - f_y}{f_u - f_y}\right)^m, \ f_y < \sigma \leqslant f_u
\end{cases}
\tag{3}
$$

Two kinds of stress-strain data are adopted in this paper：one is the code value from austenitic stainless steel 1.4401 in EN3-1-4，and the other is the test data from austenitic stainless steel 316 in[3]. Both the grades of 1.4401 and 316 correspond to grade 06Cr17Ni12Mo2 in GB/T 20878—2007. The main characteristic of the two kinds of material is given in Table 1.

TABLE 1 VALUES OF MATERIAL CHARACTERISTICS

Material	E/MPa	$f_{0.2}$/MPa	f_u/MPa	n
Test 316 ($t = 6$ mm)	182 000	279	595	7
Test 316 ($t = 8$ mm)	192 000	382	626	10
EN code 1.4401	200 000	220	520	6

Model Foundation

The finite element analysis software ANSYS11.0 was used to develop numerical models for cover plate bolted connections，seen in Figure 3，of which carbon steel Q345 is set for cover plates，stainless steel is for inner plates，and the bolts adopt 10.9 grade high strength bolts. The characteristic of stainless steel in the model values according to Table 1. The characteristics of cover plates and bolts are provided in Table 2. The 3D solid element SOLID92 and SOLID95 are used to model the plates and the bolts. CONTA174 and TARGEI170 are used to model the contact. Pretension which comes out by PRETS179 is applied though PSMESH order. Vov-Mises criterion is adopted as the yield criterion. Multi-linear hardening criterion is adopted as the hardening criterion.

TABLE 2 VALUES OF MATERIAL CHARACTERISTICS FOR COVER PLATES AND BOLTS

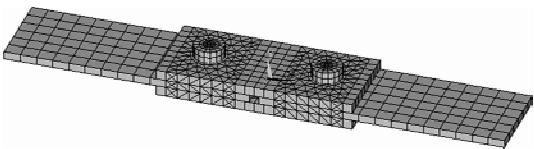| Grade	Use	f_y/MPa	f_u/MPa	E/MPa
Carbon steel Q345	Cover plates	345	500	2.01×10^5
High strength 10.9	bolts	995	1 160	2.01×10^5

Figure 3   Finite element model

FE Model Validation

Validation of the FE models was made against the test on bolted connections in aluminum alloy by Guixiang Zhang[7] . One series of test data was picked out to verify the FE model. The inner plates are from aluminum alloy 6061 - T6, $t = 3$ mm, and the cover plates are from carbon steel Q345, $t = 15$ mm. The diameter of the bolt is 16 mm. The end distance is $2.5d_0$.
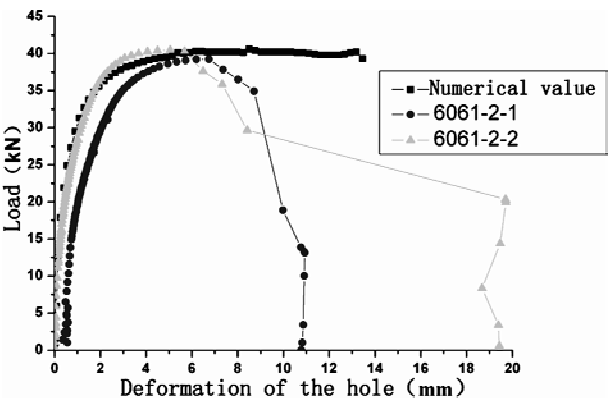

Figure 4   Load-deformation curves from tests and numerical models

According to Figure 4, before the fully plastic yield point, the FE model simulated the value of the test well. Therefore, the FE model could coincide with the experimental results well, which proved its correctness for the bearing performance of the cover plate bolted connection.

Parameter and Failure Criterion

The diameter of the bolt, the end distance and the thickness of the inner plate are selected as the parameters for the analysis. The size of the hole is 2 mm bigger than the diameter of the bolt according to EN3-1-4, $d_0 = d + 2$ mm. The value of the parameters is given in Table 3.

TABLE 3   VALUES OF THE PARAMETERS

Parameter	Value				
Diameter	12 mm	16 mm	20 mm	24 mm	—
End distance	2.0 d_0	2.5 d_0	3.0 d_0	3.5 d_0	4.0 d_0
Thickness	3 mm	6 mm	8 mm	10 mm	12 mm

There are two kinds of failure criterion for bearing performance of the bolt connection[7] :
Strength criterion: the load peak in the load-deformation curve in spite of the deformation
Deformation criterion: the load value when the deformation of the hole rises to some limit value

According to[8]，when the deformation of the bolt hole rises to 20% of d_0，the bearing performance is considered failure. Tests show that the level of the deformation could effectively represent the overall bearing performance of the connection.

PARAMETER ANALYSIS

Analysis for Ultimate Bearing Capacity

Shown in Figure 5，the dimensions are：(a) $d = 20$ mm，$2.5d_0$，$t = 3 \sim 12$ mm；(b) $d = 20$ mm，$t = 8$ mm，$2d_0 \sim 4d_0$；(c) $t = 8$ mm，$2.5d_0$，$d = 12 \sim 24$ mm.

According to Figure 5，the conclusions are：(1) The ultimate bearing capacity increases gradually with the increase of the stainless steel thickness as the end distance is $2.5d_0$ and $d = 20$ mm. As shown in Figure 5 (a). (2) The ultimate bearing capacity increases with the increase of the end distance as $d = 20$ mm and $t = 8$ mm. But when the end distance increases to $3.0d_0$，there is no obvious increase for bearing capacity. As shown in Figure 5(b). (3) The ultimate bearing capacity increases with the increase of the diameter of the bolt as the end distance is $2.5d_0$ and $t = 8$ mm. But when the diameter increases to 20 mm，the diameter is no longer the controlling factor for ultimate bearing capacity. As shown in Figure 5(c).

(a) Thickness

(b) End distance

(c) Diameter
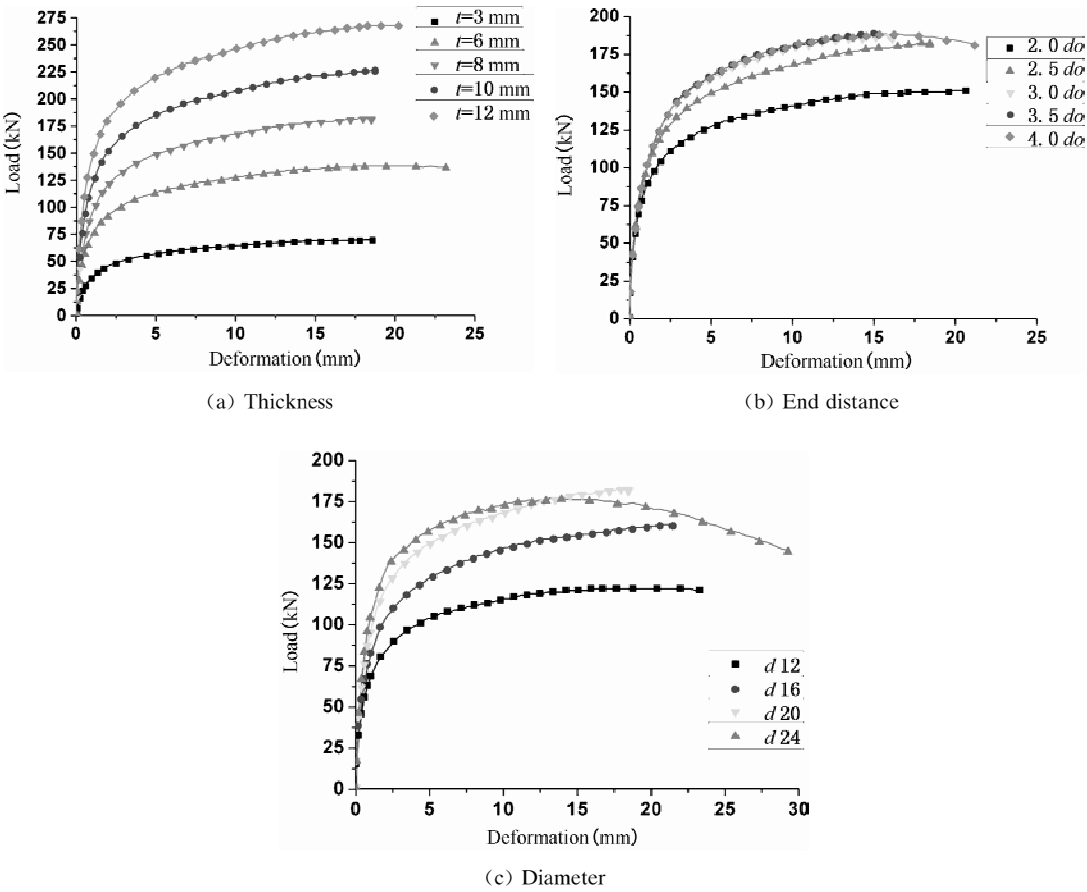
Figure 5 Load-hole deformation curves for different parameters with material data in EN3-1-4

(a) Thickness

(b) End distance

(c) Diameter
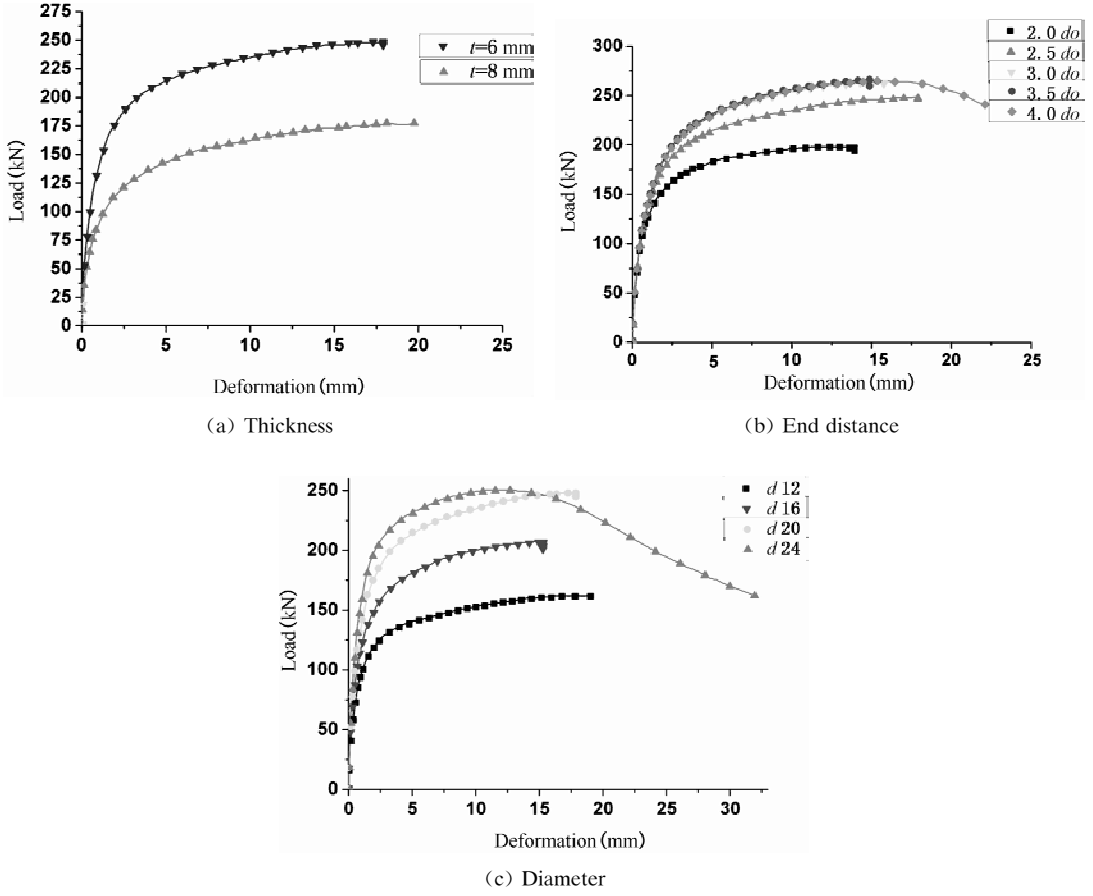
Figure 6   Load-hole deformation curves for different parameters with material data in test[3]

According to Figure 5 and 6，the conclusions are：（1）As $t = 6$ mm，the bearing capacity with the data from tests is 28.27% higher than that with data from EN3-1-4；As $t = 8$ mm，the capacity is 36.08% higher with tests than with EN3-1-4. That's because the mechanical property of 316 from EN3-1-4 and 1.4401 from tests are quite different from each other. （2）In spite of the difference from the mechanical property of the materials，the variation with the variation of the three parameters does not change.

Analysis for Deformation Bearing Capacity

According to[8]，the connection is considered to have failed when the hole deformation increase above 30% of the end distance in this paper.

Shown as Figure 7，the conclusions are：（1）The deformation bearing load increases linearly with the increase of the thickness of the stainless steel inner plate. As shown in Figure 7(a). （2）The deformation bearing load increases nonlinearly with the increase of the end distance. When the end distance increases above $3.0d_0$，there is no obvious increase for the bearing load. As shown in Figure 7(b). （3）The deformation bearing load increases almost linearly with the increase of the diameter of the bolt. When the diameter increases above 20 mm，the increase effect to bearing load reduces. As shown in Figure 7(c).

(a) Thickness

(b) End distance

(c) Diameter
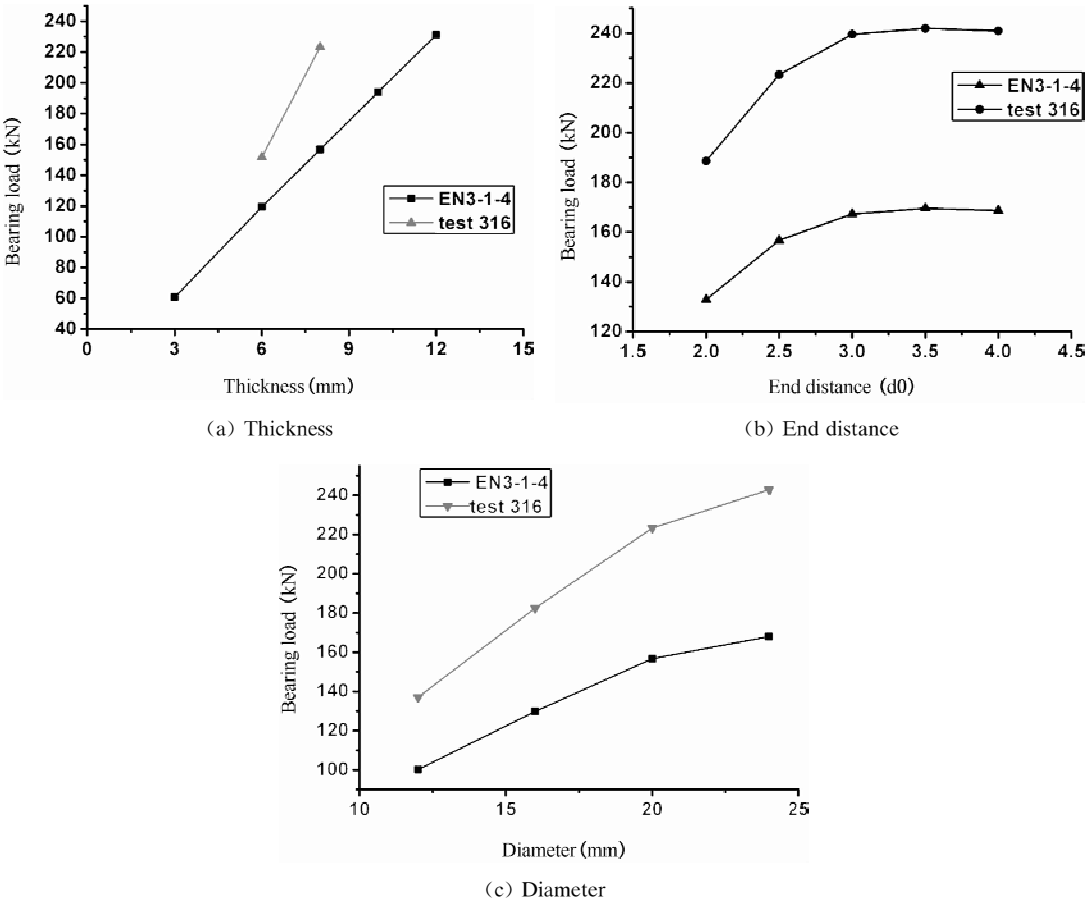
Figure 7　Deformation bearing load-parameter curves with material data in EN3－1－4 and the test

CONCLUSION

The ultimate bearing capacity of the cover plate bolted connection for stainless steel increases gradually with the increase of the thickness of the stainless steel plate，the end distance and the diameter of the bolt. But as the diameter or the end distance exceeds a certain value，this effect reduces and the diameter or the end distance is no longer the controlling factor for the ultimate bearing capacity. The deformation bearing capacity increases linearly with the increase of the thickness of the stainless steel plate，and nonlinearly with the end distance. As the thickness of the inner stainless steel plate is 8 mm，the diameter of the bolt is 20 mm，the connection could get better bearing capacity when the end distance is $3.0d_0$. Because of the difference of the material property for austenitic stainless steel 316 and 1. 4401，the bearing capacity with test 316 is about 30% higher that with EN 1. 4401. Comprehensive analysis should be considered for the design of the cover plate bolted connection.

ACKNOWLEDGEMENT

REFERENCES

［1］Bouchair，A.，Averseng，J. and Abidelah，A.，"Analysis of the behaviour of stainless steel bolted connections"，Journal of Constructional Steel Research，2008，64(11)，pp.1264-1274.

［2］Bouchaïr，A. and Baptista，A.，"Strength and deformation of stainless steel bolted joints with reference to Eurocode 3"，3rd Eurosteel conference，2002，pp.879-888.

［3］Chang，T.，"Experimental Study on the Mechanical Properties of Stainless Steel and the Deformation Behavior of Stainless Steel Beams"，Dalian University of Technology，2011.

［4］Gao，B.，"Research on nonlinear deformation and stability of stainless steel flexural members with welded I-sections"，2011.

［5］Salih，E.L.，Gardner，L. and Nethercot，D.A.，"Numerical investigation of net section failure in stainless steel bolted connections"，Journal of Constructional Steel Research，2010，66(12)，pp.1455-1466.

［6］Mirambell，E. and Real，E.，"On the calculation of deflections in structural stainless steel beams：an experimental and numerical investigation"，Journal of Constructional Steel Research，2000，54，pp.109-33.

［7］Zhang，G.X.，Wang，Y.Q. and Shi，Y.J.，"Analysis and Design Method of Bearing Strength of Bolted Connection in Aluminum alloy"，Journal of Guilin University of Technology，2006，26(04)，pp.501-505.

［8］Kim，H.J.，Joseph，A. and Yura.，"The effect of ultimate-to-yield ratio on the bearing strength of bolted connections". Journal of Constructional Steel Research，1999，49 (3)，pp.255-263.

［9］Guan，J.，Wang，Y.Q. and Zhang，Y.，"Research on stainless steel connections and application in engineering". ASSF-2010. pp.125-140.

［10］EN 1993-1-4. Eurocode 3"Design of steel structures-Part1-4：General rules-Supplementary rules for stainless steels". 2006.

THE EFFECT OF YIELD-TO-ULTIMATE RATIO ON THE BOLTED CONNECTION UNDER STATIC SHEAR

* B. Pan，Y.J. Shi and Y.Q. Wang

Key Laboratory of Civil Engineering Safety and Durability of China Education Ministry，
Department of Civil Engineering，Tsinghua University，Beijing 100084，China
* Email：panb_thu@163.com

KEYWORDS

Yield-to-ultimate ratio，shear resistance，bearing resistance，net cross-section design resistance，long joints.

ABSTRACT

Eurocode 3 Annex D allows the use of high strength steel. But there are no special conditions or restrictions for bolted connections for high strength steel in Annex D. Especially there are significantly fewer investigations on the influence of end distance，edge distance or bolt spacing on the bearing resistance of high strength steel in comparison to other grades. Ductility degradation due to the increase of yield-to-ultimate ratio makes a dent in bolted connection under static shear，which limited the application of high strength steel. The paper summarized experimental research on bolted connection under static shear of different strength grade steel，and the effect of yield-to-ultimate ratio on bolted connection was analyzed. It was found that for a particular type of fastened the variation in shear strength caused by the type of connected material was usually very small. The reduction in bearing resistance for small e_2 or p_2 didn't need to be so large. The design resistance according to yielding of the gross cross-section was critical for mild steel，to prevent large member elongation. But for high strength steel，the design resistance given by rupture of the net area was critical because the tensile resistance of the net section was reached before the yielding of the gross area.

INTRODUCTION

The ductility of steel material is very important for bearing resistances of bolted connections under static shear [1]. The ductility of steel material depends on yield strength (Y)，tensile strength (T) and the yield to ultimate tensile strength ratio (Y/T). The bolt hole made by drilling or pinching，may cause net cross-section weaken and may therefore cause stress concentration. Stress concentration around the bolt hole may cause yielding before required to yield the gross area. The yielding area of the structural element depends on the material's strain hardening ability. If the ability of the material is limited，then the concentration of stresses may cause cracks in the material，resulting in brittle failure of the net cross-

section. Therefore，the ability of the material to maintain ductility is important.

With the development of steel structures，which has been closely linked to the development in material properties and production methods，high strength steels with nominal yield strength more than 460 MPa have begun to be applied in many steel structures including buildings and bridges since the first application of high strength steel more than 460 MPa in Japan in 1960s [2, 3]. Especially with the application of "new" production processes for carbon steels such as the thermo-mechanical rolling and the quenching and tempering process，it becomes possible for such steels both having a high construction strength and good fabrication properties，which makes it fit to be used in steel construction. Compared to ordinary steel，application of high strength steel has many advantages，increasing the steel strength can reduce the steel member section size and the structure weight，and create larger functional space as well. But high strength steels are less ductile than the usual mild structural steels. Their application in structures has in the past been limited.

In recent years，several tests and studies have been carried out regarding to the problems for the use of HSS，but only few studies on bolted connections are available [4, 5]. Kim and Yura [6] investigated the effect of end distance on the bearing strength of one-bolt and two-bolt lap connections. Two different steels with different ultimate-to-yield stress ratios were used to explore the effect of steel strength on bearing capacity. The test results were compared to bearing resistance according to AISC standard and to EC 3 standard，and the latter was found to be more conservative. Aalberg and Larsen [7, 8] implemented similar tests using steel grades S690 and S1100，which included that the strength and ductility of bolted connections didn't have any difference between high strength steels and mild steels. They also studied the block shear on welded I-sections in high strength steels [9]. Puthli and Fleisher [10] carried out 25 bolted connection tests using 17.5 mm thick S460 grade steel plates，which observed the influence of bolt spacing and edge distance. The experimental failure loads were compared with resistance according to EN 1993-1-8. It was concluded that the reduction of the design bearing resistance prescribed in EC3 for edge distances less than 1.5 times the bolt hole diameter or 3.0 times the bolt spacing may not be necessary for the parameters in the tests. Može，Beg and Lopatič [11] carried out extensive experimental research on net cross-section failures of plates with holes（23 tests）and bolted connections（20 tests）made of high strength steel S690. All failures showed local ductility by necking of net cross-section or by bolt hole elongation. Even a small reduction in gross section didn't result in its yielding and consequently to large plastic deformations of the whole member. Može and Beg [12] presented experimental research of 38 tension splices with bolts in double shear made of S690 steel. The high strength steel plates in bolt bearing showed ductile behavior in terms of large hole elongations with plate squashing. In this paper，the effect of yield-to-ultimate ratio on the bolted connection is summarized according to recent researches on high strength steel bolted connections.

HSS MATERIAL PROPERTIES

Shi [13] carried out several high strength steel coupon tests in Tsinghua university and Delft university of technology，including Q420，Q460，S690 and S960. Q420 and Q460 steels are two kinds of Chinese high strength low alloy structural steels，with the nominal yield stress of 420 MPa and 460 MPa. S690 and S960 steels are two grades of European high strength structural steels，with the nominal yield stress of 690 MPa and 960 MPa，respectively. The stress-strain curves obtained from coupon tests are shown in Figure 1. It can be concluded that：High strength steels，such as S690 and S960，don't display instinct yielding stage

compared to mild steels; the yield-to-ultimate ratio increases as yield strength of steel grades increase; high strength steels have lower ductility than mild steels, because the elongation decreases with the increasing of yield strength; however, the ductility of S690 high strength steels still satisfy the European code requirements [14, 15].
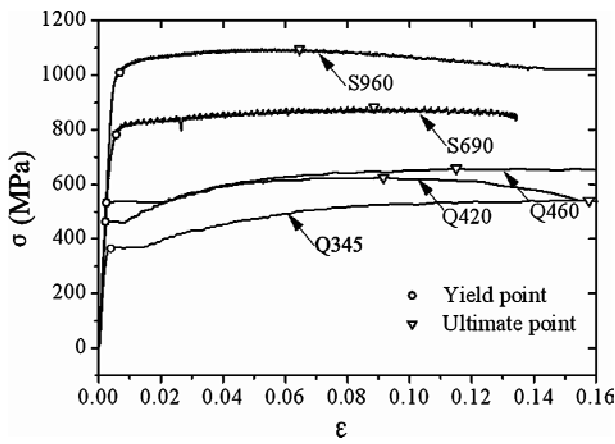

Figure 1   HSS stress-strain curves

THE EFFECT OF YIELD-TO-ULTIMATE RATIO ON THE SHEAR STRENGTH

Wallaert [16] carried out compression lap shear tests using A440 and Q8T ($f_u = 844$ MPa) steel plates and Wang [17] carried out tension lap shear tests using 16 Mn and A₃ steel plates. The test results are shown in Figure 2. It can be concluded that the shear strength has nothing to do with yield-to-ultimate ratio of steel plates. But the deformation decreases with the increasing yield strength of steel grades. However, in Japan the test results presented show a little decrease of the shear strength, using SS41, SM50 and SM58 high strength steel plate.
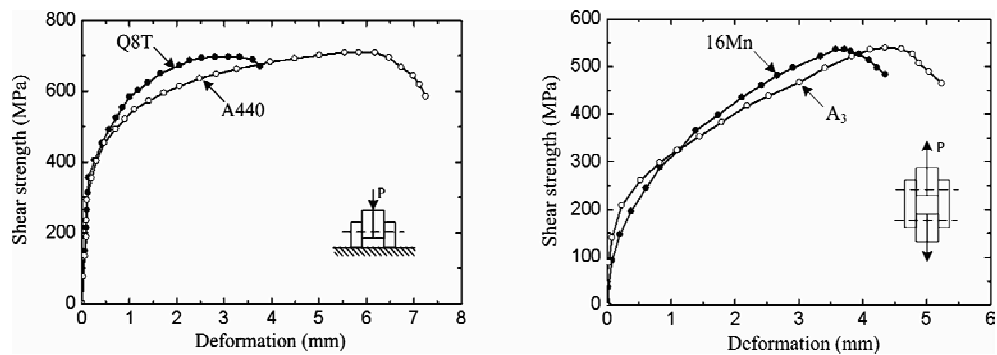
Figure 2   The effect of yield-to-ultimate ratio on the shear strength

THE EFFECT OF YIELD-TO-ULTIMATE RATIO ON THE BEARING RESISTANCE

In Eurocode 3 the design bearing resistance of bolted connection can be checked according to the expression as below:

$$F_{b, EC} = k_1 \alpha_b f_u dt / \gamma_{M2} \tag{1}$$

Where f_u is nominal ultimate tensile strength of the plate, d is bolt diameter, t is plate thickness and partial factor γ_{M2} with the recommended value of 1.25. Parameters k_1 and α_b are defined as follows and take into account mainly geometrical parameters:

In the direction of load transfer

$$\alpha_b = \min(\alpha_d; f_{ub}/f_u; 1) \tag{2}$$

$$\text{for end bolts} \quad \alpha_d = e_1/3d_0 \tag{3}$$

$$\text{for inner bolts} \quad \alpha_d = p_1/3d_0 - 1/4 \tag{4}$$

Perpendicular to the direction of load transfer

$$k_1 = \min(2.8e_2/d_0 - 1.7; 1.4p_2/d_0 - 1.7; 2.5) \tag{5}$$
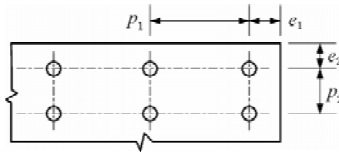
Figure 3　Definition of end e_1, edge e_2 distance and pitches p_1, p_2

Where f_{ub} is defined as the nominal ultimate tensile strength of the bolt and d_0 is a bolt hole diameter. End distance e_1, edge distance e_2, and pitch p_1 and p_2 are defined in Figure 3. Minimum distances set lower limit for the bearing resistance: end distance $e_1 \geqslant 1.2d_0$, $e_2 \geqslant 1.2d_0$, $p_1 \geqslant 2.4d_0$ and $p_2 \geqslant 2.4d_0$.
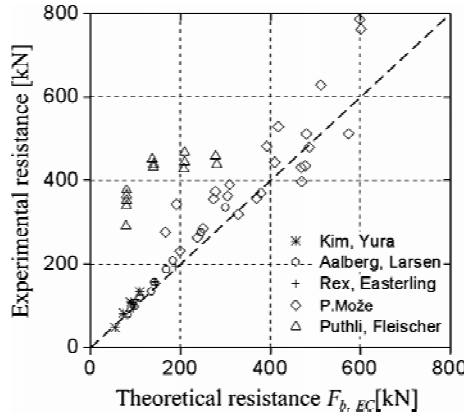
Figure 4　Comparison of experimental and theoretical resistances

Experimental results of high strength steel bolted connections are summarized in Figure 4 according to the documents [6~10, 12, 18]. And the test results are compared to bearing resistance according to AISC standard or EC 3 standard. The theoretical resistances are mostly found to be more conservative, especially for the smaller edge distance e_2 or pitch p_2[10]. It's proved that geometrical parameters influence the bearing strength of bolted connections to a great extent.

Parameter k_1

From Eqn. 5, parameter k_1 is determined by edge distance e_2 and pitch p_2. According to the test results of high strength steel, Eurocode 3 is found to be too conservative as shown in Figure 5 when the edge

distance $e_2 < 1.5d_0$ or pitch $p_2 < 3.0d_0$. The stress redistribution of high strength steels is different from mild steels with greater yield-to-ultimate ratio，so the values of parameter k_1 should be revised.
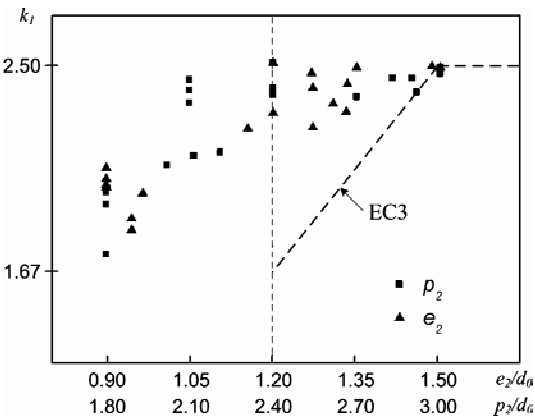
Figure 5　Parameter k_1 in relation of the edge distance e_2 and pitch p_2

Parameter α_b

From Eqn. 2，parameter α_b is determined by end distance e_1. It should be necessary to investigate the effect of end distance on the bearing strength of different strength grade steels. Kim[6] carried out one-bolt and two-bolt lap connections tests using two kinds of steels ($f_y/f_u = 0.62$ or 0.89). It's concluded that when end distance e_1 stays unchanged，the ratio of bearing resistance P_{max} to ultimate tensile strength F_u almost unchanged，which has nothing to do with yield-to-ultimate ratio.
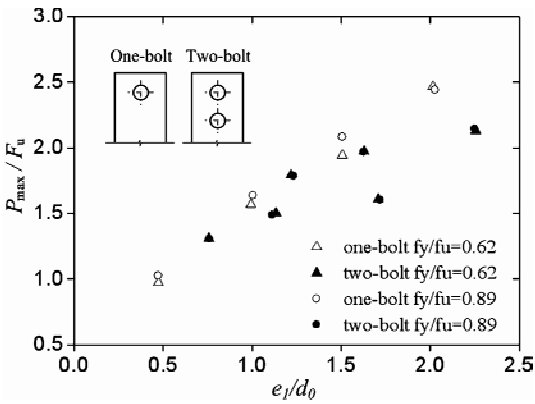
Figure 6　Parameter α_b in relation of yield-to-ultimate ratio

THE EFFECT OF YIELD-TO-ULTIMATE RATIO ON CROSS-SECTION RESISTANCE

The bolt hole blocks the effective transmission of tensile stress in bolted connections under shear. Therefore stress concentration around the hole is produced，which may cause yielding before required to yield the gross area. If the ability of the material is limited，then the concentration of stress may cause cracks in the material，resulting in brittle failure of the net cross-section. However，the steel of enough

ductility can conduct stress redistribution to ease the concentration of stress and prevent the brittle failure of steel plate.

In Eurocode 3 the design resistance of the cross-section of bolted connections should be controlled by both the ultimate design resistance of the net cross-section $N_{u, Rd}$ and the plastic design resistance of gross cross-section $N_{pl, Rd}$:

$$N_{u, Rd} = 0.9 A_{net} f_u / \gamma_{M2} \tag{6}$$

$$N_{pl, Rd} = A f_y / \gamma_{M0} \tag{7}$$

Where f_u is ultimate tensile strength of the plate, f_y is yield strength of the plate, A is gross cross-section area and A_{net} is net cross-section area, partial factor γ_{M2} and γ_{M0} with the recommended value of 1.25 and 1.0. The ultimate design resistance of the net cross-section $N_{u, Rd}$ prevents the brittle failure of the net area at bolt holes. The plastic design resistance of gross cross-section $N_{pl, Rd}$ prevents the excessive elongation owing to the yielding of gross area. If the design strength of bolted connection is governed by the plastic design resistance of gross cross-section $N_{pl, Rd}$, the yielding of the gross area may happen before the brittle failure of the net area. That's to say, $N_{u, Rd} > N_{pl, Rd}$.

$$N_{u, Rd} > N_{pl, Rd} \Rightarrow A_{net} / A > 1.4 f_y / f_u \tag{8}$$

For mild steels, commonly the ultimate design resistance of the net cross-section $N_{u, Rd}$ isn't the governing factor, because A_{net} / A is greater than 0.8 in most circumstance. However, the yield-to-ultimate ratio increases as yield strength of steel grades increase, so high strength steels may be controlled by the brittle failure of the net area, which is proved by the test results of S690 in P. Može [11].

CONCLUSION

The paper summarized experimental research on bolted connection under static shear of different strength grade steel. The test results are compared to the design resistances, and following conclusions are derived:

1) The elongation of high strength steels decreases and the yield-to-ultimate ratio increases, compared with mild steels.

2) The shear strength of bolted connections has nothing to do with yield-to-ultimate ratio of steel plates. But the deformation decreases with the increasing yield strength of steel grades.

3) Eurocode 3 is found to be too conservative when the edge distance $e_2 < 1.5 d_0$ or pitch $p_2 < 3.0 d_0$. The effect of end distance e_1 on bearing resistances has nothing to do with yield-to-ultimate ratio.

4) Commonly, the cross-section resistance of mild steel is controlled by the yielding of gross area while high strength steel is governed by the brittle failure of the net area.

ACKNOWLEDGEMENT

REFERENCES

［1］Pavlina，E. J. and Van，T. C. J.，"Correlation of yield strength and tensile strength with hardness for steel"，Journal of Materials Engineering and Performance，2008，17(6)，pp.888-893.

［2］Pocock，G（2006）．"High Strength Steel Use in Australia，Japan and the U. S. Journal of The Structural Engineer"，84，21，pp.27-30.

［3］IABSE（2005）．"Use and Application of High-Performance Steels for Steel Structures"．Zurich

［4］Reidar Bjorhovede．"Development and use high performance steel"．Journal of Constructional Steel Research，Vol.60，pp.393-400，2004.

［5］Chang，Y. F.，Wei，M. and Liu，L. X.，"Development of high strength thick plate for building structures"．Proceeding of Annual Conference of China Steel Construction Society，1-5，2007．（in Chinese）

［6］Kim，H. J. and Yura，J. A.，"The effect of ultimate-to-yield ratio on the bearing strength of bolted connections"．Construc Steel Res，1999，49(3)，pp.255-269.

［7］Aalberg，A. and Larsen，P. K.，"Bearing strength of bolted connections in high strength steel"．In：Proceedings of nordic steel construction conference. 2001.

［8］Aalberg，A. and Larsen，P. K.，"The effect of steel strength and ductility on bearing failure of bolted connections"．In：Lamas A，Simoes da Silva L，editors. Proceedings of the 3rd European conference on steel structures，Eurosteel 2002，2002.

［9］Aalberg，A. and Larsen，P. K.，"Strength and ductility of bolted connections in normal and high strength steels. Norwegian University of Science and Technology"，Department of Structural Engineering；March 1999.

［10］Puthli，R. and Fleischer，O.，"Investigation on bolted connections for high strength steel members"．Construct Steel Res 2001，57(3)，pp.313-326.

［11］Može，P.，Beg D. and Lopatič，"Net cross-section design resistance and local ductility of elements made of high strength steel"．J Construct Steel Res 2007；63(11)，pp.1431-1441.

［12］Može，P. and Bog，D.，"High strength steel tension splices with one or two bolts. J Construct Steel Res，2010，66(8)，pp.1000-1010.

［13］Shi，G. and Ban，H. Y.，"Engineering Application and Recent Research Advances of High Strength Steel Structures"［C］. 12th International Conference on Scientometrics and Informetrics，Rio de Janeiro，Brazil，2009.

［14］European Committee for Standardisation. EN 1993-1-1：Eurocode 3：Design of Steel structures. Part 1.1：General rules for buildings. Brussels，2005.

［15］European Committee for Standardisation. prEN 1993-1-12：Eurocode 3：Design of steel structures. Part 1.12：Additional rules for extension of EN 1993 upto steel grades S700. Brussels，2006.

［16］Jama，J. W. and John，W. F.，"Shear strength of high-strength bolts，Journal of the Structural Division"，ASCE，Vol.91，No.3，June 1965，pp.99-125.

［17］Wang，B. Q.，Chen，L. L. and Lu，X. F.，"Guide to Design Criteria for High Strength Bolted Connections"，Metallurgical Industry Press，1991.

［18］Clinton，O.，Rex，P. E. and W. Samuel，E.，"Behavior and Modeling of a Bolt Bearing on a Single Plate，Journal of the Structural Division，" AS，CE，Vol.129，No.6，June 2003，pp.792-800.

［19］John，W. F. and Lynn，S. B.，"Criteria for designing bearing-type bolted joints"，Journal of the Structural Division，ASCE，Vol.91，No.5，October 1965，pp.129-153.

THE INFLUENCE OF THE ANGLE OF RIBBED STIFFENER AND THE MULTI-DIRECTIONAL LOADS ON THE WELDED HOLLOW SPHERICAL JOINTS

J. T. Yu，* Y. M. Zhang，K. Q. Yu and B. Tang

Research Institute of Structural Engineering and Disaster Reduction，Tongji University，
Shanghai，200092，China
* Email：abeier04201@126.com

KEYWORDS

Hollow spherical joints，ultimate bearing capacity，influence factors，enhancing coefficient.

ABSTRACT

This paper presents the experimental and numerical study on four groups（12 in total）of welded hollow spherical joints with ribbed stiffener tested under uniaxial compression or tension loads. Through loading test，the relationship between load and deformation is obtained and the values of joints' bearing capacities are compared with results calculated according to specifications. With the adoption of elasto-plastic model and consideration of geometric and material nonlinearity，the whole loading processes were simulated with the help of ABAQUS. Through combining the test data and computing results. The relationships between bearing capacity and various influence factors including the multidirectional loads and the stiffener's direction and number were analyzed. The bearing capacity of the joint under multidirectional loads depended on the axial force of the branch tube. When the axial force of the branch tube was very small，the decline of the bearing capacity was not significant；when it was large，the bearing capacity decreased significantly. At the end of this paper，it is recommended the reduction coefficient should be introduced to ensure the sufficient capacity of the kind of joint in the specifications.

INTRODUCTION

Welded hollow spherical joints（WHSJ in short）are extensively used as a node pattern for grid structures in China for its convenience. Recently，extensive theoretical and experimental research on the mechanical of WHSJ under uniaxial loads was carried out by researchers at home and abroad. At home，the formulas for the ultimate bearing capacity of the welded hollow spherical joints（diameter 120 mm～500 mm）were obtained on the basis of regression analysis of the experimental data according to a large amount of test，and have been presented in the Chinese specifications which are "Technical Specification for Latticed Shells" [1]（denoted "specification TSLS"），"Specification for design and construction of trussed structure" [2]（denoted "specification SDCTS"）and "Technical Specification for Spatial Grid Structure" [3]（denoted "specification TSSGS"）. But in the current Chinese specifications，the design

formulas for WHSJ are not only applied to joints with diameters less than 500 mm，but also to joints with diameters less than 900 mm. It was found in the practice that it is not safe to design the WHSJ with large diameter using the design value from the calculating formulas. Additionally，the values of the calculating formulas are different among those specifications，which at last lead to different design values. For safety concerns，the engineers are always prone to select the conservative one from three computing results，which will inevitably increase the construction cost. In the specification [1] mentioned above，the failure properties of WHSJ are assumed to be strength collapse under uniaxial loads，but from the existing test data［Ultimate bearing capacity of the welded hollow spherical joints in spatial reticulated structures］，it was found stability failure really happened when WHSJ was subjected to compressive load. Addition to that，the calculating formulas of WHSJ do not distinguish the loading condition of compression or tension，as means the bearing capacities of the joint under compression loads or under tension loads are same according to the specification. Thus it is a fair question to propose a more accurate and valuable calculating formula for the engineers.

As to the bearing capacity calculation of WHSJ，Zhihua Chen [6] pointed out，the tensile capacity were apparently larger than the compressive one and it was irrational and insecurity for the calculating formulas basing on the tension capacity，however ignoring the compression failure mode. The same results were also conducted by Qinghua Han [7] through testing 64 groups of compression and tension joints with the same dimension. As to the analysis on the influencing factors，Nianliang Yao [8]，Lanchao Jiang [9] studied the main factors influencing the bearing capacity of the joints and its influence degree on the basis of the experimental and theoretical analysis. Mingzhou Su[10] investigated the ultimate bearing capacity of the joint under unidirectional，bidirectional，three-directional loads by FEM，the results of the analysis indicated that the bearing capacity under unidirectional load was slightly larger than the capacity under multi-directional loads. The simulation of the WHSJ which was under triaxial load or a combination of triaxial load and moment also was done by Xingfei Yuan[11]，and the calculating formula for bearing capacity of the WHSJ under three-directional loads was obtained. But current specifications[1, 2, 3] don't provide more details about the calculating formula for bearing capacity of the WHSJ under multidirectional loads. In this aspect，this needs further study in the future.

Additionally，to enhance the bearing capacity or even vary the collapse mode of the WHSJ，ribbed stiffeners are popularly set to the WHSJ. Effects of the stiffener's direction and number on the bearing capacity should be considered in the design process. But currently there are very few research results on it at home and abroad. In the current specifications，the ribbed stiffeners enhancing coefficients of compression and tension welded spheres were 1. 4 and 1. 1 respectively. In the new "Technical Specification for Spatial Grid Structure" [3]，comparing to calculating formula for the bearing capacity of WHSJ in the latticed shells specification，two modulations were presented：①all the coefficients was 0. 9 of the old，which was identical with the space truss specification；②when the diameter of the hollow sphere was more than 500 mm，an adjustment coefficient of 0. 9 needed to be multiplied on the basis of ①. The enhancing coefficient of the ribbed stiffeners' bearing capacity that was mentioned in the current specifications of China did not count in the influence of the location and number of the ribbed stiffener precisely. So as to all the ribbed stiffeners，the same enhancing coefficients were used to confirm the effectiveness on the ultimate bearing capacity，of which the precision was doubtful. In this paper，the location and number of different ribbed stiffeners were researched emphatically. With the help of the full-scale tests of 4 groups of 12 welded hollow spherical joints in total that had been done，the ABAQUS software was used to simulate the whole loading process of the spherical joints to get some

results of useful value, which can be supplements to the bearing capacity formulas in the current specifications.

According to the above discussion, the following aspects are of interest in this paper:

1) How to Figure out the rationality of computing formulas among different codes.

2) Effect of the multi-directional axial force and the stiffener's direction and number on the bearing capacity.

EXPERIMENTAL PROCEDURE

Specimens Design

12 WHSJ in 4 groups were selected randomly for loading, the details of which were shown in Table 1 and the constructions of the WHSJ were shown Figure 1 and Figure 2. Take the specimen WHSJ 1 for example, whose diameter is 800 mm, the thickness of hollow sphere is 36 mm; the diameter and the thick of steel tube connecting to the sphere is 377 mm, 28 mm respectively.

TABLE 1   DETAILS OF THE TESTED WHSJ

Case.	Diameter / thickness /mm	tube diameter / tube thickness/mm	ribbed stiffener thickness /mm (direction)	Loading condition
1	D800×36	377×28	30(45°)	compression
2	D750×25	325×18	28(45°)	tension
3	D650×18	273×14	24(45°)	tension
4	D400×10	180×8	30(45°)	compression
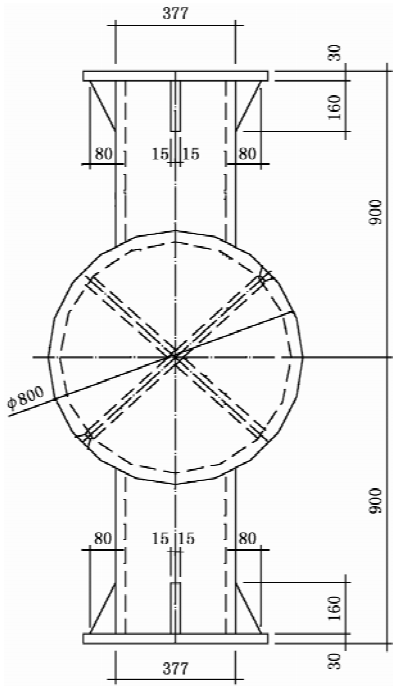
Figure 1   Elevation view of the D800×36

Figure 2   The picture of the joint

Loading Device and Loading Diagram

Electro-hydraulic servo machine with capacity of 20 000 kN and two hydraulic jacks YQ－400 were used for axial compression and tension tests respectively. DH3185 data acquisition system was used for data acquisition. All specimens were subjected to the monotonic increasing axial load until failure. The load was applied under load control mode. Before the formal test，the preloading was applied to the specimens by three stages. In the formal test，there was an interval of 3 minutes between every two loading steps in order to make the stress and strain stable. For the WHSJ 1 D800×36 and WHSJ 4 D400×10（under compression load），the loading grades were 1 200 kN and 300 kN respectively. And for the WHSJ 2 D 750×25 and WHSJ 3 D650×18（tension test），the loading grades were 250 kN and 150 kN respectively. In the final stage of the test，multi-stage unloading scheme was made to unload WHSJ.

Instrumentation

BF－120－2A electric resistance strain gages and YHD－200 displacement transducers（minimum division value was 0.005 mm）were used to measure the stress and displacement of steel sphere and steel tube in each step respectively.

Test Results and Discussion

The load-deformation curves of the WHSJs are shown in Figure 3. From the Figure 3，the loading processes of tension and compression specimens can be divided into three phases: elastic phase，elastic-plastic phase and failure phase. Take WHSJ 1 D800×36 for example，in the earlier stage of the loading process（when load was less than 6 000 kN），the deformation of the sphere and the tube was quite small and the strain showed the material was in an elastic phase. With the increase of the load，the load-displacement curve became flat，indicating the beginning of plastic phase. When the load was 7200 kN～12 000 kN，the deformation of the sphere and tube increased rapidly，even the sound of the welding line rupturing could be heard when loading. While the load reached 12 000 kN，the joints buckled evidently，and the tests were stopped. In the final stage，the failure load（12 000 kN）was unloaded by four stages. The unloading grade was 3 000 kN. During the unloading process，it was found that the residual plastic deformation was much larger than the elastic deformation. With regard to WHSJ 3 D650×18，when the load was less than 3 000 kN，the deformation of the sphere and tube was very small，and the load and the deformation had linear relationship. Then when the load was more than 3 000 kN and less than 4 500 kN，the deformation of the sphere increased rapidly，and the tensile rigidity decreased. Differentiating from that，the slope of the load-displacement curve of the tube was unchanged，which indicated that the tube still was under elastic state. When the load was more than 4 500 kN，the deformation rate of the specimens increased rapidly，and the slope of the load-displacement curve decreased. When the load reached 6 000 kN，the tests were stopped. In the final loading stage，the failure load（6 000 kN）was unloaded by three steps（4 000 kN，2 000 kN，0 kN）.

The test results and the values of the calculating formulas for bearing capacity in terms of the specifications[1, 2, 3] are compared in Table 2. Through comparison，it is indicated the test results are in good accordance with the values of the calculating formulas for tension capacity in terms of the "specification-TSLS"[1] and "specification-SDCTS"[2]，but not with the values of the calculating formulas for compression capacity. The value of "specification-TSLS"[1] is somewhat larger，especially for the
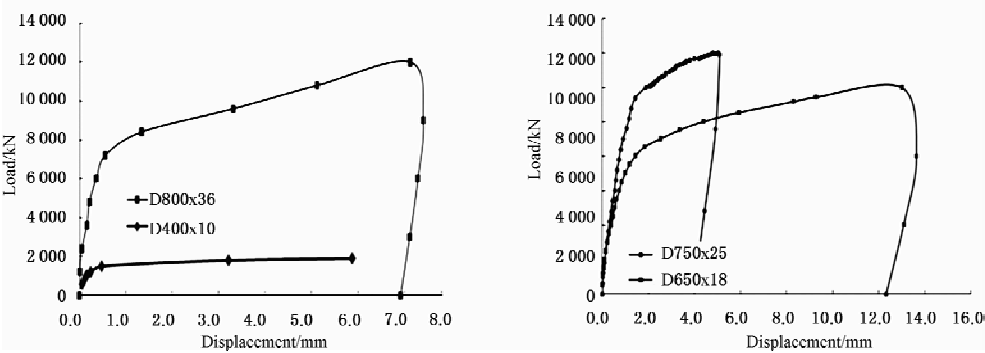
Figure 3   The load-displacement curves of WHSJs

spheres whose diameters are larger than 500 mm. Thus the check coefficients are generally less than the specified value 1.6, which make the design value insecure. When the diameter is larger than 500 mm, the check coefficients according to "specification-SDCTS"[2] are more than 1.6, and the values of the calculating formulas for bearing capacity are somewhat conservative. So it is inappropriate to use "specification-SDCTS"[2] to calculate the bearing capacity of joints with large diameter. The check coefficients of "specification-TSSGS"[3] were closer to 1.6. So it is concluded that the design formula of "specification-TSSGS"[3] has the highest accuracy among the three codes.

TABLE 2   COMPARISON OF TEST RESULTS, DESIGN VALUES OF BEARING CAPACITY

Case	Test value /kN	TSLS /kN	Check coefficient	SDCTS /kN	Check coefficient	TSSGS /kN	Check coefficient
D800	11 985	9 709	1.23	3 313.08	3.62	7 864.80	1.53
D750	7 024	4 883	1.44	4 553.34	1.54	3 955.30	1.78
D650	5 834	3 058	1.91	2 753.86	2.18	2 477.13	2.36

ANALYSES OF THE INFLUENCE FACTORS ON THE BEARING CAPACITY OF WHSJ

The Influence of The Ribbed Stiffeners' Direction and Number On the Ultimate Bearing Capacity

In order to study the influence of ribbed stiffeners' direction and number on the ultimate bearing capacity of the spherical joint, similar analysis were adopted to perform the FEM simulations of 6 groups of ribbed stiffener layout, as shown in Figure 4. Each group includes 4 models of different diameters, namely 400 mm, 650 mm, 750 mm and 800 mm. To highlight the effect of ribbed stiffener, the rigidity of the steel tubes were assumed infinite in the computing process to ensure the failure occurring in the sphere region.

The computing results of the ultimate bearing capacity of the ribbed stiffened welded spherical joints are listed in Table 3 and the enhancing coefficients are shown in Table 4, from which the following conclusions can be drawn: when the load is parallel to at least one plane of ribbed stiffeners (90° single joint, 90° cross joint or, 90° double joint), the enhancing values is commonly larger than 1.4. The bearing capacity increases significantly. From this point, the provisions of specifications are somewhat conservative. When the load is perpendicular or at an angle to the plane of the ribbed stiffeners (0° single joint, or 45° cross joint), the enhancing coefficients was less than 1.4, and the tension enhancing coefficient was less than 1.1, so the specifications were somewhat unsafely.
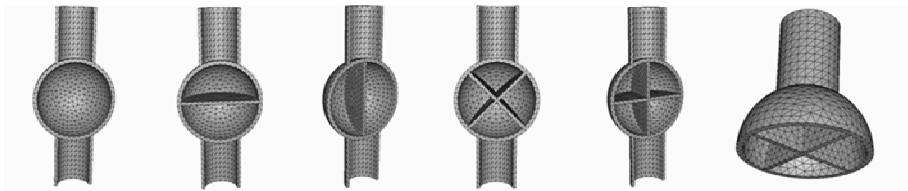
(1) No stiffener　　(2) 0° single　　(3) 90° single　　(4) 45° cross　(5) 90° cross　(6) 90° double

Figure 4　Ribbed stiffeners layout

TABLE 3　COMPUTING VALUES OF TENSION AND COMPRESSION BEARING CAPACITY OF THE JOINTS

No.	Sphere diameter / Ribbed stiffeners	400 mm		650 mm		750 mm		800 mm	
		Compression	Tension	Compression	Tension	Compression	Tension	Compression	Tension
1	no	1 966	2 933	4 572	6 463	6 490	8 015	10 923	15 410
2	0° single	1 969	3 191	4 604	6 704	6 498	8 108	10 930	15 506
3	90° single	3 980	6 087	7 968	11 138	9 803	12 536	16 687	21 602
4	45° cross	2 340	3 024	4 974	6 780	6 807	8 303	11 911	16 566
5	90° cross	4 010	6 212	10 120	11 176	11 654	12 361	16 905	24 455
6	90° double	6 142	9 221	10 988	16 128	12 484	16 966	17 281	28 700

TABLE 4　ENHANCING COEFFICIENTS OF THE RIBBED STIFFENERS TO THE HOLLOW SPHERICAL JOINTS

No.	Sphere diameter / Ribbed stiffeners	400 mm		650 mm		750 mm		800 mm	
		Compression	Tension	Compression	Tension	Compression	Tension	Compression	Tension
1	no	—	—	—	—	—	—	—	—
2	0° single	1.002	1.088	1.007	1.037	1.001	1.012	1.001	1.006
3	90° single	2.024	2.075	1.743	1.723	1.510	1.564	1.528	1.402
4	45° cross	1.190	1.031	1.088	1.049	1.049	1.036	1.090	1.075
5	90° cross	2.040	2.118	2.213	1.729	1.796	1.542	1.548	1.587
6	90° double	3.124	3.144	2.403	2.495	1.924	2.117	1.582	1.862

The 90° single joints has higher bearing capacity than that of the 45° cross joint，so the enhancement of the bearing capacity is not necessarily in proportion to the number of ribbed stiffeners. The difference between the bearing capacity of 90° single joint and the 90° cross joint is not significant，whereas the enhancing amplitude is remarkable in case of 90° double joint. The influence of different layouts of ribbed stiffener in ascending order is：no stiffener ＜0° single ＜45° cross ＜90° single ＜90° cross ＜90° double.

From the above results it indicates that：(1) in case of different ribbed stiffeners，the bearing capacity of tension is generally larger than that of the compression；(2) the tension and compression bearing capacity of ribbed stiffened joints is larger than that of hollow spherical joints；(3) when the load is parallel to the plane of stiffener，the compression enhancing coefficients are larger than 1.4，and the tension enhancing coefficients are larger than 1.1. When no stiffener is parallel to the direction of load，the compression

and tension enhancing coefficients are all close to 1.0, which implies limited effect of stiffeners. （4）
from the maximum value of compression and tension enhancement，namely 3.124 and 3.144 respectively，
we know an appropriate layout of stiffeners will be highly efficient.

Bearing Capacity of Whsj Under Multi-Directional Loads

In practice，the WHSJ in spatial reticulated structures are always under multidirectional loads. In the
literatures[10, 13]，the study of the joints under multi-directional orthogonal loads was carried out，and the
result indicated that when the load applied on the lateral branch tube was comparatively small，the stress
state of the joint under multi-directional loads was similar with under uniaxial load. Currently there are
very few research results on the ultimate bearing capacity of joint under multi-directional and non-
orthogonal loads. In this section，the bearing capacity of the joints concluding cross-shaped joint，$60°$ K-
type joint and double K-type joint under 36 cases was analyzed by FEM. The FEM model of the double K-
type joint was shown in Figure 5 as follow.
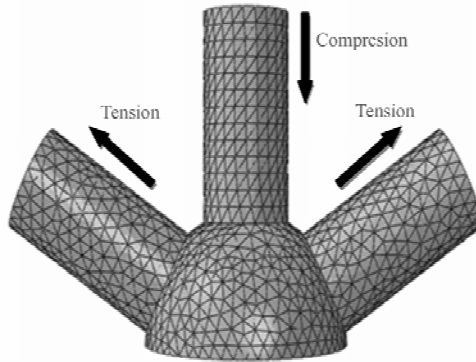
Figure 5   FEM model of WHSJ under multidirectional loads

The FEM model was established without ribbed stiffener to avoid the irrelevant influence. To eliminate
the impact of tube's diameter，the main tube's diameter was set the same as branch tube's. The uniaxial
load of the main tube and the branch tube was taken as $F1$ and $F2$ respectively. The relationship between
the F_1 and F_2 is

$$F_2 = \lambda F_1 \qquad\qquad (1)$$

where λ is the ratio of the branch tube's uniaxial load to the main tube's uniaxial load. In the analogue
computation，the values of λ are 0.3，0.6 and 1.0 respectively. The results of FEM analysis are compared
in Fig 6.

It can be concluded as follows：
（1）With the increase of λ，the bearing capacities of joints decrease. When $\lambda = 0.3$，compared to the
uniaxial tension value of $5\ 925.98$ kN and uniaxial compression value of $4\ 603.32$ kN，the bearing
capacities of joint under multi-directional loads drop by 11.0% in tension and 10.2% in compression
respectively. When $\lambda = 1.0$，the drops are 45.8% and 32.8% at maximum，respectively.
（2）From the $90°$ joint to the $60°$ double K-type joint，the bearing capacities decrease. As to the cross

(a) The main tube under compression   (b) The main tube under tension
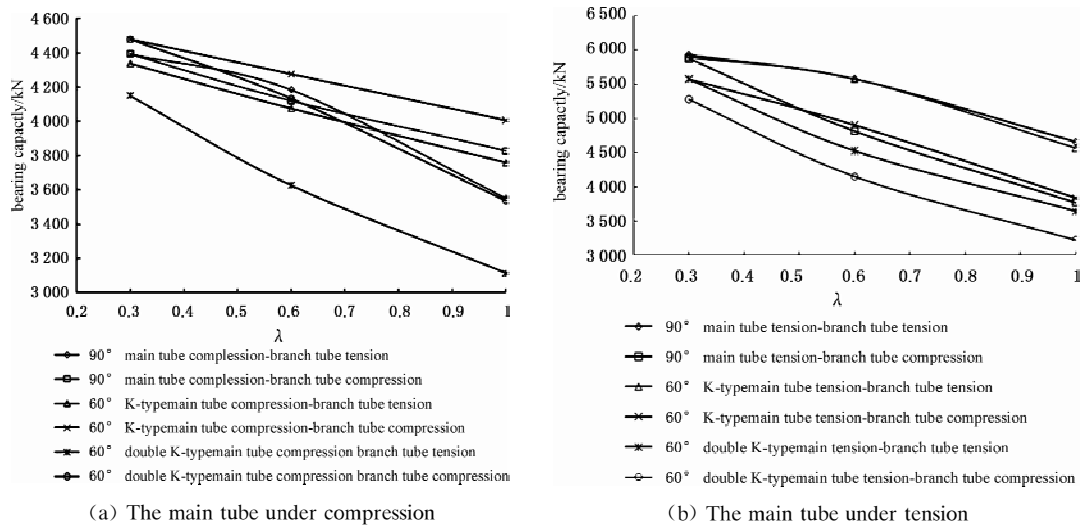
Figure 6　Bearing capacity of WHSJ under multidirectional loads

joint and the 60° K-type joint，when λ = 0.3，the tension and compression bearing capacities drop by 6.1% and 6.5% respectively；when λ = 0.6，the tension and compression bearing capacities drop by 18.8% and 11.5% respectively；when λ = 1.0，the tension and compression bearing capacities drop by 36.0% and 22.8% respectively. As to the 60° double K-type joint，the bearing capacity drops significantly，when λ = 1.0，the tension and compression bearing capacity drop by 45.0% and 32.8%，respectively.

CONCLUSIONS

According to the experiment and FEM analyses of the influence of multi-factors on the performance of WHSJ，the conclusions are listed as follows：

1）Compared with the test data，the design value obtained from the specification TSSGS is proved most reasonable among the three applicable specifications；

2）The direction and number of the stiffeners have significant influence on the bearing capacity. The ribbed stiffener parallel to the axial load really contribute more to the bearing capacity than that perpendicular or at an angle to loading direction. The enhancing coefficients corresponding to the load-parallel ribbed stiffeners are larger than the recommended value of specifications；While the enhancing coefficients of other cases are less than the recommended value；

3）When the axial force of the branch tube is comparatively small，the decline of joint's bearing capacity is negligible；With the increasing of force provided by the branch tube，from the 90° cross joint to the 60° double K-type joint，the influence become significant. From the author's point of view，the reduction coefficient should be introduced to ensure the sufficient capacity of joint in the future revision of specification.

In general，there are numerous factors affecting the mechanic properties of WHSJ，in-depth studies in this area are still needed.

REFERENCES

［1］JGJ 61-2003，"Technical Specification for Latticed Shells"，2003.

［2］JGJ 7−91,"Specification for design and construction of trussed structure", 1991.

［3］"Technical Specification for Spatial Grid Structure (approval of the draft)", 2007.

［4］JGJ 78−1991,"Standard for Quality Inspection and Assessment of Trussed Structure", 1991.

［5］GB 50152−92,"Standard for Test Methods of Concrete Structures", 1992.

［6］Chen, Z.H. and Liu, X.L., "Research on the Bearing Capacity of Welded Hollow Spherical joints", The 11th space structure academic conference, Nanjing, China, 2005.

［7］Han, Q.H., Pan, Y.D. and Liu, X.L., "Analysis for The Ultimate Tensile and Compressive Bearing Capacity of Welded Hollow Spherical Joints", China Civil Engineering Journal, 2003,36(10),pp.1−6.

［8］Yao, N.L., Dong, M. and Yang, L.P., etc. "Analysis for The Bearing Capacity of Welded Hollow Spherical Joints", Building Structure, 2000,30(4),pp.36−38.

［9］Jiang, L.C., Gao, R. and Xu, G.B., "Study on Influence of Different Factors on Support Capacity of Hollow Spherical Connectors", Journal of Northern Jiao Tong University, 1998,22 (4),pp.41−44.

［10］Su, M.Z., Gu, Q. and Lu, X.S., "FEM analysis on the Bearing Capacity of Welded Hollow Spherical Joints", Xi'an Univ. of Arch. & Tech, 1998,30(2),pp.119−123.

［11］Yuan, X.F., Peng, L.Z. and Dong, S.L., "Loading-Carrying Capacity of Welded Hollow Spherical Joints Subject to Combined Planar Tri-Directional Axial Force and Bending Moment", Journal of Zhejiang University (Engineering science), 2007,41(9),pp.1436−1442.

［12］Xue, W.L. and Zhang, Q.L., "Destructive Mechanism and Experimental Study of Welded Hollow Spherical Joints Connected with Circular Steel Tubes", Journal of Building Structures, 2009,30 (5),pp.155−161.

［13］Qin, L.Y., Xu, D.G. and Zhou, A.M., "Study on the Bearing Capacity of Welded Hollow Spherical Joints", Journal of Zhengzhou University, 2006,27(3),pp.25−29.

ANALYSIS OF MOMENT-ROTATION CURVE FOR SEMI-RIGID JOINT OF EXTENDED END PLATE CONNECTION

* L. Wang[1]，B. S. Liu[2]，X. T. Dong[1]

[1] Shandong Provincial Key Laboratory of Civil Engineering Disaster Prevention and Mitigation(Shandong University of Science and Technology)，Qingdao，266590，China
[2] Zhejiang southeast space frame company，Hangzhou，311209，China
* Email：wlkdtjxy@sina.com

KEYWORDS

Flush end plate connection，extended end plate connection，semi-rigid，static behavior，seismic behavior，moment-rotation curve，ANSYS.

ABSTRACT

The traditional design of steel structure always simplify the joint as ideal rigid or hinged. However，joint is neither ideal rigid or hinged in the actual project，it is semi-rigid. After establishment finite element model of semi-rigid end plate，the static performance was analysed. Consider the end-plate thickness，bolt diameter，bolt spacing，beam height and column web stiffeners five factors，study the various factors effects on the end plate of semi-rigid joint capacity，deformation characteristics and moment - rotation curve characteristics.

INTRODUCTION

70% of the damage have occurred in the steel connection joint in the previous earthquake，and unreasonable joint design will lead to brittle failure. The traditional design of steel structure always simplify the joint as ideal rigid or hinged. However，joint is neither ideal rigid or hinged in the actual project，it is semi-rigid.[1] Some research indicated that，compared with the rigid，semi-rigid connection is more suitable for the seismic design of steel structure. For semi-rigid nodes design，European standard Eurocode 3（1992）gives the basic design method and assembly method. In contrast，our specification for semi-rigid joints design stipulation is too pale. At the same time，as a result of our country and foreign standard calculation theory，material properties are not identical，the foreign standard does not completely accurately guide our practical engineering. Therefore，performance and design method of semi-rigid joints research is imperative.

This paper uses finite element software ANSYS to establish end plate semi-rigid joints finite element model for static performance analysis，change of end-plate thickness，bolt diameter，bolt spacing，beam

section height and column stiffener five factors to study various factors effects on semi-rigid connections of bearing capacity，deformation and moment-rotation curve.

ESTABLISHMENT OF FINITE MODEL

Element Type And Material Properties

In this paper，all model selection is solid element. beam，column，end plates and bolts for steel component SOLID92 simulation；the contact element of end plate and column flange，screw and the side wall of the bolt hole use the target cell TARGE170 and contact element CONTA174 simulation. [2-3] Through the command PSMESH generated three-dimensional pretension element PRETS179 to pretension high strength bolt. [4]

Beam，column and the end plates are made of Q345B steel，the monotonic load model using bilinear isotropic hardening constitutive model，as shown in Figure 1. High-strength bolts used 10. 9 friction type high strength bolts，using multiple linear hardening model，as shown in Figure 2. The Poisson's ratio is 0. 3，the anti-slip coefficient of the end plate friction is 0. 44.
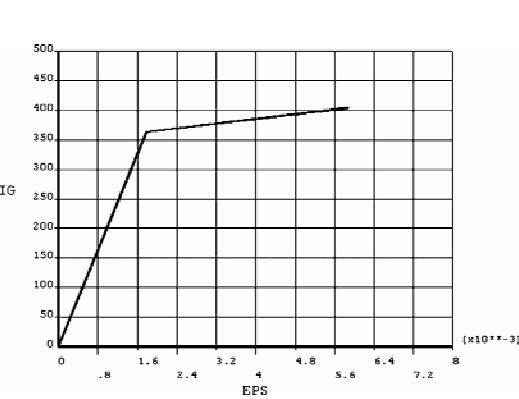
Figure 1   Stress-strain curve of beam-column and end plate
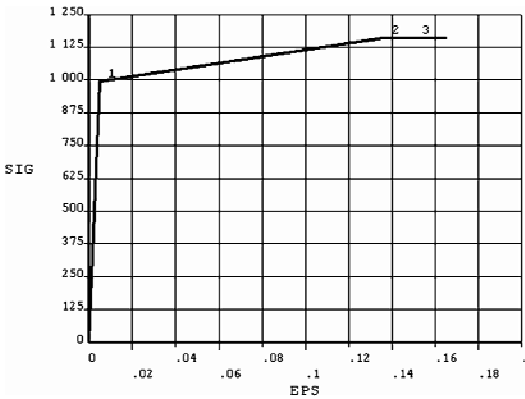
Figure 2   Stress-strain curve of high strength bolts
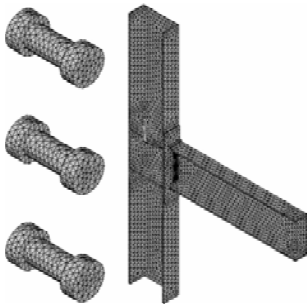
Figure 3   Meshing of B20 and bolts
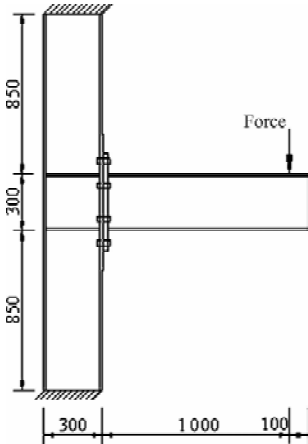
Figure 4   Forced diagram of finite element models

Boundary Condition

The loading process consists of two steps：the first step，applying bolt pre-tension load；the second step，from the center line 1 150 mm of the column using force control loading methods，grading loading，so that the beam generated displacement. Each load step use automatic time step. Model mesh as shown in Figure 3，the model of the force diagram as shown in Figure 4.

MODEL VALIDATION

In order to verify the accuracy and reliability of the ANSYS simulation，use the test parameters from specimens SC3（protruding end-plate connections）of reference[5] to simulate the extended end-plate semi-rigid connections，and the simulated results were compared with experimental data. End plate joints deformation simulation results contrast with test results of reference[5] as shown in Figure 5，the ANSYS results of the moment-rotation curve contrast with the test curve of reference[5] as shown in Figure 6. It can be seen from the Figure that the finite element results agree well with the experimental results. This shows：the finite element method the paper used can simulate the bearing capacity and bending moment-rotation curve of end-plate connections semi-rigid joint.
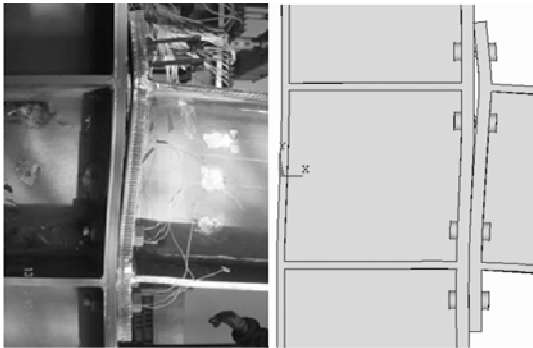
Figure 5   Displacement of extended end-plate connection   Figure 6   Comparison of moment-rotation curve
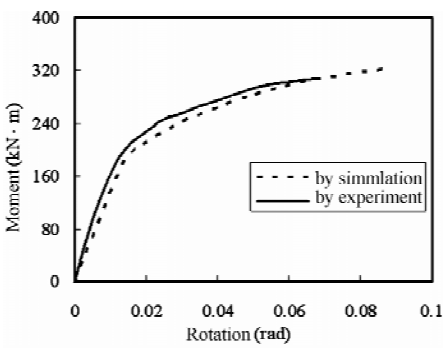
MOMENT-ROTATION CURVE OF EXTENDED END PLATE CONNECTIONS

In theory，the joint rotation is the change of joint connected beam axis of rotation angle for the load phasor value of zero. [6] End plate connection node angle refers to the upper and lower beam end flange at the center line of the relative rotation angle. For extended end plate connections，mainly includes two parts；the rotation ϕ_{ep} caused by the relative deformation between the extended end plate and column flange and shear deformation ϕ_s caused by the corner，as shown in Figure 7.
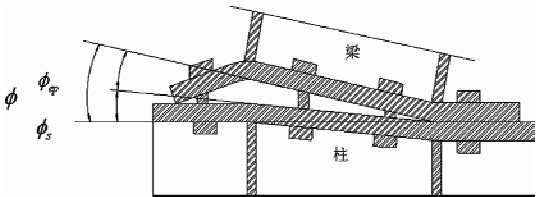
Figure 7   Rotation of extended end-plate joints

Use of the finite element analysis software ANSYS to analysis the effect of end-plate thickness，bolt diameter，bolt spacing，beam section height and column stiffener five factors to the end plate semi-rigid connection moment-rotation curve.

The End Plate Thickness

The end plate thickness of the model as shown in table 1. The moment-rotation curve and the effect of end plate thickness on the initial stiffness of the joint as shown in Figure 8 and Figure 9 respectively. Beam and column section size of the model are H300×200×8×12 and H300×250×8×12 respectively.

TABLE 1　END-PLATE THICKNESS OF MODELS IN THIS GROUP

model	end plate thickness(mm)	model	end plate thickness(mm)
WB8	8	WB20	20
WB12	12	WB24	24
WB16	16	WB28	28
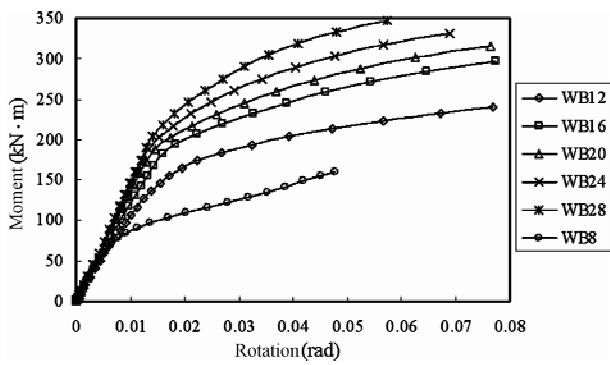
Figure 8　Joints moment-rotation curve of different end-plate thickness
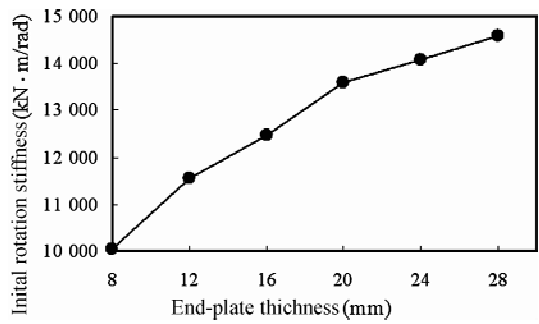
Figure 9　Influence curve of end-plate thickness to initial rotation stiffness

By the Figure 8 and 9 can be seen：with the end plate thickness increases，the initial stiffness of the joint increases，the plasticity bending bearing capacity increases，and the deformation capacity decrease accordingly. The effect of end plate thickness on the end plate connection performance showed the following rules：when the end plate thickness is relatively small，with the increase of the thickness of end plate，node moment-rotation curve changes obviously，the initial rotational stiffness and the plastic bending bearing capacity greatly improve；when the end plate thickness is larger，with the end plate

thickness increases，node moment-rotation curve changes a little or no change，the initial rotational stiffness and the plastic bending bearing capacity increase is not obvious.

The resulting moment-rotation curves of variation of the above reasons maybe：with the end plate thickness increases，the node failure mode has shifted. When the end plate thickness is relatively small，node failure mode is end plate buckling，then increase the end plate thickness the node performance greatly changed，as with the end plate thickness increases，node moment-rotation curve changes obviously，the initial rotational stiffness and the plastic bending bearing capacity greatly improve；when the end plate thickness increases to a certain value，the node failure mode change by the end plate buckling into bolt snapped，then it was not obvious to increase the end plate thickness on the node's performance，as with the end plate thickness increases，the moment-rotation relationship curve is very small，the initial rotational stiffness and the ultimate flexural capacity force unchanged.

The Bolt Diameter

The end plate and column flange was connected by high-strength bolts in end plate semi-rigid nodes，as the standard WB20 model，to analysis the effect of diameter change to the moment rotation curve of flush end plate and extended end plate semi-rigid connections by changing the diameter of the bolt. The bolt diameter of this group model as shown in Table 2.

TABLE 2　BOLT DIAMETERS OF MODEL IN THIS GROUP

model	WBM16	WB20	WBM24
bolt diameter	M16	M20	M24

The moment-rotation curve of the model as shown in Figure 10. It can be seen from the Figure that with the bolt diameter increases，the initial stiffness and ultimate flexural bearing capacity have been enhanced in different degree both flush end plate connection and extended end plate connection and overall increase marginally. When the bolt is improved from M16 to M20，the joint initial rigidity and bearing capacity of two kinds of end plate connection larger increase，when the bolt is improved from M20 to M24，the initial stiffness and bearing capacity smaller increase.
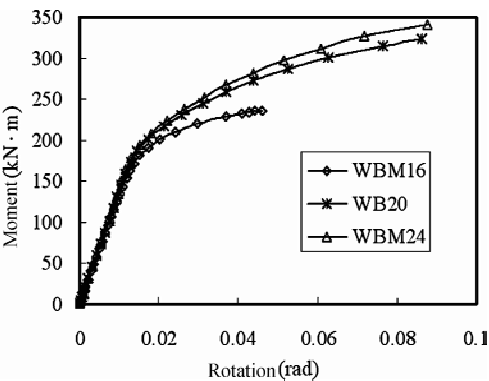
Figure 10　Joints moment-rotation curve of different diameter

The phenomenon is caused by the bolt joint failure mode change with changes in the diameter. When the bolt is M16，the node failure mode of two kinds is the screw broken，when the bolt is M20 and M24，the

node failure mode is end plate buckling. Therefore，when the bolt diameter smaller or larger thickness of end plate，increasing the diameter of the bolt can effectively improve the initial rotational stiffness and the bearing capacity，but when the bolt diameter is relatively large or end plate thickness is relatively small，increasing the bolt diameter to improve the initial rotational stiffness and the bearing capacity can not play a good effect.

Bolt Pitch

The bolt pitch of this model as shown in table 3.

TABLE 3   BOLT PITCHES OF MODELS IN THIS GROUP

model	WBD156	WB20	WBD196
bolt pitch(mm)	156	176	196

The moment-rotation curve of this model as shown in Figure 11. By the graph can be seen：with the bolt spacing increases，the deformation do not change，failure mode is not changed，moment-rotation curve does not change obviously，the initial rotational stiffness and the ultimate flexural bearing capacity increases a little.
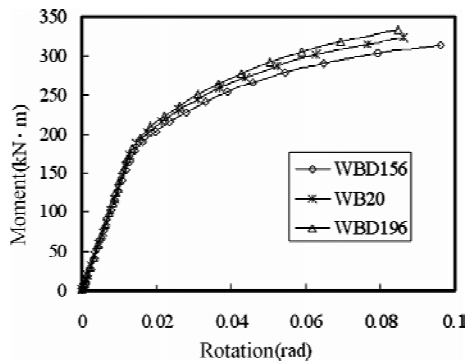
Figure 11   Joints moment-rotation curve of different bolt pitches

Beam Section Height

The beam section height of this model as shown in table 4.

TABLE 4   BEAM SECTION HEIGHT OF MODELS IN THIS GROUP

model	WBH250	WB20	WBH350
beam section height(mm)	250	300	350

The moment-rotation curve of the model as shown in Figure 12. It can be seen from the Figure that there are no obvious influence on node deformation when change of beam section height. The moment-rotation curve of the model changed significantly as the change of beam section height；the initial rotational stiffness and the ultimate flexural capacity is rising rapidly，while the joint deformation capacity decreased as the beam section height increased.
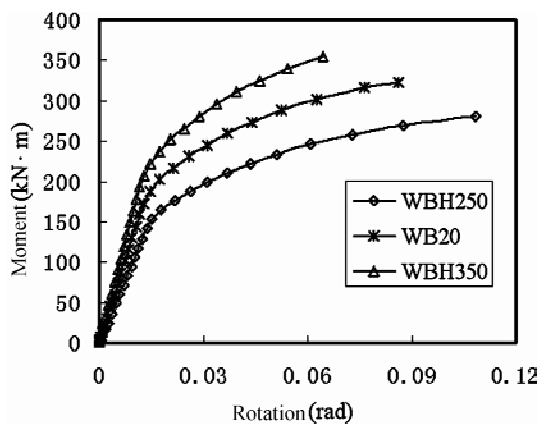
Figure 12   Joints moment-rotation curve of different beam section height

Column Stiffeners

In order to study the influence of column stiffeners on the end plate semi-rigid connection properties，removed the column stiffeners in the WB20，while other parameters unchanged，design model of WB20 -N. Using ANSYS to analyze them and compare with the model WB20.
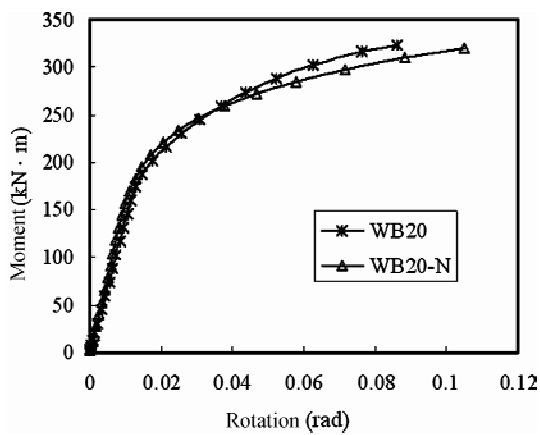
Figure 13   Joints moment-rotation curve of models in this group

Figure 4.13 shows that column stiffeners have great influence on the deformation characteristics of the extended end plate connections. For the model WB20，the beam flange at the end plate deformation larger，more obvious deformation occurred in node domain；remove the stiffener，the model WB20-N nodes in a large domain deformation，and the column flange under the beam flange buckling serious.

This shows that the column web stiffeners can control the domain deformation and improve joint stiffness remarkable both in end-plate connections and extended end-plate connections.

It can be seen from Figure 4.13 that the moment-rotation curves change little with or without stiffening，the initial rotational stiffness and the ultimate flexural capacity increase smaller. Therefore，it is not obvious to set column stiffeners in order to improve the initial rotational stiffness and the ultimate flexural

capacity.

CONCLUSIONS

（1）The finite element analysis method this paper used can well simulate the end plate semi-rigid connection of the overall force performance，bearing capacity and moment-rotation curve，thus provided a reliability method to simulate a variety of form and structure of the end plate connection by the finite element software ANSYS.

（2）End plate thickness and height of the beam feature a greater impact on end-plate semi-rigid connections. With the end plate thickness increases，the initial stiffness of the joint increases，the plasticity bending bearing capacity increases，and the deformation capacity decrease accordingly. The effect of end plate thickness on the end plate connection performance showed the following rules：when the end plate thickness is relatively small，with the increase of the thickness of end plate，node moment-rotation curve changes obviously，the initial rotational stiffness and the plastic bending bearing capacity greatly improve；when the end plate thickness is larger，with the end plate thickness increases，node moment-rotation curve changes a little or no change，the initial rotational stiffness and the plastic bending bearing capacity increase is not obvious.

（3）Along with the bolt diameter or bolt spacing increases，the initial stiffness and ultimate flexural bearing capacity of extended end plate connection improve a little. Compared with column stiffeners joint，the moment-rotation curves of no column stiffeners node have not obvious change，the initial rotational stiffness and the ultimate flexural capacity have a smaller increase，but the node domain have large deformation，as ductility improvement.

REFERENCE

［1］Chen，H. F.，"Stability design of steel frames"，Translated by Suiping Zhou，World Book Publishing Company，1999.

［2］Deng，F. P.，"ANSYS10. 0 finite element analysis of self-study manual"，People's Posts and Telecommunications Press，2009.

［3］Gong，S. G.，Xie，G. L. and Huang，Y. Q.，"ANSYS parametric programming and command manual"，Machinery Industry Press，2010.

［4］Li，W.，"Civil engineering application examples of ANSYS"，China Water Conservancy and Hydropower Press，2007.

［5］Shi，G.，"Static and Seismic Behavior of Semirigid End-plate Connections in Steel Frames"，Tsinghua University，2004.

［6］Shi，G.，Shi，Y. J.，Wang Y. Q.，Li，S. F. and Chen，H.，"Experimental study of semirigid end-plate connections in multi-story steel frames"，Journal of Tsinghua University（natural science edition），2004，3(44)，pp. 391-394

STUDY ON TENSILE BEARING BEHAVIOR OF REINFORCED GUSSET PLATE CONNECTIONS TO SLOTTED TUBES

* X. P. Shu[1], Z. S. Yuan[1], Z. L. Ding[1], H. Zou[1], Y. S. Ding[2]

[1] Steel Structural Institute of Civil Engineering College，Hunan University，Changsha，410082，China
[2] China Aeronautical Project and Design Institute，Beijing，100088，China
* Email：shuxingping@sina. com

KEYWORDS

Reinforced gusset plate connections to slotted tubes，tensile bearing behavior，experimental research，shear lag.

ABSTRACT

A number of studies on gusset plate connections to slotted tubes have been carried out in the last few years，however，it mainly focuses on those connections which are not reinforced. So，in order to study the tensile bearing behavior of reinforced gusset plate connections to slotted tubes，the experimental study and simulation by ANSYS were conducted to a total of six specimens of gusset plate connections to slotted tubes，in which two were not reinforced，two were reinforced by weld hollow sphere and the other two were reinforced by plates. Test results showed that the failure modes of all these specimens were tensile failure occurred in the tube where the gusset plate entered it，and a clear necking had taken place before failure in the tube of specimens GPT-3 and GPT-6 which were reinforced by plates. A good agreement is observed between the results of test and FEA. The study indicates that the phenomenon of shear-lag is rather serious in the process of tensile loading and the quality of welds at the slotted end has great impact on the ultimate tensile bearing capacity of gusset plate connections to slotted tubes. In addition，the tensile bearing capacity of reinforced gusset plate connections to slotted tubes is higher than the relevant connections which are not reinforced，but the increasement of connections reinforced by plates is more remarkable.

INTRODUCTION

In bracing structures or long-span tube trusses，the tubes are frequently slotted into gusset plates to simplify fabrication and avoid intersection line cutting[1]. Because the gusset plate only connects to a part of the tube section，shear-lag occurs at the circumference where the hollow section connected to the gusset plate[2]，the unconnected circumference of the hollow section is not fully engaged and contributes only in part to the resistance of the member. And an early failure may happen in connections because of the stress concentration at the slotted ends. The present study mainly focuses on gusset plate connections

to slotted tubes which are not reinforced，such like the experimental program and associated numerical analysis carried out by Cheng J. J. R. [3]，and those ultimate tensile strength calculated formulas given by American code[4] and Canadian code[5]. But the relevant study about the gusset plate connections to slotted tubes which are reinforced is little. So，an experimental study and associated numerical analysis were carried out on four reinforced gusset plate connections to slotted tubes with two relevant connections which were not reinforced.

EXPERIMENTAL PROGRAM

Specimens Design and Test Setup

The experimental study comprised of six specimens shown in Figure 1. Among them，specimens GPT-1 and GPT-4 are not reinforced，GPT-2 and GPT-5 are reinforced by welded hollow sphere，specimens GPT-3 and GPT-6 are reinforced by steel plate which has the same thickness as the steel tubes. The fillet weld sizes in all the specimens are 8 mm，and the specimens' material is Q235. The physical dimensions of specimens and the material properties are shown in Table 1. According to the characteristic of the specimens in this paper，test setup is constructed as shown in Figure 2，so that the pressure of the jack can transform to tension of the specimen through distribution beams.
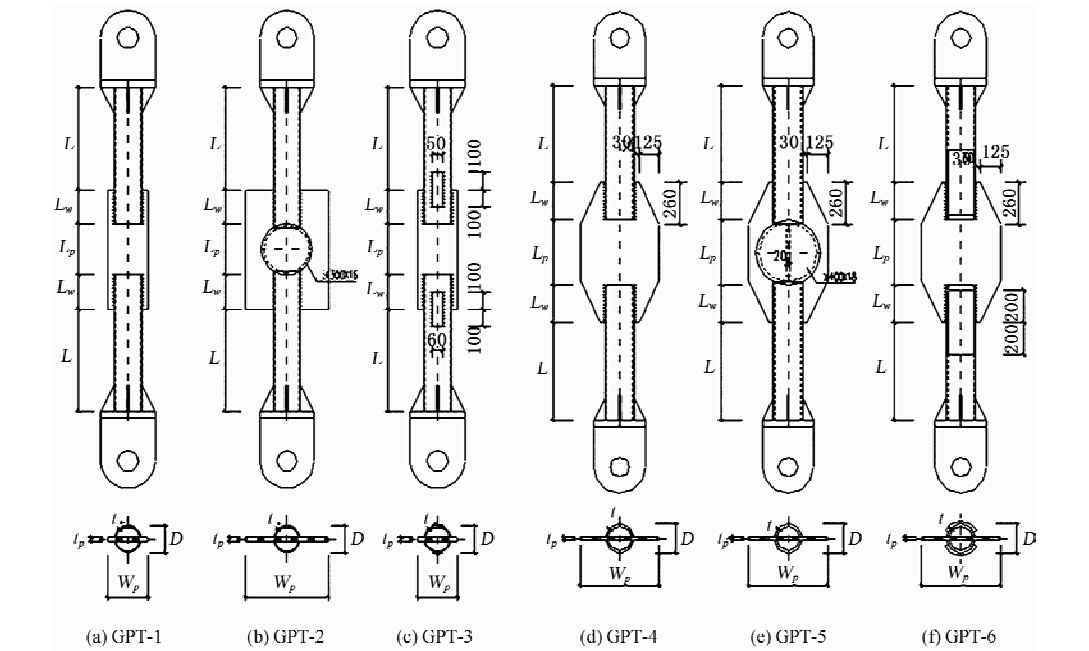
Figure 1 Dimensions of test specimens

TABLE 1 DIMENSIONS OF TEST SPECIMENS

Specimens	D /mm	t /mm	W_p /mm	t_p /mm	L_p /mm	L_w /mm	L /mm
GPT-1	159. 0	6. 0	239	22. 0	300	200	600
GPT-2	159. 0	6. 0	490	22. 0	300	200	600
GPT-3	159. 0	6. 0	239	22. 0	300	200	600

							continued
Specimens	D /mm	t /mm	W_p /mm	t_p /mm	L_p /mm	L_w /mm	L /mm
GPT–4	180.0	10.0	490	22.0	400	230	600
GPT–5	180.0	10.0	490	22.0	400	230	600
GPT–6	180.0	10.0	490	22.0	400	230	600

Properties of steel: yield strength, $f_y = 278.9$ MPa; tensile strength, $f_u = 440.3$ MPa; modulus of elasticity, $E = 2.07 \times 10^5$ MPa
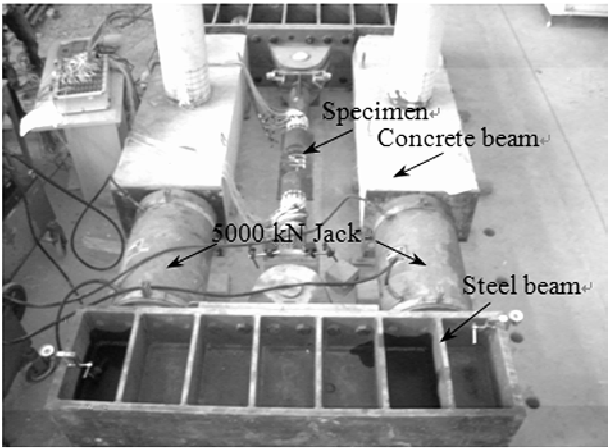
Figure 2   Test set-up of specimens

Loading Program and Test Content

According to the pre-estimated ultimate tensile bearing capacity of the specimen，we loaded on it at different stages. The pre-estimated ultimate strength was the smaller one of the finite element analysis result. Loading process included preloading，standard loading and failure loading. Preloading consisted of three steps，and the load in every stage was twenty percent of standard load，then it was unloaded in 2-3 steps. The time interval between every step was 10 minutes. In standard loading stage，we loaded as much as 10% of the preestimated ultimate strength in every step to 90% of the strength or obvious plastic deformation appeared. And the time of dead loading in every step should not be less than 30 minutes in order to reduce the difference between the short-term test loading and the long-term practical loading. In failure loading stage，we loaded as much as 5% of the preestimated ultimate strength in every step until the specimen damaged.

During the test，a total of four strain gauges were arranged on the exterior surface of the tube，then the internal force of the tube in elastic working stage can be attained through the strain data of strain gauges，and the loading case of jack can be monitored. In order to investigate the complicated stress of the hollow section at the slotted end and obtain the stress development situation and the elastic-plastic deformation in this region，strain rosettes were located on the exterior surface of the hollow section at the slotted ends，as shown in Figure 3. Two string-displacement meters were located on both sides of the tubes in order to obtain the axial deformation of the specimens.
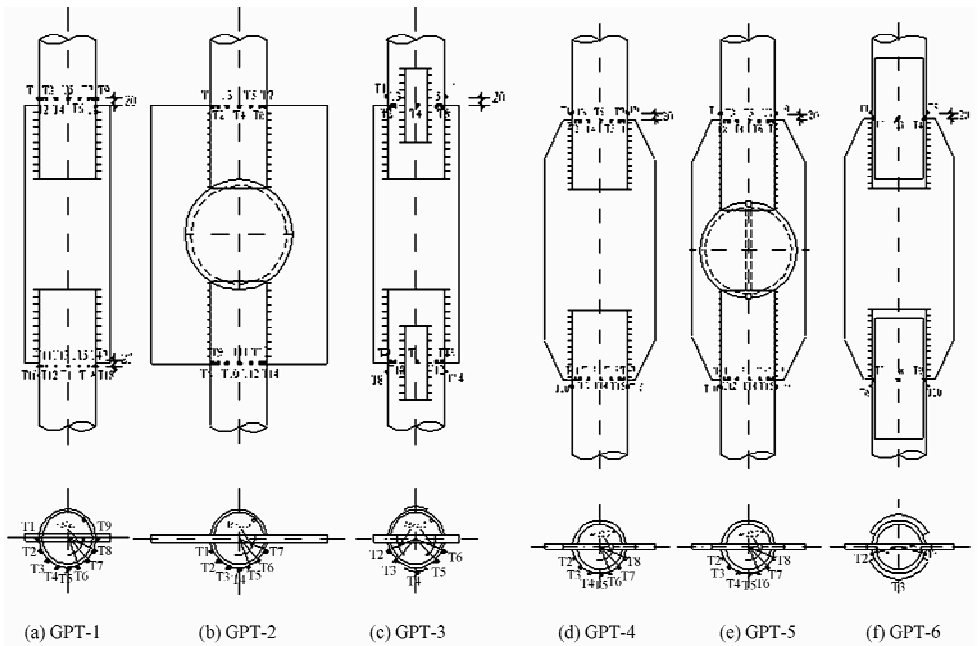
Figure 3　Strain gauge and rosette locations on specimens

EXPERIMENTAL RESULTS AND ANALYSIS

Failure Modes of Specimens

The test showed that the failure of all these cases occurred in the tube where the gusset plate entered it，and obvious necking of the specimens GPT-3 and GPT-6 reinforced by plate had taken place in the tube before failure. In the process of tensile loading，the phenomenon of shear-lag was very serious. Figure 4 and Figure 5 show the final failure modes of the GPT-1 and GPT-2 after test. In the loading process of specimen GPT-1，when the load reached 902.5 kN，cracks appeared at the toe zone of welds of the slotted end. When the load reached 1 092.5 kN，tension failure occured at the slotted end of the circumference of hollow section，and the load couldn't increase any more. For GPT-2，when the load reached 950.0 kN，crack appeared at the toe zone of welds of the slotted end. When the load reached 1 140.0 kN，tension failure occured at the slotted end of the circumference of hollow section. In the process that the specimen GPT-3 was loaded，a clear necking had taken place on the tube，as shown in Figure 6，and crack appeared at the toe zone of welds of the slotted end when loaded to 997.5 kN. When the load exceeded 1 192.5 kN，the cracks developed faster and faster. After the load reached 1 245.0 kN，the circumference of hollow section at the slotted end was tensioned to failure. For the sake of welding，the quality of welds at the slotted end of specimen GPT-4 was poor and the size of welds at the slotted end was not enough. When the load reached 1 500.0 kN，the toe zone of welds at the slotted end began to crack. When the load reached 1 602.5 kN，the specimen lost its bearing capacity. So，for the reason above，the ultimate bearing capacity of specimen GPT-4 was smaller than the pre-estimated value. The failure mode is shown in Figure 7. The failure mode of specimen GPT-5 was quite the same as that of specimen GPT-4，as shown in Figure 8. Its cracking load was 1 707.5 kN，and the ultimate strength was 1 913.8 kN. In the process that specimen GPT-6 was loaded to 1 862.5 kN，crack appeared at the toe

zone of welds at the slotted end. As the load increased，the development of cracks became slowly，and necking on the tube was found，as shown in Figure 9，and the loading stopped with the load of 2 497.5 kN.
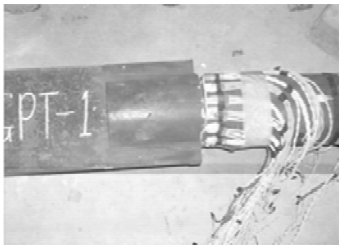
Figure 4　Fracture of GPT-1
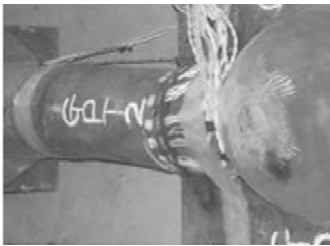
Figure 5　Fracture of GPT-2
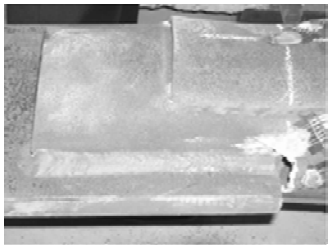
Figure 6　Necking and fracture of GPT-3

Figure 7　Fracture of GPT-4
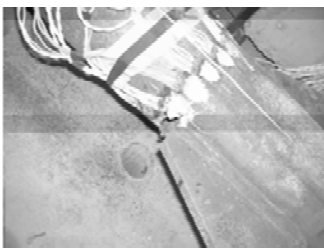
Figure 8　Fracture of GPT-5
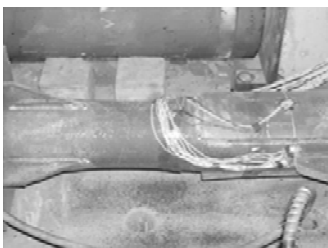
Figure 9　Necking and fracture of GPT-6

Stress Distribution on the Hollow Section at the Slotted Ends

Because of the effect of shear-lag and stress concentration，not every part of the hollow section at the slotted end is effective，and the circumference around unconnected place displays only part of the potential bearing capacity. So，it is necessary to know the stress distribution on the hollow section at the slotted end. In these tests，the disposal of strain gauge is taken into account of this situation，as Figure 3 shown. According to the strain of test points and the characteristic of material，we can transform these complex stresses which are taken from test points into Mises equivalent stress σ_e. The distribution curves of these equivalent stresses on the hollow section at the slotted end are shown in Figure 10 to Figure 13.

From Figure 10 and Figure 12，we can see that the stress distribution on the hollow section at the slotted end is non-homogeneous and test point at the slotted end yields firstly comparing with the others on the same cross-section. Moreover，test points far from the slot are still in elastic stage when the joint destroyed. Because the weld quality of specimen GPT-4 at the slotted end is poor，the stress distribution is much more non-homogeneous than that of specimen GPT-1. From Figure 10 and Figure 11，we can see that the difference of stress distribution between GPT-2 and GPT-1 is not very obvious. Comparing Figure 12 and Figure 13，we can see that the distribution of equivalent stress on the cross-section of GPT-5 is more homogeneous. For the existence of reinforced plate，the stress distribution at the slotted end can't be measured，so the equivalent stress distribution of GPT-3 and GPT-6 are not described in this paper.
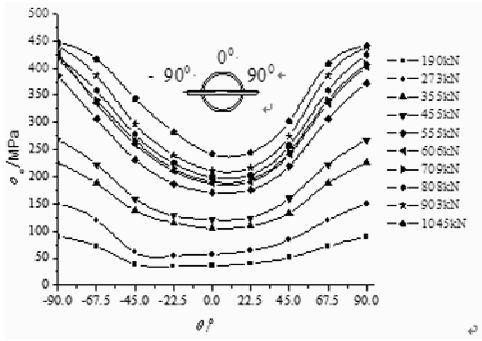
Figure 10　Equivalent stress distribution around circumference of the round hollow section（GPT‑1）
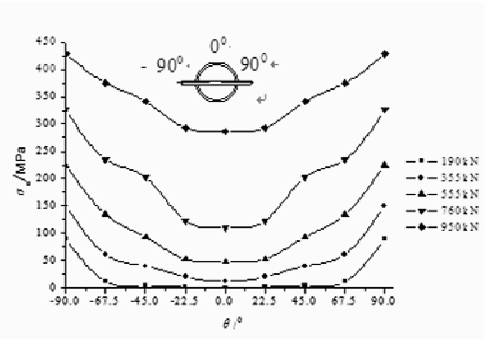
Figure 11　Equivalent stress distribution around circumference of the round hollow section（GPT‑2）
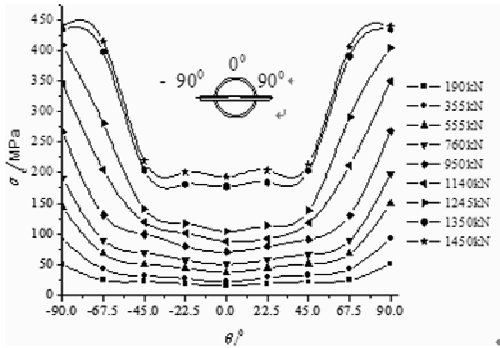
Figure 12　Equivalent stress distribution around circumference of the round hollow section（GPT‑4）
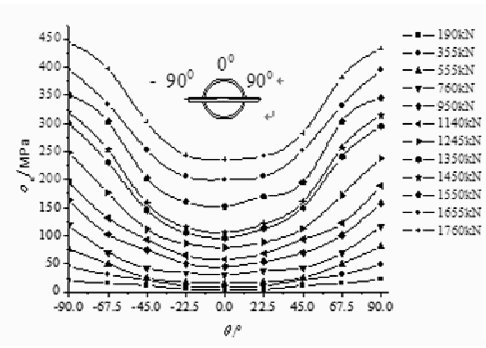
Figure 13　Equivalent stress distribution around circumference of the round hollow section（GPT‑5）

Comparison between Test Results and Results of Finite Element Analysis

In this paper，the six specimens were simulated and computed with Shell 93 in ANSYS. Stress-strain relationship in ideal elastic-plastic and the Von Mises yield criterion were adopted. But the effect of welds and residual stress were not taken into account. The contrast between load-axial displacement curves from test and the results from finite element are shown in Figure 14 to Figure 19. From Figure 14，Figure 15，Figure 16，Figure 18 and Figure 19，we can see that the maximum load from FEA is close to the test maximum load，but the displacements calculated from FEA are not matching well with that got from the tests. The main reasons may as follows：Firstly，in order to get the whole load-displacement curves of the specimen in FEA，the whole loading process was controlled by displacement. But in test，loading process was controlled by load because of the limit of testing device. Secondly，cracks appeared at the slotted ends when the specimens were under loading for the effect of stress concentration and weld residual stress. But the effect of cracks was not taken into account in FEA. From the contrast of Figure 14 and Figure 17，we can see that the strength of the connections is restricted by the quality of the return welds at the slotted ends. From the load-displacement curves of all specimens as shown in Figure 14 to Figure 19，it can be found that the strength and ductility of the reinforced specimens are higher than that of which are not reinforced. Because the welded hollow sphere can transfer part of tensile force，the strength and ductility of gusset plate connections to slotted tubes members GPT‑2 and GPT‑5 which are reinforced by welded hollow sphere are higher than specimens GPT‑1 and GPT‑4. Since the tubes necking may increase the axial displacement of the tubes，the ductility of specimens GPT‑3 and GPT‑6 is

much better than that of GPT-1 and GPT-4. At the same time，for the development of the cracks of the hollow section at the slotted end is restricted by the reinforced gusset plates，the strength of specimens GPT-3 and GPT-6 is obviously higher than the strength of GPT-1 and GPT-4. The necking position of the specimen GPT-6 is different from GPT-3 because of the different dimensions of reinforced plates. Finally，test ultimate strength of all specimens is compared with the FEA results，as shown in Table 3. From Table 2 it can be seen that the test ultimate strength of specimens match well with the FEA results except GPT-4，for the strength of the joint is restricted by the quality of the return welds at the slotted end，but the FEA hasn't taken the effect of weld into account.

TABLE 2   COMPARISON BETWEEN CALCULATED VALUES FROM FEA AND TEST VALUES

Specimens	FEA values N_{tu}^{FEA}	Test values N_{tu}^{T}	$N_{tu}^{FEA} / N_{tu}^{T}$
GPT-1	1 006.4 kN	1 092.5 kN	0.92
GPT-2	1 115.8 kN	1 140.0 kN	0.98
GPT-3	1 187.8 kN	1 245.0 kN	0.95
GPT-4	1 705.7 kN	1 602.5 kN	1.06
GPT-5	1 902.3 kN	1 913.8 kN	0.99
GPT-6	2 322.7 kN	2 497.5 kN	0.93
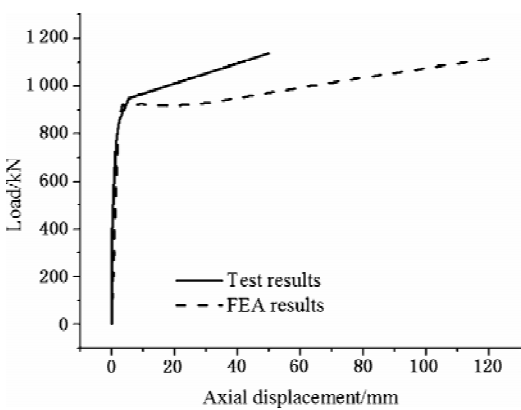
Figure 14   Load-displacement curves of GPT-1
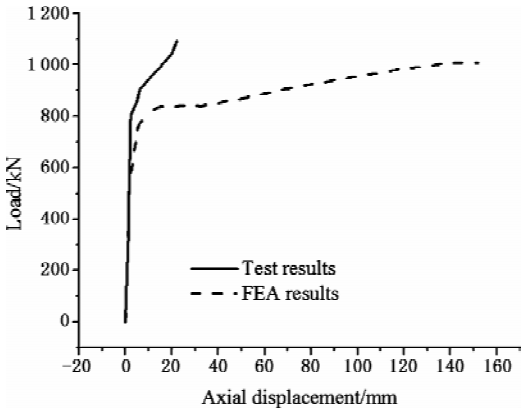
Figure 15   Load-displacement curves of GPT-2
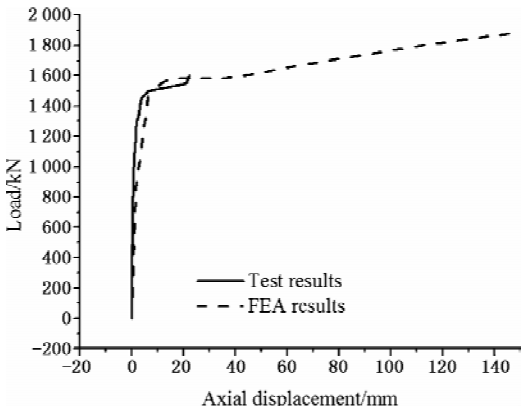
Figure 16   Load-displacement curves of GPT-3
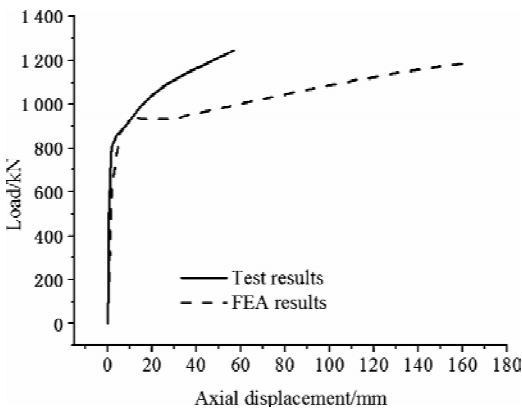
Figure 17   Load-displacement curves of GPT-4
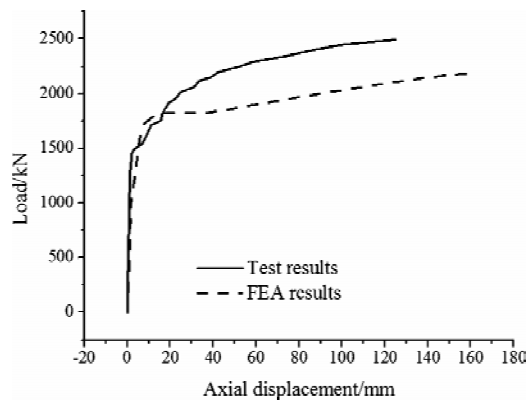
Figure 18   Load-displacement curves of GPT–5
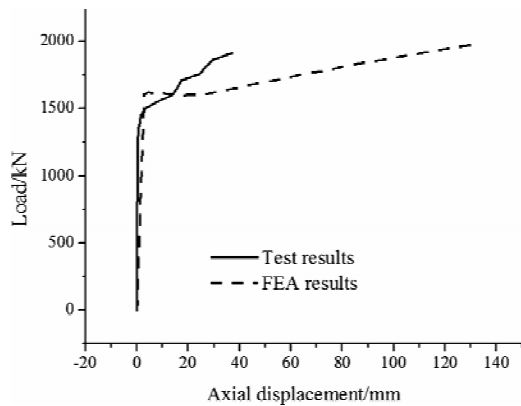
Figure 19   Load-displacement curves of GPT–6

CONCLUSIONS

An experimental program and associated finite element analysis on four reinforced gusset plate connections to slotted tubes and two relevant connections not reinforced were carried out，and the conclusions are summarized as follows：

(1) The failure of all specimens occurred at the circumference of the hollow section at the slotted ends，and shear-lag was serious in the process of tensile loading.

(2) The tensile strength of the connection is restricted by the quality of the return welds at the slotted end. Therefore，attention should be paid on this detail of gusset plate connections to slotted tubes in practical projects.

(3) The tensile strength and ductility of the gusset plate connections to slotted tubes reinforced by welded hollow sphere or plates are higher than that which are not reinforced，and the strength of the connections reinforced by plates enhances more remarkably.

ACKNOWLEDGMENT

REFERENCES

［1］Ding，Y.S.，"Discussion on some design problems in circular tubular joints"，Spatial Structures，2002，8(2)，pp. 56–64.

［2］Chen，S.F.，"Design of steel structures（The third edition）"，Science Press，2005.

［3］Cheng，J.J.R.，Kulak，G.L. and Khoo，H.，"Strength of slotted tubular tension members"，Canadian Journal of Civil Engineering，1998，25(4)，pp.982–991.

［4］American Institute of Steel Construction，Specification for structural steel buildings，2005.

［5］Canadian Standards Association，Limit states design of steel structures，2003.

FULL-SCALE EXPERIMENT RESEARCH ON K AND KK JOINTS

[*] X. P. Shu，Y. Yao，S. N. Zhu，Z. S. Yuan and B. R. Lu

Steel Structural Institute of Civil Engineering College of Hunan University，Changsha，P. R. China
[*] Email：shuxingping@sina. com

KEYWORDS

CHS joints，full-scale experiment，FEA，code design formula.

ABSTRACT

In order to obtain the failure modes，the stress distributions and the ultimate capacity of circular hollow sections（CHS），full-scale tests on five specimen joints were carried out，including two K joints and three KK joints. Three kinds of failure patterns of specimen joints were observed in the tests，namely weld crack failure connecting tensile brace and chord，the local buckling failure at compressive brace end adjacent to the chord and the failure combined weld crack of tensile brace with local buckling of compressive brace. The distribution and development of the equivalent stress were rather complicated and non-uniform. As the specimens used in the tests had the peculiarity of strong chord and weak brace，the failure modes of joints were different from that stipulated in the codes（GB 50017-2003 and Eurocode3），in which the chord failed due to the excess of plastic deformation. Therefore calculation for the ultimate capacity could not apply the formulas given in the codes. Good agreement had been found between the results of laboratory tests and Finite Element analyses（FEA）. FEA method was an efficient method of solving ultimate capacity of such joints.

INTRODUCTION

With the invention of intersecting line cutting machine，CHS joints become more and more widely used in long-span space structure. Experimental and theoretical researches were done over last several years[1-6]. K joints and KK joints are two of the most common forms in CHS joints. In order to investigate the stress distribution，deformation and ultimate capacity of K joints and KK joints，full-scale experiments and FEA on five joints were carried out.

TEST PROFILE

Joint Specimens

In the test，CHS were used in both chords and braces of all the specimens. Five specimens including two

K-type joints and three KK-type joints were divided into two groups. Geometrical parameters of joints are shown in Figure 1-2 and Table 1-2.
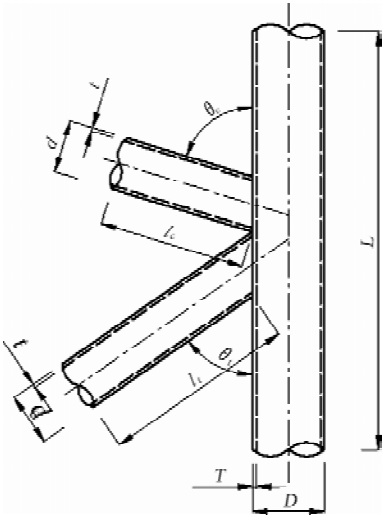
Figure 1   Geometrical parameter of K-type joints
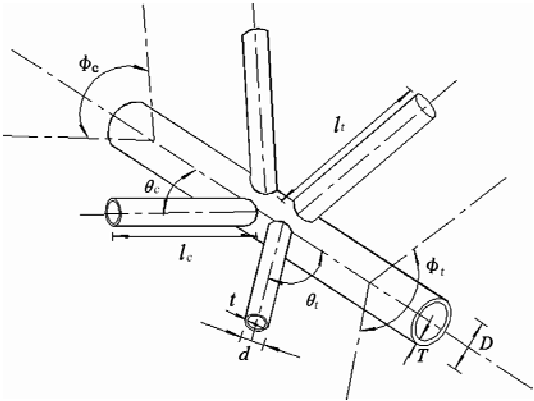
Figure 2   Geometrical parameter of KK-type joints

TABLE 1   GEOMETRICAL PARAMETER OF K-TYPE JOINTS

Specimens	D/mm	T/mm	d/mm	t/mm	L/mm	l_c/mm	l_t/mm	θ_c /(°)	θ_t /(°)
K1	299	20	89	4	1 500	350	925	61.9	61.3
K2	245	14	180	12	2 000	500	660	73.0	55.2

TABLE 2   GEOMETRICAL PARAMETER OF KK-TYPE JOINTS

Specimens	D/mm	T/mm	d/mm	t/mm	L/mm	l_c/mm	l_t/mm	θ_c /(°)	θ_t /(°)	φ_c /(°)	φ_t /(°)
KK1	299	16	159	6	2 000	500	500	56.7	53.3	52.6	58.6
KK2	299	20	159	6	2 000	450	530	72.5	61.0	34.4	35.1
KK3	339	40	159	6	2 000	560	550	69.0	62.7	37.4	39.7

All the tubular joints used Q235B Steel. Through data analysis and statistic of 12 groups of material property experiments，the actual material parameters of joint specimens were obtained：yield strength f_y equals 273.2 MPa，tensile strength f_u equals 442.9 MPa，elongation δ equals 22.5%，material elastic modulus E equals 2.057×10^5 MPa.

Test Equipment and Loading Process

In order to inspect the damage forms and ultimate strength of CHS，special loading device was designed which could withstand above 2 000 kN，as shown in Figure 3. The loading device was a plane steel frame composed of two H-columns and two H-beams connected with bolts. The K-type joints were directly

connected to the loading device with bearing while KK-type joints made use of distributing beams for its spatial brace tubes. The stiffeners were layout for the local stability of the loading device. Supporting frame perpendicular to the plane was set up to guarantee the stability of the specimens out of plane. Two boot beams were set up at the bottom to raise the stability of the loading device out of the plane.

In this experiment，a similar loading program was adopted for both K-type joints and KK-type joints. The program loaded directly to the chords through a hoisting jack and made the braces loaded passively. When the chords were loaded upward，the lower braces are in tension while the upper braces are in compression. Figure 3 and 4 separately show the loading scene of K-type joints and KK-type joints.
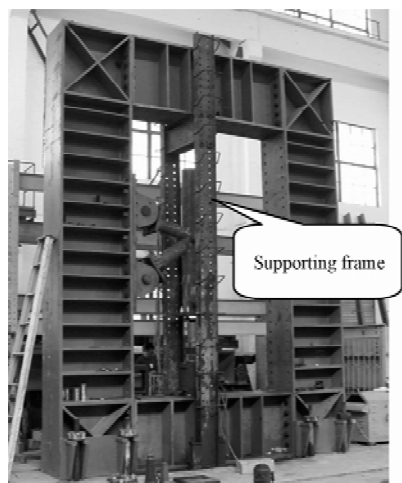
Figure 3   Test loading of K-type joints

Figure 4   Test loading of KK-type joints

Based on the predicted ultimate load bearing capacity of joint specimens，each loading level is 10% of the predicted ultimate load bearing capacity. When reaching 90% of the predicted ultimate load bearing capacity or there is an obvious plastic deformation，the load level should decrease to 5% of the predicted ultimate load bearing capacity until the joints damaged by reaching its ultimate load bearing capacity.

The Measurement

The measurement focuses on strain measurement，displacement measurement and bearing capacity measurement. During testing it layouts strain gauges in the centre of both chords and braces which are set each $90°$ around the section. The internal force and the bending moment of each member in the elastic range can be calculated through strain data by strain gauges，meanwhile，the loading of the hoisting jack and the plastic state of each tube are monitored. In order to investigate the complex stress states and the development of stress in the cross region of chords and braces and the elastic-plastic deformation of chord wall，three-element strain gauges are layout on chord wall about 10mm away from the brace roots，as shown in Figure 5.

In order to investigate the local deformation of chord wall and axial deformation of the chords，displacement meters are layout between one side or both sides of brace axis and chord axis to measure local deformation of chords wall and relative displacement between the braces and chords，as shown in Figure 6.

(c)

(d)

(e)
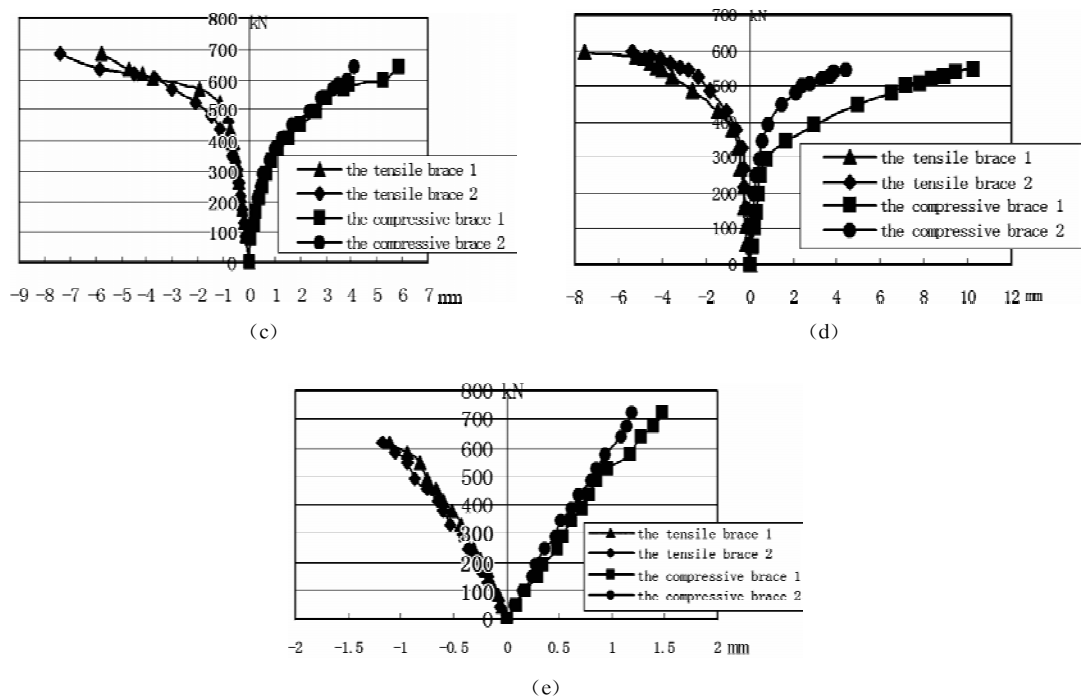
Figure 9   The load-displacement curves of the joints

Comparison with the Test Results，FEA Results and Code Formula Calculating Values

Using the finite element program ANSYS as a calculating tool，ultimate capacity analysis on five joints in this experiment are done respectively. Calculating models make use of 3D four-node element Shell181 in ANSYS Cell Library，taking the geometric nonlinearity and material nonlinearity into consideration at the same time. The experiment's loading and binding situation is simulated during analysis. Calculation model of K-type joints and KK-type joints are shown in Figure 9. Material is regarded as the ideal elastic-plastic material which obeys Von-Mises yield criteria and plastic flow criteria. Ultimate capacity changes made by residual stress and welds are not considered in this paper. There is a comparison between FEA results，experimental results and code formula calculating values[7-8]. As shown in Table 3.

TABLE 3   COMPARISON BETWEEN THE TEST RESULTS，FEA RESULTS AND CODE FORMULA CALCULATING RESULTS

specimens	Test results N_{u1}/kN	FEA results N_{u2}/kN	Calculating results of GB 50017—2003 N_{u3}/kN	Calculating results of Eurocode3 N_{u4}/kN	N_{u2}/N_{u1}
K1	287	244	742	854	85%
K2	1 776	1 690	822	794	95%
KK1	654	698	874	855	107%
KK2	700	597	983	1 063	85%
KK3	958	838	1 800	3 032	87%

By comparison in Table 3，we can see that the deviation between joint ultimate capacity calculated by FEA and testing results is between -15% and $+8\%$. Deviation is mainly caused by different material

(a) Calculating model of K-type joints   (b) Calculating model of KK-type joints
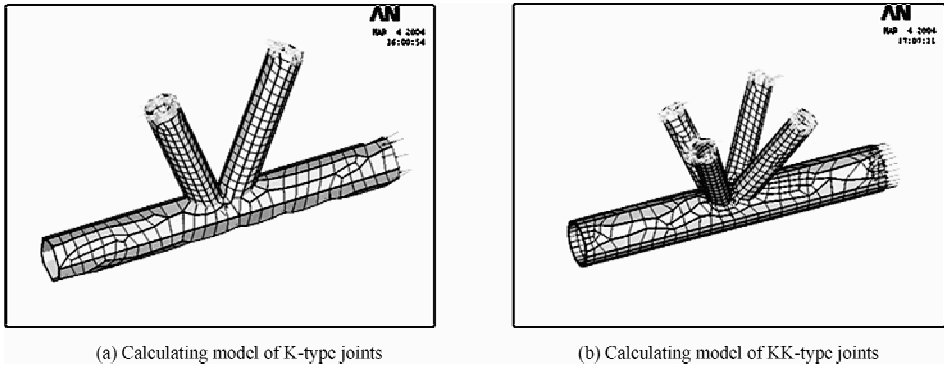
Figure 10   Calculating models

stress-strain curves between FEA and experiment，effect by welds and different models between FEA and joint specimens. Inspite of the deviation，joints ultimate capacity calculated by finite element analysis are basically in agreement with tested results.

Tested joint's ultimate capacity is significantly less than code formula calculating values except for K2 joint. The reason of the large difference mainly because that the code formula calculation of intersection joints capacity is based on the chord wall failure of the excessive local plastic deformation while the failure modes of joints in the test are the brace roots local buckling and weld's sudden fracture connecting the chords and the braces in tension，although the geometric parameters of the test joints are consistent with the code requirements and joint's ultimate capacity could not be calculated by code formulas. For K2 joint which is destroyed by slight plastic deformation of the chord wall intersecting the braces，the weld crack failure of tensile brace and local bucking failure of compressive brace，the ultimate capacity calculated by code formula is significantly higher. The calculation results of ultimate capacity are conservative when joints are destroyed by the large plastic deformation on the chord wall.

CONCLUSIONS

Full-scale tests on five circular hollow sections（CHS）were carried out. After Comparison with the test values，FEA calculating values and code formula calculating values，we obtain several main following discussions.

First，chords walls have no obvious deformation under the axial force from the brace. The joint failure damage patterns are mainly divided into three forms，namely weld crack failure connecting tensile brace and chord，the local buckling failure at compressive brace end adjacent to the chord and failure combined weld crack of tensile brace and local bucking of compressive brace.

Secondly，equivalent stress distribution on chord walls is very uneven. Some testing joints entered the plastic stage at a very early moment while the others at elastic stage all the time. Equivalent stress σ_e of K-joints and KK-joints is roughly symmetrical to chord axis. Regions where stress is larger and grows faster more concentrate on joints' toe and heel.

Thirdly，it is an effective method to analyze the ultimate capacity of intersecting joints with FEA，and

the results are true and credible.

Finally，because joints in this paper have stronger chords and relatively weaker brace，the damage forms don't belong to the form of excessive plastic deformation on chords defined in the code. It can not be calculated by code formula of our country.

ACKNOWLEDGMENT

REFERENCES

［1］Dexter，E.M. and Lee，M.M.K.，"Static Strength of Axially Loaded Tubular K-Joints Ⅰ：Behavior"，Journal of Structural Engineering，ASCE，1999，125(2)，pp.194-201

［2］Dexter，E.M. and Lee，M.M.K.，"Static Strength of Axially Loaded Tubular K-Joints Ⅱ：Ultimate Capacity"，Journal of Structural Engineering，ASCE，1999，125(2)，pp.202-210

［3］Gazzola，F.，Lee，M.M.K. and Dexter，E.M.，"Design Equation for Overlap Tubular K-Joints under Axial Loading"，Journal of Structural Engineering，ASCE，2000，126(7)，pp.798-808

［4］Lee，M.M.K. and Wilmshurst，S.R.，"Strength of Multiplanar tubular KK-joints under antisymmetrical axial loading"，Journal of Structural Engineering，ASCE，1997，123(6)，pp.755-764.

［5］Chiew，S.P.，Soh，C.K. and Wu，N.W.，"Experimental and Numerical SCF Studies of Multiplanar Tubular XX-Joint"，Journal of Structural Engineering.，ASCE，2000，126(11)，pp.1331-1338

［6］Shen，Z.Y.，Cheng，Y.J. and Chen，Y.Y.，"Experimental Study on Overall Roof Structure and Joints of a 80 000-seat Stadium in Shanghai"，Journal of Building Structures，1998，19(1)，pp.2-10.

［7］Ministry of Construction of the PRC，Code for design of steel structures（GB50017-2003），2003，Beijing，pp.101-102

［8］European Committee for Standardization，Eurocode 3：Design of steel structures-Part 1-8：Design of joints，CEN，2005，pp.109

STATIC BEHAVIOR OF PARTIALLY OVERLAPPED TUBULAR N-JOINTS OF SQUARE CHORDS WITH CIRCULAR BRACES

* X. P. Shu，Z. S. Yuan，Z. R. Zhu，Y. Yao and B. R. Lu

Steel Structural Institute of Civil Engineering College，Hunan University，Changsha，410082，China
* Email：shuxingping@sina. com

KEYWORDS

Tubular N-joint，static behavior，experimental research，parametric analysis.

ABSTRACT

An experimental program and associated parametric analysis of the ultimate load behavior of partially overlapped tubular N-joints of square chord with circular braces were carried out. Two partially overlapped N-joints of square chords with circular braces were tested to failure under overlapping brace axial compression and chord axial loading. Then，tests results including the failure mode and ultimate capacity were compared with the FEA results，showing good agreement. A detailed parametric study is subsequently conducted to examine the failure modes and the ultimate bearing capacity of this kind of joints. The analytical results show that there are several possible failure modes of the joint under overlapping brace axial compression namely the chord face plastification，the overlapping brace local bucking and the combination of the two. Additionally onset of cracking is also one of the failure modes appear in some joints. Among these failure modes，the chord face plastification is found to be the most common type of failure mode at high chord width-to-its thickness ratio. Furthermore，the effect of geometric parameters on the joints is analyzed and comparision of results between FEA and code formula is conducted.

INTRODUCTION

Hollow sections are widely used in steel structures for their simple and aesthetic appearance. Usually two shapes of hollow sections are used，circular hollow section（CHS）and rectangular hollow section（RHS）. Circular hollow sections are used almost exclusively in offshore structures. This is due to the following factors：relatively lower drag coefficient，equal lateral strength in all directions，minimal stress concentration in joints，and outstanding buckling strength. Rectangular hollow sections provide a simpler geometry so the joints can offer a more economical design than the equivalent circular sections with respect to fabrication costs. For the reasons above，tubular joints of square chords with circular braces are used. A series of experimental and theoretical studies have been carried out on the load-carrying capacity of circular hollow section joints[1-8]，and the formulae have been built[9-12]. However，the research on

tubular joint of square chords with circular braces is rare，especially on N-joints.

A full-scale experimental research on two partially overlapped N-joints of square chords with circular braces under axial force of chord and brace was carried out. Then，tests results including the failure mode and ultimate capacity were compared with the FEA results and associated parametric analysis were conducted using the FE model simulating the experiment.

EXPERIMENTAL PROGRAM AND FE MODEL

Test Specimens and Test Set-up

The configuration and geometric variables of the two partially overlapped tubular N-joints of square chord with circular braces are illustrated in Figure 1 and Table 1. The hidden seams of the joints were welded. Figure 2 shows the test set-up of N-joints. A planar reaction frame which could balance itself was designed in the experiment. The plane frame was made up of two frame columns and two frame beams. They were connected together with bolts. The diagonal brace (i. e.，the overlapped brace) was hinged on the plane frame while the left end of the chord was connected to the column of the frame with bolts.
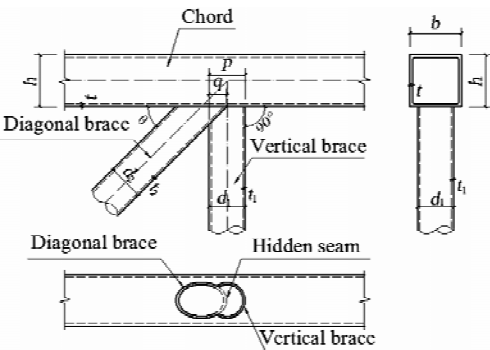
Figure 1   Geometric parameters of N-joints
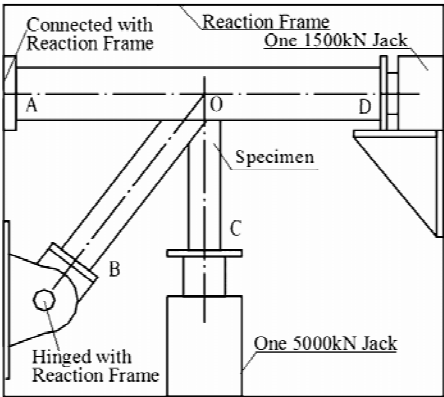
Figure 2   Schematic drawing of test set-up

TABLE 1   GEOMETRIC PARAMETERS OF OVERLAPPED N-JOINTS

Specimen name	b	h	t	d_1	t_1	d_2	t_2	θ	O_v
N1	300 mm	300 mm	10 mm	180 mm	8 mm	203 mm	10 mm	52.3°	57.0%
N2	300 mm	300 mm	14 mm	219 mm	12 mm	219 mm	12 mm	52.3°	60.3%

Properties of steel：yield strength，$f_y = 349.5$MPa；tensile strength，$f_u = 524.2$ MPa；modulus of elasticity，$E = 2.04 \times 10^5$ MPa

Test Procedure and Failure Modes

Axial pressure was applied on the right end of the chord and the lower end of the vertical brace simultaneously by hydraulic jacks，which made the chord and the vertical brace in compression and the diagonal brace in tension. During the test，the load was increased by 10% of the design load which calculated from FEA. When it reached 80% of the design load or there was obvious plastic deformation，5% of the design load was increased in every step until the joint damaged. The load on the chord and the brace were applied in the same proportion. For the specimen N1，there was local buckling failure of the

vertical brace near the connection，with the local weld fracture between the two braces. Meanwhile，the weld near the connection of the chord fractured and the surface of the chord cracked，as shown in Figure 3. For the specimen N2，there were local buckling failure of the chord near the connection and buckling failure of square chord side-web on the chord. Almost the entire weld between the two braces fractured，and the weld between the diagonal brace and the chord locally fractured，as shown in Figure 4.
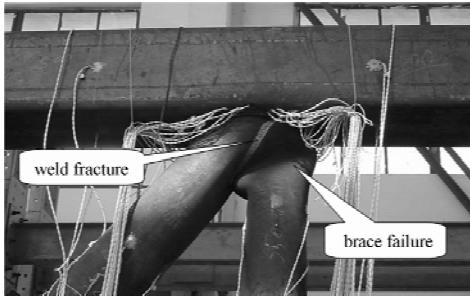
Figure 3   Failure mode of the specimen N1
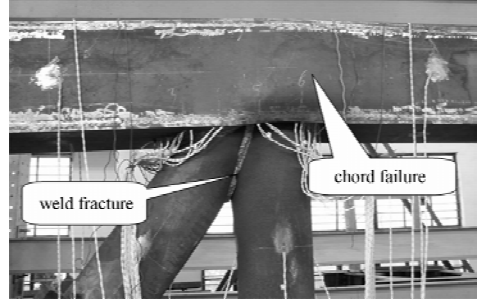
Figure 4   Failure mode of the specimen N2

Finite Element Model

The finite element models of the two specimens were created using ANSYS program. Numerical modeling of the joints included the following considerations：both the tubes and the welds were modeled using twenty-node brick elements（SOLID95 in ANSYS）. Finer meshes were used near the intersection region in order to obtain more accurate results，as shown in Figure 5. The left end of the chord and the end of the diagonal brace were pinned to simulate the boundary condition in the test，as shown in Figure 6. The actual geometric definition of the weld was included in both finite element models. Since the accurate geometry of intersection welds varies around the perimeters and is difficult to be obtained exactly，triangular outlines were used to model the cross section of weld geometry. Material nonlinearity was accounted for in the analysis through a classical plasticity model based on the Von Mises yield criterion and associated plastic flow，with material properties taken from tensile coupon tests. Table 2 shows the ultimate bearing capacity obtained from tests and from FEA，which is defined as the ultimate load of the vertical brace. It can be seen that the finite element analysis results match well with the test results. Figure 7 and Figure 8 show the contour of Von Mises stress when the joints damaged. It can be found that the FE models were reasonable in reproducing similar responses as the test results，though some differences existed. The main reasons may be that the differences in assumed and true constraint conditions and the cracking mechanism were not involved in the finite element modeling. The following parametric analysis is based on this FE model.
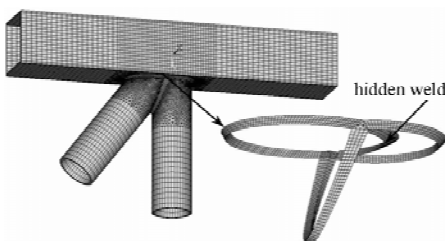
Figure 5   Finite element meshing of the specimen N2
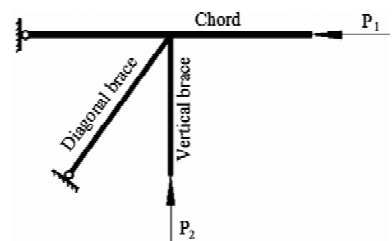
Figure 6   Loading condition of the specimens
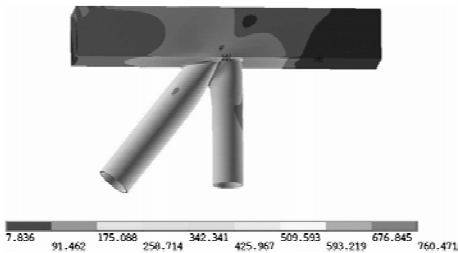
Figure 7   Mises stress contour of the specimen N1
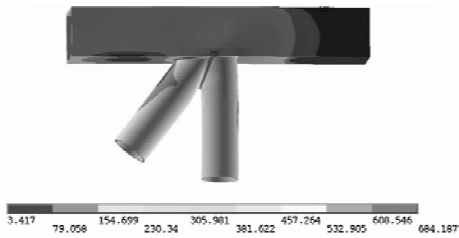
Figure 8   Mises stress contour of the specimen N2

TABLE 2   COMPARISON BETWEEN TEST VALUES AND CALCULATED VALUES FROM FEA

Specimen name	Test results N_{u1}	FEA results N_{u2}	N_{u2}/N_{u1}
N1	1 405 kN	1 433 kN	1.02
N2	2 112 kN	2 180 kN	1.03

PARAMETRIC ANALYSIS

Geometric Parameters

The prime objective of the work presented here is to study the effect of geometric parameters on the ultimate bearing capacity of N-joints of square chords with circular braces. Considering the large number of geometric parameters，to the convenience of analysis as well as comparison，this paper sets $b = 200$ mm as the length of chord side，$L = 1\,200$ mm as the chord length，and $l = 600$ mm as the braces length and $\theta = 45°$. While the varying geometric parameters include β，γ，τ and O_V，with β the ratio of the brace diameter to the length of chord side ($\beta = d_i/b$)，γ the ratio of the length of chord side to wall-thickness ($\gamma = b/t$)，τ the thickness ratio of brace to chord ($\tau = t_i/t$) and O_V the amount of overlap. Three groups，altogether 81 overlapped joints are designed for non-linear finite element analysis，according to the above varying parameters，as shown in Table 3. The finite element model acquired above is applied in the geometric study，and the axial load of the chord P_1 is $0.2A \cdot f_y$.

Distribution of Failure Modes

Three joint failure modes are identified in this paper as the ultimate load is reached，namely，brace local buckling failure（BLB），chord plasticity（CP）and cracking（C）. Sometimes，the failure mode is the combination of the two. Brace local buckling failure and chord plasticity are common failure modes of tubular joints which are judged by checking the deformation shape of joint model and stress. Cracking，as the failure criterion，was deemed to have occurred when 20% tensile strain was attained at any location （determined by scanning the values of maximum principal strains at the element Gauss points)[4]. Finite element analysis of 81 overlapped N-joints are carried out in this paper，among which 16%'s brace local buckling failure，57%'s combination of brace local buckling and chord plasticity failure，11%'s chord plasticity，while another 13 joints are combination of cracking and chord plasticity failure accounting 16% of all the joints.

TABLE 3   GEOMETRIC PARAMETERS OF OVERLAPPED N-JOINTS

Geometric parameters	The value of geometric parameters		
β	0.4	0.6	0.8
γ	10	20	30
τ	0.4	0.7	1.0
O_v	30%	60%	90%

Effect of Geometry

Analysis of β's effect on the ultimate bearing capacity of overlapped N-joints of square chords with circular braces when $O_v = 30\%$, $O_v = 60\%$ and $O_v = 90\%$ is carried out. Because of limited extent of this paper, only the curve of effect of $O_v = 60\%$ of the joints is illustrated in Figure 9, but similar cases are found when $O_v = 30\%$ and $O_v = 90\%$. As shown in Figure 9, β's effect on N-joints' ultimate bearing capacity is quite the same as that on K-joint that ultimate capacity basically increases in linear trend with the changing value of β. Joints with thicker chord wall ($\gamma = 10$) make the most increase of ultimate bearing capacity. This is because when $\gamma = 10$, failures seen are mainly of brace local buckling failure modes. With the increasing value of β, brace section is widen, which raises the ultimate capacity of brace. When $\gamma = 30$, which suggests a relatively thinner joint chord wall, ultimate capacity seems the least increase, because joint like this is more likely to see combination of brace local buckling and chord plasticity failure. So given the increasing β, chances of brace local buckling would increase instead, as a result, there is no notable increase in ultimate bearing capacity.

Figure 10 illustrates the effect of γ on overlapped N-joints of square chords with circular braces strength, which are similar in cases when $O_v = 30\%$ and $O_v = 90\%$. As shown in Figure 10, ultimate capacity of overlapped N-joints with the same β and τ would tend to decrease as γ increases. This is quite the same as gap joints. Ultimate capacity of joints reduces faster when the value of range from 10–20, while slower when range from 20–30. In addition, the ultimate capacity of joints with γ ranging from 0.7–1.0 reduces less than those with γ equaling to 0.4.
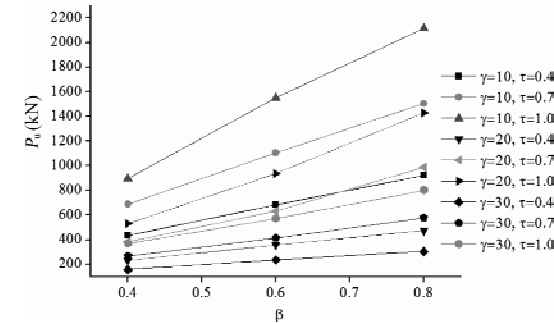
Figure 9   Effect of β on N-joint strength ($O_v = 60\%$)
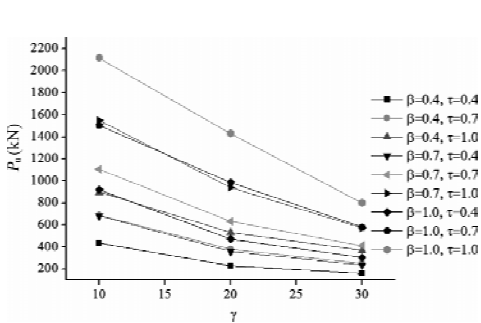
Figure 10   Effect of γ on N-joint strength ($O_v = 60\%$)
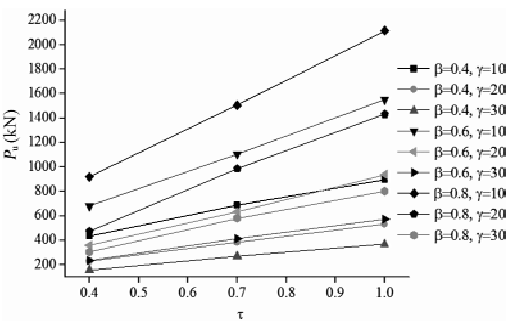
Figure 11   Effect of τ on N-joint strength $(O_v=60\%)$
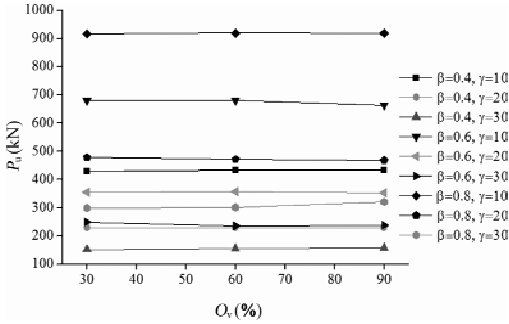
Figure 12   Effect of O_v on N-joint strength $(\tau=0.4)$

Effect of τ on overlapped N-joints of square chords with circular braces strength is illustrated in Figure 11，which are quite the same in case when $O_v = 30\%$ and $O_v = 90\%$. Figure 11 shows ultimate strength of overlapped N-joints increases linearly with the increasing of τ. Generally speaking，ultimate capacity increases slower when the value of γ is relatively greater，vice versa.

Because of the overlap of braces，part of axial load is transferred between them，so the ultimate bearing capacity of overlapped joint is not all the same as that of gap joint. In order to investigate the influence of overlap on joint ultimate bearing capacity，illustrations are made when thickness ratio of brace wall to chord wall τ equals to 0.4，0.7 and 1.0，as shown in Figure 12 to Figure 14. From Figure 12 it can be concluded that when τ equals to 0.4，or the brace wall is thin，the overlap of brace has little effect on joint ultimate capacity，because failures of joints are mostly of brace local buckling failure mode when τ is relatively small，the overlapped braces are unable to enhance the strength performance of joints. On the contrary，bearing capacity tends to decrease slowly as O_v increases. This is because load transferred directly among joint braces increases as overlap raises，meanwhile，configuration of joint gets more complicated，as a result the escalating concentration of stress makes joint apt to reach ultimate capacity because of brace local buckling. From Figure 13 and Figure 14，it can be seen that ultimate strength of overlapped joint with γ equalling to 20 and 30 tends to increase obviously with the rising of overlap，when the value of τ is relatively great. The ultimate strength of overlapped joint with γ equalling to 10，however，remains almost the same as overlap increases.
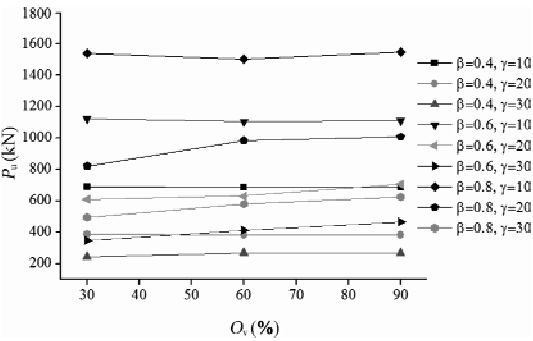
Figure 13   Effect of O_v on N-joint strength $(\tau=0.7)$
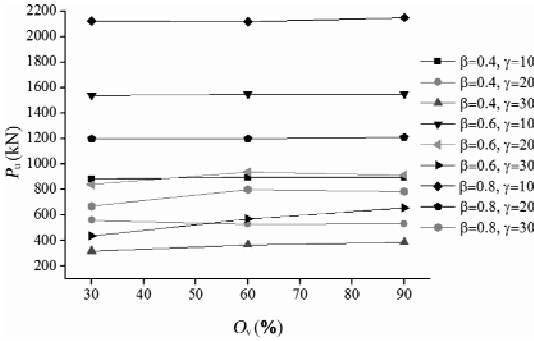
Figure 14   Effect of O_v on N-joint strength $(\tau=1.0)$

Comparison of Results between FEA and Code Formula

In Code for Design of Steel Structures[9]，N-joint is classified as K-joint. The design formula for N-joints

with the local weld fracture between the two braces. For the specimen N2，there were local buckling failure of the chord near the connection and buckling failure of square chord side-web in the chord. And the main failure modes are identified in parametric analysis，namely，brace local buckling failure（BLB），chord plasticity（CP），cracking（C），and the combination of them.

(2) The effect of β，γ and τ on N-joints' ultimate bearing capacity is quite the same as that on CHS K-joint，that is，ultimate capacity increases linearly with the increasing β and τ，while it tends to decrease with the increasing γ.

(3) When τ equals to 0.4，or the brace wall is thin，the overlap of brace has little effect on joint ultimate capacity. However，ultimate strength of N-joints of square chords with circular braces with γ equaling to 20 and 30 tends to increase obviously with the rising of overlap.

(4) As overlap increases most of ultimate strength ratio（P_u / P'_u）of FEA to code formula[9] tends to decrease，and when τ equals to 0.4，and $O_v = 60\%$ or $O_v = 90\%$，the ultimate strength of N-joints calculated by FEA is lower than that by code formula. Furthermore，with relatively smaller γ，the result gained from the code design formula leans toward the unsafe side.

ACKNOWLEDGMENT

REFERENCES

［1］Kurobane，Y.，"Ultimate resistance of unstiffened tubular joints"，Journal of Structural Engineering，ASCE，1984，106(2)，pp.385-400.

［2］Yeoh，S. K.，Soh.，A. K. and Soh，C. K.，"Behaviour of tubular T-joints subjected to combined loadings"，Journal of Constructional Steel Research，1995，32(3)，pp.259-280.

［3］Kang，C. T，Moffat，D. G. and Mistry，J.，"Strength of DT tubular joints with brace and chord compression"，Journal of Structural Engineering，ASCE，1998，124(7)，pp.775-783.

［4］Dexter，E. M. and Lee，M. M. K.，"Static strength of loaded tubular K-joints. I：Behavior"，Journal of Structural Engineering，ASCE，1999，25(2)，pp.194-201.

［5］Dexter，E. M. and Lee，M. M. K.，"Static strength of axially loaded tubular K-joints. Ⅱ：Ultimate capacity"，Journal of Structural Engineering，ASCE，1999，125(2),pp.202-210.

［6］Gazzola，F.，Lee，M. M. K. and DEXTER，E. M.，"Design equation for overlap tubular K-joints under axial loading"，Journal of Structural Engineering，ASCE，2000，126(7)，pp.798-808.

［7］Chiew，S. P，Chee，K. S. and Nai，W. W.，"Experimental and numerical stress analyses of tubular XT-joint"，Journal of Structural Engineering，ASCE，1999，125(11)，pp.1239-1248.

［8］Chiew，S. P.，Chee，K. Soh. and Nai，W. W.，"Experimental and numerical SCF studies of multiplanar tubular XX-joint"，Journal of Structural Engineering，ASCE，2000，126(11)，pp.1331-1338.

［9］Ministry of Construction of the PRC，Code for design of steel structures，2003.

［10］American Institute of Steel Construction，Specification for structural steel buildings，2005.

［11］European Committee for Standardization，Eurocode 3：Design of steel structures，part 1-8：Design of joints，2005.

［12］CIDECT，Construction with hollow steel sections，2005.

DEVELOPMENT AND RESEARCH ON A SERIES
OF PLATE JOINT

M. H. Wang and * S. S. Shi

Beijing University of civil engineering and architecture，zhanlanguan 1，Beijing，100044，China
* Email：shisongsongsss@126.com

KEYWORDS

Bolted spherical joints，welded hollow spherical joints，large-span structure，ultimate bearing capacity，failure mechanism，finite element analysis，mechanical behavior.

ABSTRACT

Bolted spherical joints and welded hollow spherical joints greatly promote the development of space grid structure；however，accessories processing complex and a large number of on-site welding problems limit its deployment and increase the project cost. In this paper，a new series of plate joint（In the motherboard connected four chord members and in the ribs board connected four web members，according to the different stress position in the network structure to choose chord and web members and bolt configuration forms of every lever，combination of different nodes in space board）is developed and finite element analysis software ABAQUS is leveraged for the numerical simulation. The effect of different thickness and diameter of the flattened end node on ultimate bearing capacity of research is studied，to provide a basis for future experiment. According to the experimental results and numerical simulation tests，a space board node system could be formed by achieving the standardization of components and nodes.

INTRODUCTION

In recent years，with the successful development of bolted spherical joints and welded hollow spherical joints，space grid structure has become the most common form in large-span structure of industrial and civil buildings. Meanwhile，plenty of professional manufacturers have appeared and improved the accessibility of those technologies. Because of graceful appearance，stable characteristics and excellent economical performance，they are in many designers's good graces and have been widely used in airports，gyms，TV towers，exhibition halls，conference centers and so on. However，there also exist some shortcomings：machining the various parts of Bolt-ball Net Frame is so complex that it has to be done by professional manufacturers；besides，welded ball grid structure is fulfilled with on site welding，which prolong the engineering installation cycle. All the mentioned deficiencies increase the difficulty of machining or construction of project，as a result，the cost of the project increased.

In the current space grid structure，the squash end of hollow structural section has been connected to round pip，square tube，rectangular pipe and other section steel successfully. Due to its convenient connection and wide applicability，they are widely used in the building industry，especially in large-span structure. Figure 1 is node details of one park's gate.
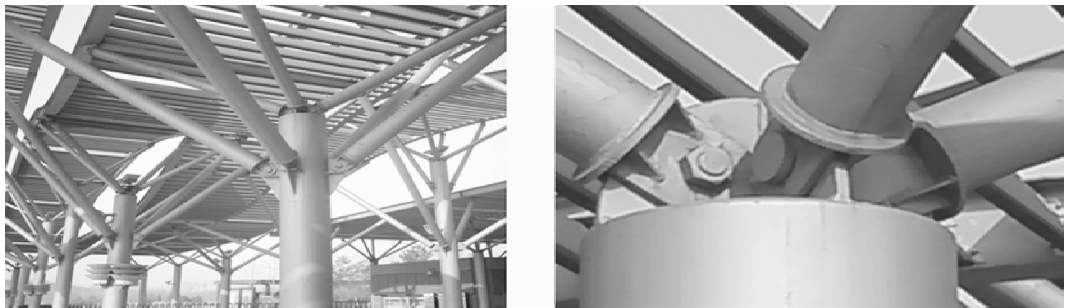

Figure 1　One park's gate

THE CONNECTION OF SQUASH END NODE AND PLATE NODE

Considering the pros and cons of the mentioned nodes above，a new design to leverage round steel instead of ball node and connect it by bolt using steel's squashed end is proposed. Its plate connect chords and ribbed slab connects web members to form plate joint（Figure 2）. This proposal has a lot of advantages，such as simple processing equipments，convenient connection to easy blanking，wide range of applicability and less need for onsite welding. After standardization of components and nodes，it will effectively improve the processing speed and reduce the project cost，thus it's a sounded alternative for bolted spherical joints and welded hollow spherical joints.
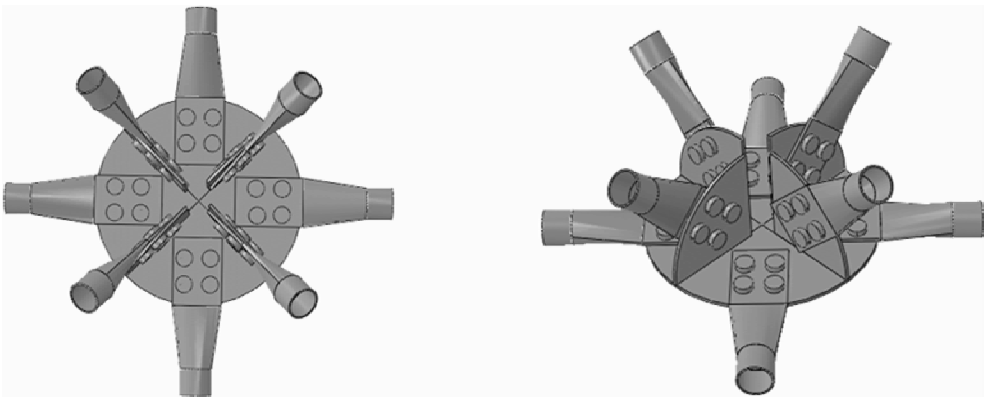
Figure 2　A series of plate joint

A SERIES OF PLATE JOINT

Shearing Bolt's Design of Regular Steel Pipe

The project utilizes nine kinds of Q235 steel pipes and a series of common bolts with 16，20，24，27，36，

39 mm in diameter. According to ultimate capacity of axial tension and construction requirement，the pipe end configurations of bolts are displayed on the following Table 1.

TABLE 1　SHEARING BOLT CONFIGURATION TABLE

Pipe size		Bolt diameter (mm)	single bolt ultimate bearing capacity（N）	tensile strength （N/mm²）	rows	calculated number per row	Real number	construction requirement		
diameter (mm)	thickness (mm)							width (mm)	minimum width	yes or no
60	3	16	28 134	215	2	1.5	2	94	86.4	yes
76	3.5	20	42 700	215	2	1.5	2	120	108	yes
89	4	20	43 960	215	2	1.9	2	140	108	yes
114	4	24	58 560	215	2	1.9	2	178	129.6	yes
159	6	27	80 117	215	2	2.7	3	250	226.8	yes
180	6	36	131 760	215	2	2.0	2	282	194.4	yes
219	6	36	131 760	215	2	2.4	3	344	302.4	yes
219	8	36	142 430	215	2	2.8	3	344	302.4	yes
219	10	39	167 158	215	2	2.8	3	344	327.6	yes

Design to Take Full Advantage Strength of Squash End Node

Above bolt configuration is designed under ultimate capacity of axial tension. However，in the practical deployment，nodes with flattened end do not always end in a state of extreme tension，so the end of the node can be designed into two forms to meet different state through reducing a row of bolts on top of the original design. Figure 3 is two proposed designs of bolt configuration，others see Table 2.
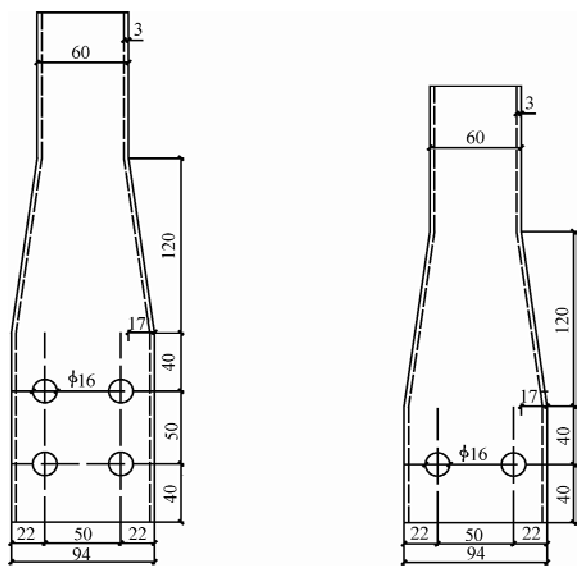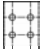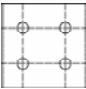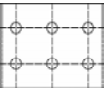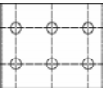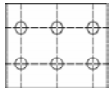
Figure 3　Two proposed designs of bolt configuration

TABLE 2   TWO KINDS OF BOLT CONFIGURATION OF ALL THE STEEL PIPES

force types	60×3	76×3.5	89×4	114×4	159×6	180×6	219×6	219×8	219×10
tension									
pressure									

Classification and Design of a Series of Plate Joint

Plate joint is tentatively scheduled to connect four chords in the floor plate while four ventral poles in the rib part. Since forces apply to different locations in gird structure，the number of chord and ventral pole as well as bolt configurations of each pipe can be selected，combined into a various plate joint.

The size of floor plate could be determined after chord and ventral pole size are normalized（see Table 3）.

TABLE 3   THE SIZE OF FLOOR PLATE OF A SERIES OF PLATE JOINT

	60×3	76×3.5	89×4	114×4	159×6	180×6	219×6
tension	400×8	500×8	600×10	700×10	800×12	900×12	1 000×12
pressure	300×8	400×8	400×10	500×10	600×12	700×12	800×12

FINITE ELEMENT STRESS ANALYSIS OF PLATE JOINT

Due to the lack of depth knowledge of its bearing capacity，specifications and related data，it will have a tremendous security risk to apply it to engineering structures，not to mention that its mechanical behavior and failure mechanism is still not clear. Therefore，there is a need for in-depth study on the subject.

Main Research Directions

On the node type，research mainly in three aspects：first，the research of anti-pulled、anti-pressed and anti-buckling to the floor part of the plate；second，the research of mechanical behavior of squashed end of the node；the last one is the research of mechanical behavior of stiffener.

Due to the insufficient time to carry out the topic，the current research focus on how the thickness of the motherboard would influent the ultimate bearing capacity when a chord is connected to the 1/4 motherboard through a bolt. According to different thickness（to keep the same sizes of the chord and the bolt），the following three simulation programs are designed（see Table 4）.

TABLE 4   SIMULATION PROGRAM

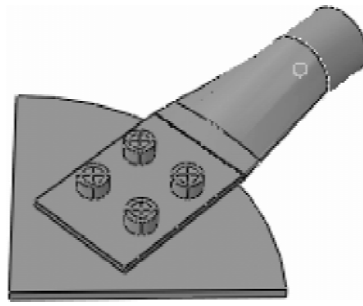|	Plate thick	Chord member	bolt diameter
Program1	6	60×3	16
Program2	8	60×3	16
Program3	10	60×3	16

Figure 4　Computational model

Establishment of The Model and Processing of The Key Technology

Establishment of the model

Based on the connection method of actual components，the 3D solid model can be established by the finite element software ABAQUS（see Figure 4）

Selection of specimen material parameters

All the specimens for analysis are Q235 steel and the yield criterion of materials complies with Von-Mises's yield criterion as well as the related flow rule. Concerning steel's stress-strain relation，two line model including the elastic stage and enhanced phase is considered. The curve is shown in Figure 5(a).

The mechanical behavior of plate joint is the key research point instead of the bolt，so the bolts' constitutive relation is only considered in the elastic stage. The curve is shown in Figure 5(b).
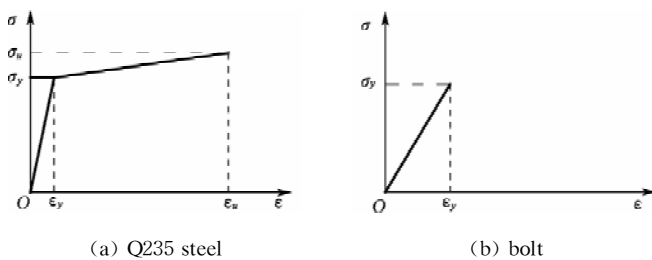

（a）Q235 steel　　　　　　　　　（b）bolt

Figure 5　Material constitutive relation

Unit selection and meshing

In the software of ABAQUS，the C3D8R belongs to the reduced-integration elements of hexahedral linear with 8 nodes and can overcome shear locking in the linear integral unit. In addition，it is able to simulate contact relationship about bolts and obtain relatively accurate displacement. Thus grids of the node are divided using the C3D8R. The model is divided into four layers along the thickness and the grid at the part of flat tube's arc is further set off. The results of divided grid are show in Figure 6.
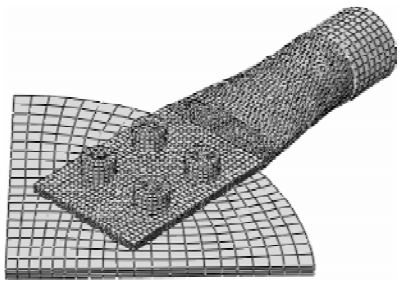
Figure 6　Mesh generation

Treatment of contact relationship

This article is a research on detailed structure of the node，so the connection of surface and surface in the ABAQUS including the connection of plate and hollow pipe，bolt head and hollow pipe as well as the bolt hole and screw is selected. Defined in accordance with the principles of the contact pair：the thicker，stiffer and larger divided surfaces are considered as main surfaces while others are treated as subsidiary ones. In the project，the main surface is the plate and the subsidiary surface is hollow pipe in the connection of plate and hollow pipe，while the main surface is hollow pipe and subsidiary surface is bolt head in the bolt head and hollow pipe.

Boundary conditions and loading system

Both sides of the motherboard should be fixed and surface loads（210 MPa）are exerted on the cross-section of hollow pipe in a linear way.（See Figure 7）
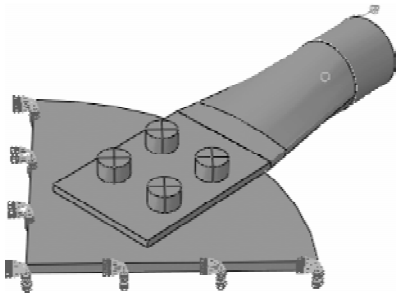

Figure 7　Boundary conditions and load

Finite element results and analysis

Figure 8 indicates that when the thickness of the motherboard is 6 mm，maximum stress of chord is 243.8 MPa while maximum stress of motherboard is 236.9 MPa，they both yield. When the motherboard is 8 mm thick，maximum stress of chord is 243.8 MPa，at this point maximum stress of motherboard is 230.3 MPa，as a result，chord yields but motherboard does not. Besides，when the motherboard thickness is 10 mm，maximum stress of chord is 243.8 MPa while maximum stress of motherboard is 166.3 MPa，not only motherboard does not yield but also has a large surplus.
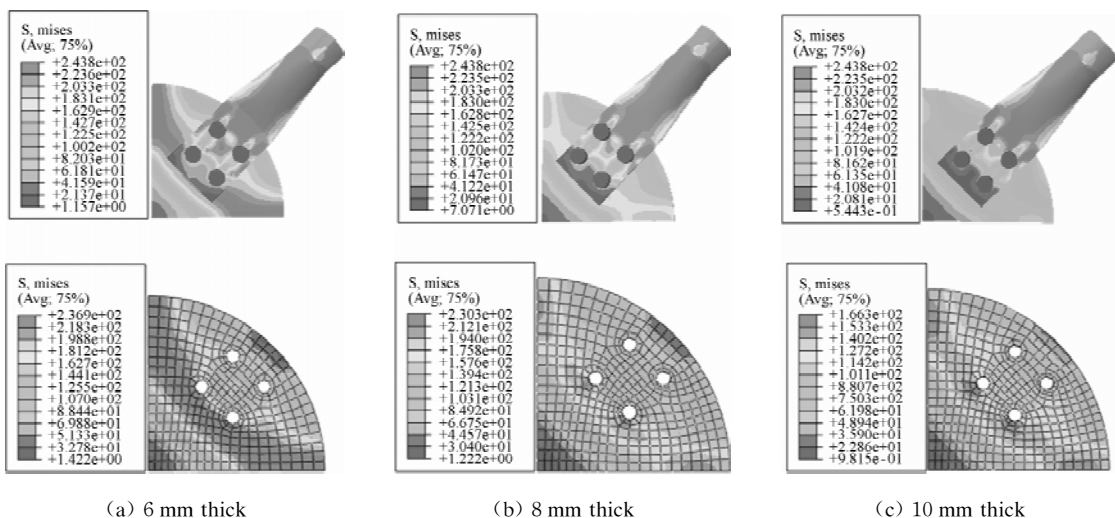
(a) 6 mm thick　　　　　　(b) 8 mm thick　　　　　　(c) 10 mm thick
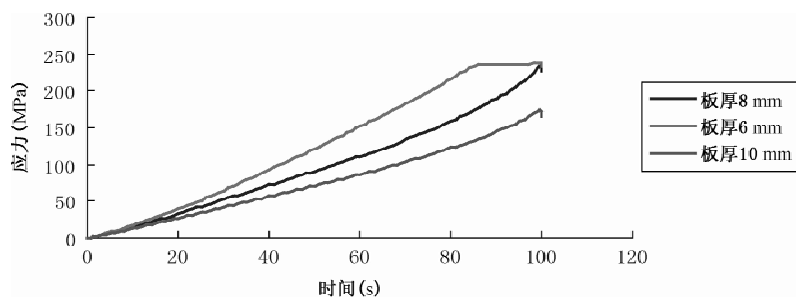
Figure 8　Stress nephogram

Figure 9　Point stress changes over time

Figure 9 presents the stress changing with time for the same point A for three thickness plate respectively. From the curve，we can see that when the motherboard thickness is 6 mm，the point comes into the plastic stage and starts yield after 80 seconds；when the thickness is 8 mm，the point stress is about 230.32 MPa，so the chord has been yielded and the component is damaged which leads to the curve gliding. When the thickness is 10 mm，the stress of the point is about 165.48 MPa. Since the chord has been yielded，the component is destructed and the curve slide which is consistent with previous results.

There may be two main reasons to make larger parts of the chord yield. The fires one is that the process of lead pipe crushed flat tube straight part of the material in the outer wall of the axial stress，inner axial tensile stress under the function collapse occurs，the other is that flat tube round arc part of the material in the outer axial tensile stress，the inner axial compressive stress under the function-oriented flat occur.

Based on the above analysis，motherboard thickness of 6 mm should be eliminated for yielding；motherboard thickness of 10 mm has the same plastic zone as 8 mm under the same load. Therefore，selecting thickness of 8 mm not only meets the force requirements but also makes full use of the strength.

FUTURE WORK

A better understanding on mechanical behavior and failure mechanism of space plate joint is reached based on the study；however，in order to verify the reliability of finite element results，a pilot study under the same conditions in future is needed to understand the different parameters. On this basis，we can summarize the practical calculation method to guide engineering practice and promote the application and development of the space plate joint.

REFERENCES

［1］J. A. Packer and J. E. Henderson，"Hollow structural section connecting Design Guide"，Science Press，2006.

［2］Shu，X. P.，"Analysis and Design of advanced steel structure"，Science Press，1997.

［3］Shi，Y. P. and Zhou，Y. R.，"ABAQUS finite element analysis example explanation"，Machinery Industry Press，2006.

［4］Wang，Y. Z. and Fu，C. G.，"ABAQUS structural engineering analysis and example explanation"，China Building Industry Press，2010.

［5］Wang，W，Chen，Y. Y and Zhao，X. Z.，"Performance-based design of steel node Status and key issues"，Civil Engineering Journal，2007，40(11)，pp. 01-08.

［6］Bjorhovde R. and Chakrabarti S. K.. "Tests of Full-size Gusset Plate connections"［J］. Journal of Structure Engineering，ASCE，Vol. 111，No. 3，March，1985.

［7］James M. Ricles and Joseph A. Yura. "Strength of Double-row Bolted-web Connections"［J］. Journal of Structure Engineering，ASCE，Vol. 109，No. 1，January，1983.

［8］James G. Orbison，Mark E. Wagner and William P. Fritz. Tension Plane Behavior in Single-row Bolted connections subject to block shear［J］. Journal of constructional steel research 1999(49)，pp. 225－239.

［9］AISC. Load and resistance factor design specification for structural steel buildings［S］. Chicago（IL）：American Institute of Steel Construction，1999.

［10］CSA. Limit states design of steel structures. CAN/CSA-S16－94［S］. Toronto（ON）：Canadian69 Standards Association，1994.

［11］CSA. Limit states design of steel structures. CAN/CSA-S16－01［S］. Toronto（ON）：Canadian Standards Association，2001.

［12］AISC. Specification for structural steel buildings［S］. Chicago（IL）：American Institute of Steel Construction，2005.